E.O. Paton Electric Welding Institute of the National Academy of Sciences of Ukraine

International Scientific-Technical and Production Journal

The Paton WELDING JOURNAL

April 2013
No.4

Published since 2000

English translation of the monthly «Avtomaticheskaya Svarka» (Automatic Welding) journal published in Russian since 1948

Founders
E.O. Paton Electric Welding Institute of the NAS of Ukraine, International Association «Welding»

Publisher
International Association «Welding»

Translators:
A.A.Fomin, O.S.Kurochko, I.N.Kutianova, T.K.Vasilenko
Editor
N.A.Dmitrieva
Electron galley
D.I.Sereda, T.Yu.Snegiryova

Address
E.O. Paton Electric Welding Institute, International Association «Welding»
11, Bozhenko Str., 03680, Kyiv, Ukraine
Tel.: (38044) 200 60 16, 200 82 77
Fax: (38044) 200 82 77, 200 81 45
E-mail: journal@paton.kiev.ua
www.patonpublishinghouse.com
URL: www.rucont.ru

State Registration Certificate
KV 4790 of 09.01.2001
ISSN 0957-798X

Subscriptions
$348, 12 issues per year, air postage and packaging included.
Back issues available.

CONTENTS

SCIENTIFIC AND TECHNICAL

Borisov Yu.S., Demchenko V.F., Lesnoj A.B., Khaskin V.Yu. and *Shuba I.V.* Numerical modelling of heat transfer and hydrodynamics in laser-plasma treatment of metallic materials 2

Poznyakov V.D., Zhdanov S.L., Maksimenko A.A., Sineok A.G. and *Gerasimenko A.M.* Weldability of sparsely-alloyed steels 06GBD and 06G2B 8

Rybakov A.A., Filipchuk T.N. and *Goncharenko L.V.* Cracks in welded joints of large diameter pipes and measures for their prevention 15

Khorunov V.F., Zvolinsky I.V. and *Maksymova S.V.* Arc brazing of low-carbon steels 21

Somonov V.V., Boehm S., Geyer M. and *Bertelsbeck S.* Study on the effect of induction heating to prevent hot cracking during laser welding of aluminum alloys 26

Ilyushenko V.M., Novoseltsev Yu.G. and *Busygin S.L.* Metallurgical peculiarities of plasma-arc welding of chrome-bronze 34

Makhnenko O.V. and *Prudky I.I.* Information systems for selection of arc welding process parameters (Review) 37

INDUSTRIAL

Kravchuk L.A., Kushneryov A.V. and *Kozhukalo V.I.* Modernisation of electron beam welding installation ELU-20 45

Titarenko V.I., Lantukh V.N. and *Kashinsky A.S.* Machines based on lathes for mill roll surfacing 48

Pereplyotchikov E.F. and *Ryabtsev I.A.* Plasma-powder surfacing of power fitting rods 53

Kolomijtsev E.V. Corrosion resistance of welded joints of ship hull materials 56

BRIEF INFORMATION

Pulka Ch.V., Senchishin V.S., Gavrilyuk V.Ya. and *Bazar M.S.* Influence of technological schematics of induction surfacing on stability of deposited layer thickness 61

«The Paton Welding Journal» abstracted and indexed in Ukrainian refereed journal «Source», RJ VINITI «Welding» (Russia), INSPEC, «Welding Abstracts», ProQuest (UK), EBSCO Research Database, CSA Materials Research Database with METADEX (USA), Questel Orbit Inc. Weldasearch Select (France); presented in Russian Science Citation Index & «Google Scholar»; abstracted in «Welding Institute Bulletin» (Poland) & «Rivista Italiana della Saldatura» (Italy); covered in the review of the Japanese journals «Journal of Light Metal Welding», «Journal of the Japan Welding Society», «Quarterly Journal of the Japan Welding Society», «Journal of Japan Institute of Metals», «Welding Technology».

NUMERICAL MODELLING OF HEAT TRANSFER AND HYDRODYNAMICS IN LASER-PLASMA TREATMENT OF METALLIC MATERIALS*

Yu.S. BORISOV, V.F. DEMCHENKO, A.B. LESNOJ, V.Yu. KHASKIN and **I.V. SHUBA**
E.O. Paton Electric Welding Institute, NASU
11 Bozhenko Str., 03680, Kiev, Ukraine. E-mail: office@paton.kiev.ua

An approximate mathematical model is proposed to describe thermal and hydrodynamic processes occurring in combined laser-plasma cladding. The scheme of a rapidly moving heat source, which generalises the known N.N. Rykalin's scheme for a case of combined convective-conductive heat transfer in molten metal, is considered. Densities of the different-power laser and plasma heat sources are assumed to be distributed on the plate surface by the normal law, having different radii of heat spots. The combined heat spot is assumed to be additive. The equation of local heat balance on the surface of a workpiece allows for heat transfer by radiation and heat losses for evaporation. It is assumed that motion of the melt under the indirect-action plasma heating conditions is driven by the Archimedes buoyancy force and thermocapillary force. Verification of the mathematical model was carried out, and results of calculation experiments on investigation of the penetration zone under the effect of the laser and combined laser-plasma heat sources are described. It is shown that the Marangoni force is a dominant force factor determining hydrodynamics of the melt. The effect of convective energy transfer on formation of the molten zone was studied. 8 Ref., 4 Tables, 8 Figures.

Keywords: *laser-plasma cladding, thermal and hydrodynamic processes, modelling, heat transfer, heat balance, cladding, penetration zone, Marangoni force*

Problem statement. One of the topical problems of welding, cladding and other metal treatment technologies using plasma-arc, laser or combined laser-plasma heating is evaluation of results of the thermal impact by the heat source on a workpiece. There are many publications dedicated to the issues of theoretical and experimental investigation of the laser and plasma-arc effect on metallic materials [1–3]. At the same time, the problem of the combined effect on metals by the microplasma arc (of a direct or indirect action) and laser beam, the interest in which has dramatically grown with emergence of the combined laser-microplasma technologies, is studied to a much lower degree.

For adequate theoretical description of the processes occurring in laser-microplasma cladding of metallic materials it is necessary to take into account the complex interaction of different physical processes and phenomena related to heating and melting of the base material under the effect of the combined heat source. It can be assumed with a sufficiently good approximation that the combined laser-microplasma energy source is additive, i.e. it can be represented as a sum of the laser and microplasma heat sources distributed on the workpiece surface.

Normally, the models of the heat source generated by laser radiation allow for absorption of the laser radiation by a metallic material and set some law of distribution of the power density on the surface of a material treated. It should be noted in analyses of a plasma component of the heat flow that combined laser-microplasma cladding is performed as a rule by using the indirect-action plasmatrons, i.e. the current does not flow through the workpiece.

Nevertheless, thermal interaction of the current-free plasma with the workpiece surface occurs due to transfer of the critical and potential energy of the plasma particles, this resulting in the formation of the law of distribution of the plasma the heat source thermal power.

Under the thermal effect of the heat source with a density of 10^4 W/cm^2 and higher, the temperature of the weld pool surface may be 10–20 K higher than the boiling temperature, as a result of which the heat losses for evaporation do not only exceed the heat losses due to convective and radiant heat exchanges taken together, but also become comparable with the den-

*The article is based on the presentation made at the 6th International Conference «Mathematical Modelling and Information Technologies in Welding and Related Processes» (29 May–1 June, 2012, Katsiveli, Ukraine).

sity of the heat source. Therefore, allowance for the evaporation heat is an important aspect of theoretical description of the thermal effect by the combined laser-plasma heat source on the material treated.

Mathematical model. Proceed from an assumption that formation of the molten metal zone takes place in a heat conduction mode. This term implies a mode in which the penetration zone of the base metal forms without formation of a pronounced keyhole.

According to this, the free surface of the molten metal is assumed to be non-deformed, and the heat source affecting the workpiece is assumed to be the surface one.

Despite a small volume of the melt forming in cladding by using the combined laser-microplasma energy source, the velocity of motion of the liquid metal in the molten metal may be sufficiently high. Hence, the convective energy transfer can play a marked role in formation of the thermal state of the workpiece being treated.

At the absence of the current flowing through the metal pool, the Archimedes thermal buoyancy force and Marangoni thermocapillary force are the force factors affecting the molten metal.

Let $\{x', y', z'\}$ be the fixed system of Cartesian coordinates related to the workpiece being welded, the z' axis of which is directed along the gravity line; and t' be the time. Add the $\{x, y, z\}$ moving coordinate system as follows: $x = x' - v_w t'$, $y = y'$, $z = z'$, and $t = t'$, where v_w is the speed of movement of the heat source.

Upon reaching the quasi-stationary thermal and hydrodynamic state, the complete system of the hydrodynamics and heat exchange equations can be written down as follows:

$$(V_x + v_w)\frac{\partial W}{\partial x} + V_y\frac{\partial W}{\partial y} + V_z\frac{\partial W}{\partial z} = \quad (1)$$
$$= \frac{\partial}{\partial x}\left(\lambda\frac{\partial T}{\partial x}\right) + \frac{\partial}{\partial y}\left(\lambda\frac{\partial T}{\partial y}\right) + \frac{\partial}{\partial z}\left(\lambda\frac{\partial T}{\partial z}\right);$$

$$\begin{cases} (V_x + v_w)\dfrac{\partial V_x}{\partial x} + V_y\dfrac{\partial V_x}{\partial y} + V_z\dfrac{\partial V_x}{\partial z} = -\dfrac{1}{\rho}\dfrac{\partial P}{\partial x} + \nu\Delta V_x; \\ (V_x + v_w)\dfrac{\partial V_y}{\partial x} + V_y\dfrac{\partial V_y}{\partial y} + V_z\dfrac{\partial V_y}{\partial z} = -\dfrac{1}{\rho}\dfrac{\partial P}{\partial y} + \nu\Delta V_y; \\ (V_x + v_w)\dfrac{\partial V_z}{\partial x} + V_y\dfrac{\partial V_z}{\partial y} + \\ + V_z\dfrac{\partial V_z}{\partial z} = -\dfrac{1}{\rho}\dfrac{\partial P}{\partial z} + \nu\Delta V_z + g\beta_T T; \\ \dfrac{\partial V_x}{\partial x} + \dfrac{\partial V_y}{\partial y} + \dfrac{\partial V_z}{\partial z} = 0, \end{cases} \quad (2)$$

where V_x, V_y and V_z are the components of the melt velocity vector; ν is the kinematic viscosity; P is the pressure; β_T is the thermal coefficient of volume expansion of the melt; g is the gravity acceleration; $W = \rho\int_0^T c\,dT + \rho\chi\eta$ is the enthalpy; ρ is the density; c is the specific heat of the material; T is the temperature; χ is the latent solidification heat; λ is the thermal conductivity factor; $\eta = (T, T_S, T_L)$ is the volume fraction of the liquid phase in the solidification temperature range; and T_S and T_L are the solidus and liquidus temperatures. Equation (1) is integrated in the $\Omega = \Omega_L \cup \Omega_S$ region, where Ω_L is the weld pool, and Ω_S is the non-melted base metal. Equation system (2) is determined in the Ω_L region.

Let $\mathrm{Pe} = (v_w l)/a$ be the Peclet thermal criterion, where l is the characteristic geometrical dimension (in this case, it is the thickness of the plate treated), and a is the thermal conductivity coefficient of the deposited material. At $\mathrm{Pe} >> >> 1$, the rapidly moving source scheme suggested by N.N. Rykalin [4] for the welding heat model formulated within the frames of the conductive mechanism of heat transfer in a workpiece is a good approximation of the three-dimensional problem for calculation of the temperature field. In the present study, the idea of the rapidly moving source covers a case of the combined convective-conductive energy transfer. The rapidly moving source scheme ignores the heat transfer in a direction of the welding heat source, the allowance being made only for the heat transfer across the workpiece treated. In addition to the above-said, assume in equations (2) that $V_x = 0$ and $\partial P/\partial x = 0$. Then the systems of equations (1) and (2) can be written down in the following form:

$$\frac{\partial W}{\partial \tau} + V_y\frac{\partial W}{\partial y} + V_z\frac{\partial W}{\partial z} = \quad (3)$$
$$= \frac{\partial}{\partial y}\left(\lambda\frac{\partial T}{\partial y}\right) + \frac{\partial}{\partial z}\left(\lambda\frac{\partial T}{\partial z}\right), \quad y, z \in \Omega^*;$$

$$\begin{cases} \dfrac{\partial V_y}{\partial \tau} + V_y\dfrac{\partial V_y}{\partial y} + V_z\dfrac{\partial V_y}{\partial z} = -\dfrac{1}{\rho}\dfrac{\partial P}{\partial y} + \nu\Delta V_y; \\ \dfrac{\partial V_z}{\partial \tau} + V_y\dfrac{\partial V_z}{\partial y} + V_z\dfrac{\partial V_z}{\partial z} = -\dfrac{1}{\rho}\dfrac{\partial P}{\partial z} + \nu\Delta V_z + g\beta_T T; \\ \dfrac{\partial V_y}{\partial y} + \dfrac{\partial V_z}{\partial z} = 0; \\ y, z \in \Omega_L^*, \end{cases} \quad (4)$$

where $\tau = x/v_w$, and $\Omega^* = \{0 < y < L_y,\ 0 < z < L_z\}$ is the cross section of the plate. Hydrodynamics equations (4) are integrated in the Ω^*_L region to be determined, which is limited by the free surface of the melt and solidification front. Geometry of the region is subject to determination from solution of the thermal problem.

Write down the boundary conditions for equation (3) in the following form:

$$\lambda \left.\frac{\partial T}{\partial z}\right|_{z = L_z} = \alpha[T(y, L_z, t) - T_{amb}] + \varepsilon\sigma[\overline{T}^4(y, L_z, t) - \overline{T}^4_{amb}]; \quad (5)$$

$$-\lambda \left.\frac{\partial T}{\partial z}\right|_{z = 0} = \alpha[T(y, 0, t) - T_{amb}] + \varepsilon\sigma[\overline{T}^4(y, 0, t) - \overline{T}^4_{amb}] + q_v(T) + q_h(y, t); \quad (6)$$

$$\left.\frac{\partial T}{\partial y}\right|_{y = 0} = 0, \quad \left.\frac{\partial T}{\partial y}\right|_{y = L_y} = 0, \quad (7)$$

where α is the heat transfer coefficient; T_{amb} is the ambient temperature; ε is the reduced emissivity of the surface; σ is the Stefan–Bolzmann constant; $\overline{T}$ is the absolute temperature; $q_v(T)$ are the heat losses for evaporation; and q_h is the density of the heat flow imparted to the workpiece surface by the plasma and laser heat sources. The heat losses for evaporation from the melt surface were evaluated by using the Knight model [5, 6].

Set distributions of heat flow density $q_h(y, t)$ both for the laser radiation and plasma energy sources in the following form:

$$q_h(y, t) = q_0 \exp(-k(\sqrt{(x_0 - v_w t)^2 + y^2})^n),$$

where x_0 is the initial displacement of the source centre from the origin of fixed coordinate system $\{x', y', z'\}$. Designate the efficient radii of the laser and plasma energy sources through r_L and r_P (it is assumed that 95 % of power of a corresponding source is released at the spot of the efficient radius), $a = \max\{r_L, r_P\}$. If x_0 is assumed to be equal to $x_0 = 1.2a$, at the origin of the moving coordinate system at $t = 0$ the density of the heat flow from the combined laser-plasma heat sources will practically be equal to zero.

Assuming the free surface of the melt to be non-deformed, write down the boundary conditions for hydrodynamics equations (4) in the following form:

$$V_z|_{z = 0} = 0, \quad v \left.\frac{\partial V_y}{\partial z}\right|_{z = 0} = -\frac{\beta_\sigma}{\rho} \left.\frac{\partial T}{\partial y}\right|_{z = 0}, \quad (8)$$

where $\beta_\sigma = \dfrac{d\sigma}{dT}$, and $\sigma = \sigma(T)$ is the coefficient of surface tension of the melt. The second of these conditions is a balance of tangential stresses written down allowing for the effect of the Marangoni thermocapillary force. The adhesion and impermeability conditions are assumed to take place at the solidification front, the following symmetry conditions being set at $y = 0$:

$$V_y|_{y = 0} = 0, \quad \left.\frac{\partial V_z}{\partial y}\right|_{y = 0} = 0. \quad (9)$$

Numeric implementation of the formulated model was carried out by using the Lagrangian–Eulerian method and schemes of splitting of equations (3) and (4) into physical sub-processes and spatial variables [7, 8].

Calculation results. The model was verified by conducting experimental studies of the shape of the penetration and heat-affected zones under the effect on the 09G2S steel plate with thickness $L_z = 1$ cm by the Nd:YAG laser source with power $P_L = 1.25$ kW (focusing lens diameter $D_F = 5$ cm, focusing lens beam diameter $D_L = 4$ cm, lens focal distance $F = 30$ cm, heat source speed $v_w = 60$ m/h). In numerical investigations, the effect of the hydrodynamic factor on formation of the molten zone of the base metal was analysed in the following variants:

- by ignoring convection of the melt;
- by allowing only for free convection;
- by allowing for the thermocapillary force effect;
- by allowing for the combined effect of the thermal buoyancy and thermocapillary forces.

Table 1. Effect of hydrodynamic factors on penetration parameters

No.	Type of evaluation		H, cm	B, cm	V_y, cm/s	V_z, cm/s	T_{max}, °C
	Experiment		0.042	0.222	–	–	–
1	Calculation	Without convection	0.051	0.168	0	0	2905
2		A	0.049	0.174	0.191	0.089	2896
3		M	0.045	0.234	51.101	16.205	2875
4		A + M	0.042	0.252	51.300	16.310	2874

Note. A — free convection; M — Marangoni convection.

The calculation results obtained at $\eta = 0.32$ and $r_L = 0.1$ cm are given in Table 1 and shown in Figure 1. The Table gives the calculation data on penetration width B and depth H, as well as on the value of maximal overheating of the metal pool surface and maximal values of components of the melt velocity vector. It follows from Table 1 that the closest coincidence of the calculation and experimental data is achieved at the effect on the melt by the thermal buoyancy and thermocapillary forces, the dominant factor determining the penetration width being the Marangoni thermocapillary convection.

Direction of the flow of the melt and its velocity (~50 cm/s) are governed by the dominant action of the Marangoni force, under the effect of which the flows of the melt transfer the most overheated metal from the paraxial part of subsurface layers of the pool to its periphery, thus leading to a one and a half times increase in the penetration width compared to the calculation variant that ignored the melt convection. Figure 2 shows comparison of the calculation results on contours of the pool and heat-affected zone (see Table 1, No.4) with the experimental data, where the calculated shape of the penetration zone (curve *1*, isothermal line $T = 1480$ °C) and boundary of the heat-affected zone (curve *2*, isothermal line $T = 750$ °C) are superimposed on the macrosection.

As follows from Figure 2, the best agreement between the calculation and experimental data is observed with the simultaneous allowance for the thermal buoyancy and thermocapillary forces. It is likely that the difference between the calculation and experimental data on the shape of the molten zone is associated with deformation of the free surface of the pool under the effect of the vapour recoil reaction. Figures 3 and 4 show the field of isothermal lines on the plate surface and in a longitudinal section of the weld (coordinate $x = 0$ corresponds to the centre of the heat source).

It follows from Figures 3 and 4 that the maximal base metal penetration depth and width are

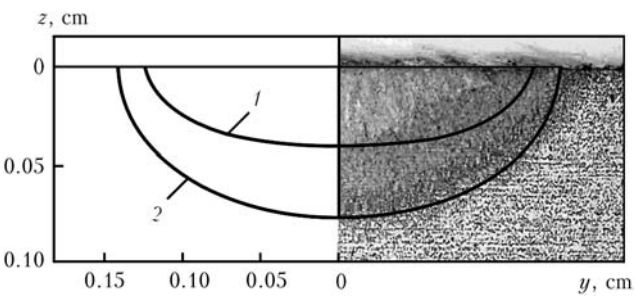

Figure 2. Penetration zone and heat-affected zone in laser heating (*1*, *2* — see the text)

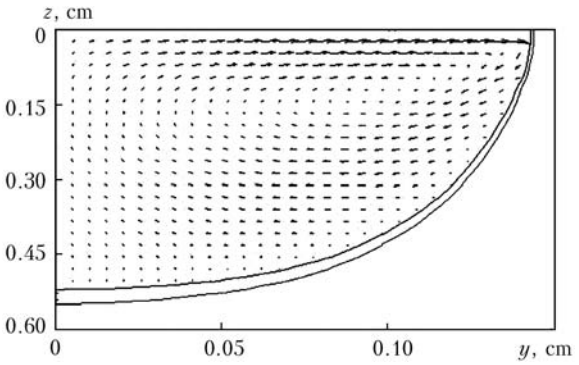

Figure 1. Field of the melt velocities in cross section of the metal pool (Table 1, variant No.4)

shifted from the source centre towards the tailing part to a distance of 0.06–0.08 cm.

Figure 5 shows thermal cycles at different sections in height of the plate. It follows from this Figure that the plate is heated to a temperature above 750 °C and to a depth of less than 0.3 cm at an average time of dwelling in the 800–500 °C range equal to 0.15 s.

Results of investigations of the effect of laser heating parameters (thermal power of laser radiation, heat spot radius, and heat source speed) are given in Tables 2–4.

Increase in power from 200 to 400 W leads to a 2.5 times increase in the penetration depth. Further increase in power ($P_L > 400$ W) does not exert a considerable effect on the penetration depth, as the maximal temperature of the surface of the molten metal pool becomes higher than the boiling temperature of the base metal of the plate, heat losses for evaporation of metal from the melt surface growing accordingly.

Consider peculiarities of heating of the plate under the effect of the combined laser-microplasma energy source. It was assumed in conducting the calculation experiment that centres of the laser and plasma heating spots coincided. The distribution of the power density of each of the

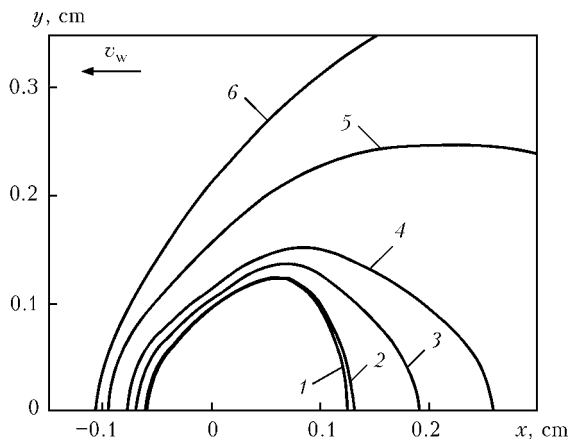

Figure 3. Field of isothermal lines on the plate surface at $T = 1480$ (*1*), 1430 (*2*), 1000 (*3*), 600 (*4*), 250 (*5*) and 100 (*6*) °C

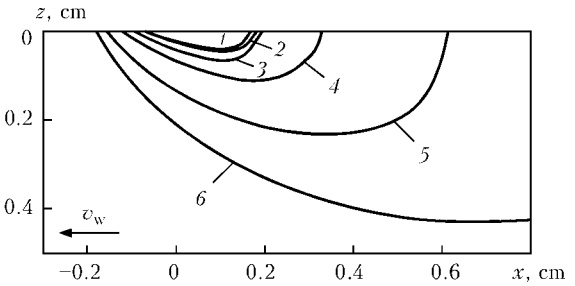

Figure 4. Field of isothermal lines in axial section of the weld at T = 1480 (*1*), 1430 (*2*), 1000 (*3*), 600 (*4*), 250 (*5*) and 100 (*6*) °C

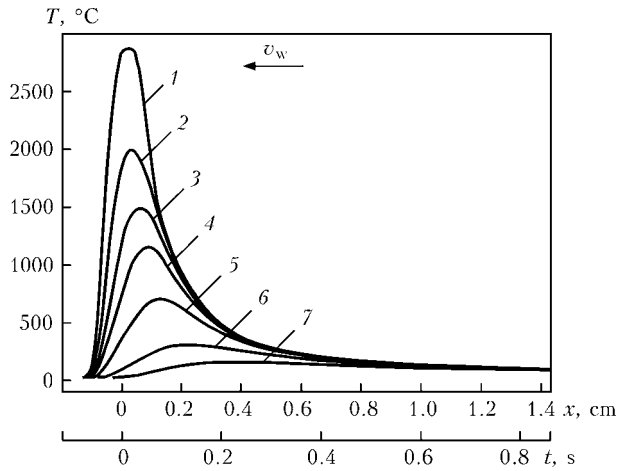

Figure 5. Temperature cycles at the weld axis for different sections in height of the plate at z = 0 (*1*), 0.02 (*2*), 0.04 (*3*), 0.06 (*4*), 0.28 (*5*), 0.36 (*6*) and 0.44 (*7*) cm

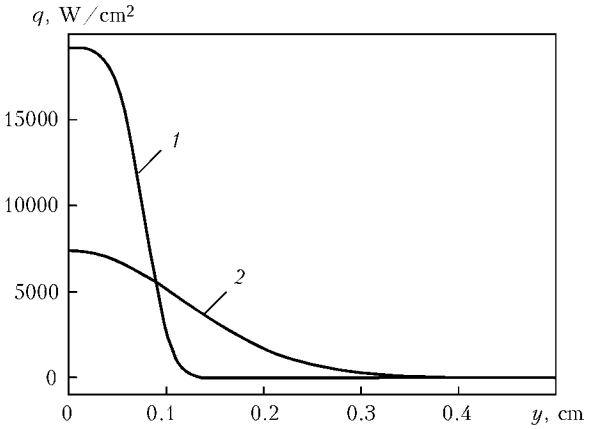

Figure 6. Distribution of specific heat flows of the laser (*1*) and plasma (*2*) heat sources on the plate surface (r_L = = 0.1 cm, efficiency = 0.32, P_L = 1250 W, r_P = 0.25 cm, efficiency = 0.5, P_P = 1300 W)

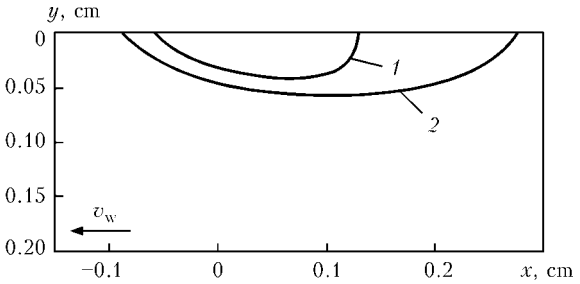

Figure 7. Shape of the penetration zone in axial section of the weld (T = 1480 °C) under the effect of the laser (*1*) and combined laser-microplasma (*2*) heat sources

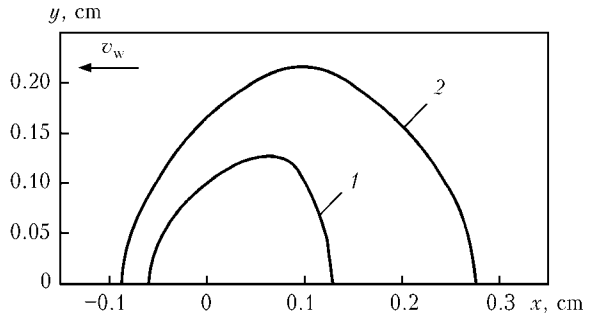

Figure 8. Shape of the penetration zone on the plate surface under the effect of the laser (*1*) and combined laser-microplasma (*2*) heat sources

said heat sources on the surface of the material treated is shown in Figure 6, where P_P is the plasma source power.

Figures 7 and 8 show the shapes of the penetration zones of the base metal in a longitudinal section and on the surface of the plate treated, respectively.

As indicated by the calculation data, under the effect of combined laser-microplasma heating

Table 2. Effect of the thermal power introduced into the plate on penetration parameters at v_w = 1.67 cm/s and r_L = 0.1 cm

P_L, W	H, cm	B, cm	T_{max}, °C	V_x, cm/s	V_y, cm/s
200	0.0165	0.1094	1886	12.8	3.7
300	0.0339	0.1872	2518	38.2	12.6
400	0.0418	0.2526	2880	51.3	16.5
500	0.0455	0.2826	2920	54.9	17.3
600	0.0475	0.3022	2944	57.1	17.9

Table 3. Effect of the heat spot radius on penetration at P_L = = 400 W and v_w = 1.67 cm/s

r_L, cm	H, cm	B, cm	T_{max}, °C	V_x, cm/s	V_y, cm/s
0.10	0.0418	0.2526	2880.65	51.30	16.50
0.12	0.0396	0.2338	2589.32	39.24	12.74
0.14	0.0346	0.2150	2274.98	27.45	8.42
0.16	0.0276	0.1920	2002.03	17.19	4.85
0.18	0.0171	0.1550	1748.69	7.62	2.04
0.20	0.0042	0.0712	1512.43	0	0

Table 4. Effect of the heat source speed on penetration at P_L = = 400 W and r_L = 0.1 cm

v_w, cm/s	H, cm	B, cm	T_{max}, °C	V_x, cm/s	V_y, cm/s
1	0.051	0.3220	2890	51.6	16.7
2	0.039	0.2320	2872	50.4	16.2
3	0.032	0.1860	2742	45.2	14.5
5	0.023	0.1480	2453	30.7	10.7
10	0.010	0.1040	1956	9.8	2.0

the width of the penetration zone increases 1.5 times, compared to laser heating. Due to this, the combined laser-microplasma treatment can provide a substantially larger size of the deposited bead.

Conclusion

With the laser heat source affecting the plate surface an intensive (~50 cm/s) sub-surface flow of the melt forms in the molten zone. This flow is caused by the dominant action of the thermocapillary force, which is generated due to a high temperature gradient (~7000 °C/cm) on the free surface of the metal pool. The flow, which is directed from the axial part of the pool towards the melting front, intensifies the energy transfer from the overheated paraxial part of the pool to its peripheral region, and favours increase in width of the molten zone. The effect of convective stirring of the pool to the penetration depth is much lower because of the mostly sub-surface flow of the melt. Application of the combined laser-microplasma energy source for cladding using powder materials (including bulk materials) allows increasing width of the deposited bead compared to laser cladding, and raising the productivity of the cladding process.

1. Duley, U. (1986) *Laser processing and analysis of materials*. Moscow: Mir.
2. Arutyunyan, R.V., Baranov, V.Yu., Bolshov, L.A. et al. (1989) *Effect of laser radiation on materials*. Moscow: Nauka.
3. Vedenov, A.A., Gladush, G.G. (1985) *Physical processes in laser treatment of materials*. Moscow: Energoatomizdat.
4. Rykalin, N.N. (1951) *Calculation of thermal processes in welding*. Moscow: Mashgiz.
5. Knight, Ch.J. (1979) Theoretical modeling of rapid surface vaporization with back pressure. *AIAA J.*, 17(**5**), 519–523.
6. Demchenko, V.F., Krivtsun, I.V., Semyonov, I.L. et al. (2009) Mathematical modelling of the processes of heating and convective evaporation of metals under the effect of pulse laser radiation. In: *Proc. of 4th Int. Conf. on Beam Technologies and Laser Application* (Saint-Petersburg, 23–25 Sept. 2009). Saint-Petersburg: StPPU, 81–85.
7. Lyashko, I.I., Demchenko, V.F., Vakulenko, S.A. (1981) Variant of the method for splitting of equations of dynamics of the viscous incompressible fluid on the Lagrangian–Eulerian networks. *Doklady AN USSR*. Series A, 43–47.
8. Demchenko, V.F., Lesnoj, A.B. (2000) Lagrangian–Eulerian method of numerical solution of multidimensional problems of convective diffusion. *Doklady NAN Ukrainu*, **11**, 71–75.

Received 24.01.2013

WELDABILITY OF SPARSELY-ALLOYED STEELS 06GBD AND 06G2B

V.D. POZNYAKOV, S.L. ZHDANOV, A.A. MAKSIMENKO, A.G. SINEOK and **A.M. GERASIMENKO**
E.O. Paton Electric Welding Institute, NASU
11 Bozhenko Str., 03680, Kiev, Ukraine. E-mail: office@paton.kiev.ua

The aim of this work was the investigation of weldability of sparsely-alloyed niobium-containing steels 06GBD and 06G2B with the yield strength of more than 390 MPa, and also evaluation of properties of their welded joints at different technological welding processes as-applied to manufacture of unique building structures (bridges, tanks of 50,000–70,000 m^3 capacity, blast furnaces). Basing on the analysis of thermokinetic diagram obtained using rapid-response dilatometer and results of tests of model thermocycled specimens the correlation at the cooling rates $w_{6/5}$ in the range of 1.3–70 °C/s between structure of metal of heat-affected zone of welded joints and their properties was established. Considering the results of tests on delayed fracture of welded joints, the range of admitted energy inputs of welding was established providing their high cold resistance and resistance to cold crack formation. The offered welding conditions and welding consumables found their application in manufacture of steels 06GBD and 06G2B welded structures of oil tanks of large capacity and bridges. 8 Ref., 5 Tables, 8 Figures.

Keywords: *sparsely-alloyed steel, weldability, thermokinetic diagram, cooling rate, structure, simulated metal of heat-affected zone, cold cracks, technological sample*

The rational application of modern sparsely-alloyed materials with high values of mechanical properties (more than 390 MPa) allows effective decreasing of metal intensity and increasing of reliability and service life of metal structures for machine building and construction. The used steels contain limited amount (up to 0.09 wt.%) of carbon, manganese and niobium. To achieve the required complex of their mechanical properties, both heat and also heat-mechanical treatment (controlled rolling) are used. In special cases, to increase corrosion resistance the copper is added into these steels in the amount of up to 0.3 wt.%.

The indisputable advantages of sparsely-alloyed steels, as compared to those known materials as steels 09G2S and 10KhSND, are their high cold resistance and good weldability [1–3]. Meantime it is known that in the process of manufacture of welded metal structures the resistance of welded joints to delayed and brittle fractures can decrease.

The aim of this work was the detailed evaluation of weldability of sparsely-alloyed niobium-contained steels 06GBD and 06G2B with yield strength of $\sigma_y \geq 390$ MPa and also investigation of properties of their welded joints at different technological processes as-applied to manufacture of unique building structures of different purpose (bridges, tanks of 50,000–70,000 m^3 capacity, blast furnaces).

The steels of grades 06GBD and 06G2B (TU U 27.1-05416923-085:2006) were developed by the Mariupol Research Institute of Structural Materials «Prometey» and are supplied of 8–50 mm thickness. By variation of modes of heat treatment and alloying, the obtaining of four levels of strength properties $\sigma_y \geq 355$, 390, 440 and 490 MPa [4–6] is controlled. The requirements to chemical composition and properties according to the technical specifications are given in Tables 1 and 2. During present investigations the steels 06GBD (class of strength C390) and 06G2B (class of strength C440) were used. The investigations carried out earlier at the E.O. Paton Electric Welding Institute prove the sufficiently high resistance of these steels to laminar and laminar-brittle fracture in the direction of the axis z [4]. According to carbon equivalent they can be referred to the class of a good weldability (C_{eq} = 0.33–0.43). However this characteristic is approximate, therefore, the additional investigations were required for final decision about fitness of these steels to welding.

To study structural transformations in HAZ metal of steel 06GBD under the effect of thermal cycles of welding the quick-response dilatometer of complex Gleeble-3800 [7] was used, where cylindrical specimens of 6 mm diameter and 86 mm length were heated up to the temperature of 1200 °C at the speed of 150 °C/s and then

Table 1. Chemical composition of steels 06GBD and 06G2B, wt.%, not more than

Grade of steel, strength class	C	Si	Mn	Nb	V
06GBD, C355	0.04–0.08	0.15–0.35	0.9–1.2	0.01–0.03	0.02–0.04
06GBD, C390	0.04–0.08	0.25–0.50	1.1–1.4	0.01–0.03	0.02–0.05
06G2B, C440	0.04–0.08	0.25–0.50	1.3–1.6	0.03–0.05	0.03–0.07
06G2B, C490	0.05–0.09	0.25–0.50	1.5–1.7	0.03–0.05	0.04–0.07

Table 1 (cont.)

Grade of steel, strength class	Mo	Ti	Cr	Ni	Cu	S	P
06GBD, C355	0.05	0.02	0.2	0.3	0.3	0.01	0.025
06GBD, C390	0.08	0.02	0.2	0.3	0.3	0.01	0.025
06G2B, C440	0.10	0.02	0.2	0.3	0.3	0.01	0.025
06G2B, C490	0.12	0.025	0.2	0.3	0.3	0.01	0.025

Table 2. Mechanical properties of steels 06GBD and 06G2B

Grade of steel, strength class	σ_y, MPa	σ_t, MPa	δ_5, %	ψ, %	ψ_z, %	KCV, J/cm^2, at T_{test}, °C		
						–40	–60	–70
	Not less than							
06GBD, C355	355	450	22	55	25	98	78	59
06GBD, C390	390	490	22	55	25	98	78	59
06G2B, C440	440	540	22	55	25	98	78	59
06G2B, C490	490	590	20	55	25	98	78	59

cooled in the temperature range of 600–500 °C at different rates (1.3–70 °C/s).

The analysis of thermokinetic diagram (Figure 1) and microstructures of simulated HAZ metal, cooled at different rates, proves that in the whole investigated range (1.3–70 °C/s) the ferrite-pearlite structure at the overheat area is observed (Figure 2). At $w_{6/5} \geq 27$ °C/s the precipitations of MAC-phase appear, the percentage correlation of which is increased from 1.20 to 5.72 % at the increase of cooling rate to $w_{6/5}$ = = 70 °C/s. Here both its hardness is increased from HV 140 to HV 171 as well as number of grains from 5 to 8–9.

In spite of similarity of structures (Figure 2, *b–d*) some distinctions on the shape of pearlite component are observed in them. Thus, at $w_{6/5}$ = = 10.1 °C/s thin pearlite plates (Figure 2, *b*) are observed in the structure along the boundaries of ferrite grains. With increase of cooling rate up to $w_{6/5}$ = 27 °C/s the plates of pearlite are refined and multiplied. Besides, separate uniaxial grains of pearlite appear (Figure 2, *c*). At the maximum cooling rate in the investigated range $w_{6/5}$ = 70 °C/s the structure is enlarged, the large pearlite colonies are appeared along with the plate precipitations of pearlite along the boundaries of pearlite grains (Figure 2, *d*).

The evaluation of mechanical properties and resistance of welded joints to brittle fracture were carried out according to the methods described in [8]. The tensile and bending tests were applied to the specimens of the sizes of 150 × 12 × 12 mm, which were cut out of the semi-products of steel 06GBD and subjected to the effect of thermal

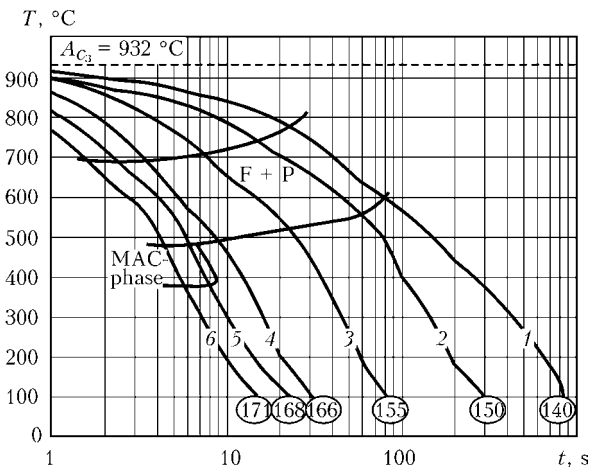

Figure 1. Thermokinetic diagram of transformation of austenite for steel 06GBD at different cooling rate $w_{6/5}$ = 1.3 (*1*), 3.1 (*2*), 10.1 (*3*), 27 (*4*), 56.7 (*5*) and 70 (*6*) °C/s

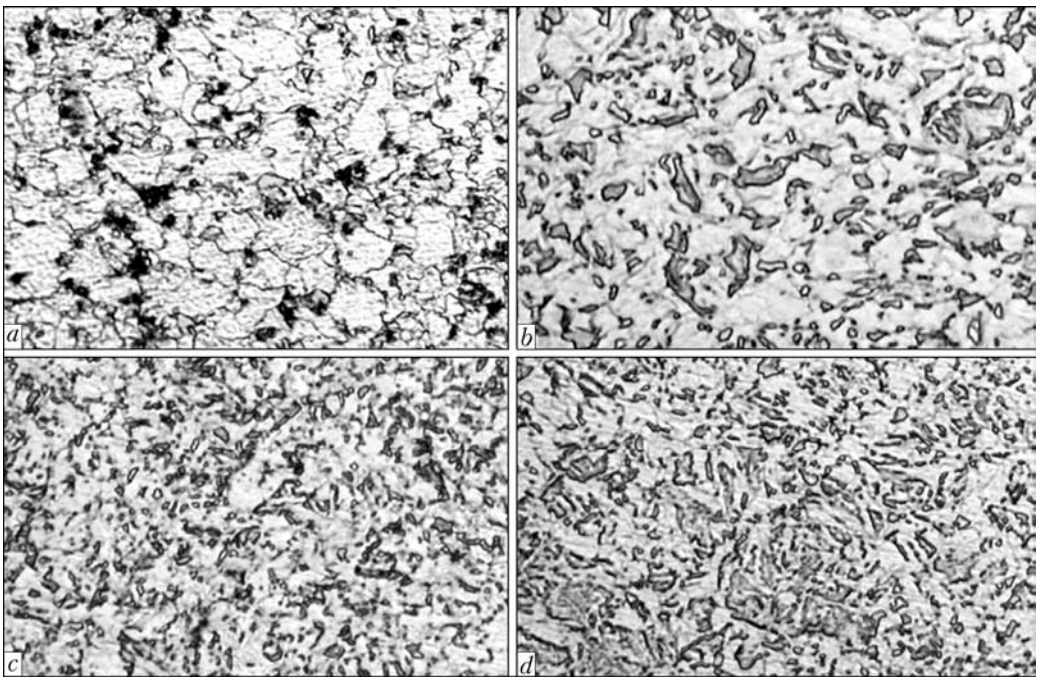

Figure 2. Microstructures (×500) of steel 06GBD specimens at $w_{6/5}$ = 1.3 (*a*), 10.1 (*b*), 27 (*c*) and 70 (*d*) °C/s

cycles of welding (heating up to 1250 °C at the speed of 150 °C/s and cooling at different rates within the range of 1.5–25 °C/s). The chemical composition of investigated rolled metal of different thicknesses δ is given in Table 3, and results of mechanical tests of the simulated HAZ metal of the investigated steel are given in Figures 3–5.

The analysis of data obtained as a result of rupture tests of specimens (see Table 3 and Figure 3, *a*, *b*) showed that with decrease of cooling rate the values σ_y and σ_t characterizing strength of metal are monotonously decreased. Values of yield strength are most intensively decreased. According to the results of mechanical tests, in the range $w_{6/5}$ = 1.5–3 °C/s the weakening of HAZ metal occurs, characterized by 25–60 MPa decrease of the values of yield strength of HAZ metal as compared to the initial data (Figure 3, *a*). At such cooling rates the HAZ metal has σ_y values lower than values established in the standard documents on steel. Meantime the tensile strength of HAZ metal in the whole investigated range of cooling rates did not decrease lower than values specified by technical specifications on steel.

The ductile properties of HAZ metal are at the high level. In spite of some negligible decrease of values of elongation with increase of cooling rate they exceed 22 % (see Figure 4, *a*). At the same time the values respectively to the reduction in area practically did not change (Figure 4, *b*).

With the decrease of cooling rate the impact toughness of HAZ metal is decreased independently of test temperature. However at 20 °C the value $KCV_{+20} \geq 170$ J/cm^2 (see Figure 5, *a*) remains considerably high in the whole range. The negative influence of cooling rate was revealed during the tests of specimens under the conditions of lowered temperatures. If for the thicknesses of 12 and 14 mm the higher values are characteristic at $w_{6/5} \geq 10$ °C/s (Figure 5, *b*), then at $w_{6/5}$ = 1.5–10 °C/s the sharp decrease of values of impact toughness (KCV_{-40} = 18–24 J/cm^2) is observed.

It was established that the required complex of mechanical properties of HAZ metal can be provided in welding at limited heat inputs when

Table 3. Chemical composition of investigated rolled metal of steel 06GBD, wt.%

δ, mm	C	Mn	Si	P	S	Cr	Mo	Cu	Nb	V
12	0.066	1.20	0.20	0.008	0.006	0.14	0.13	0.22	0.019	0.04
14	0.069	1.22	0.18	0.009	0.008	0.13	0.12	0.21	0.021	0.05
20	0.066	1.23	0.19	0.010	0.009	0.22	0.13	0.22	0.021	0.05
32	0.064	1.24	0.17	0.011	0.011	0.23	0.10	0.20	0.020	0.05
40	0.070	1.22	0.17	0.018	0.010	0.21	0.12	0.21	0.019	0.05

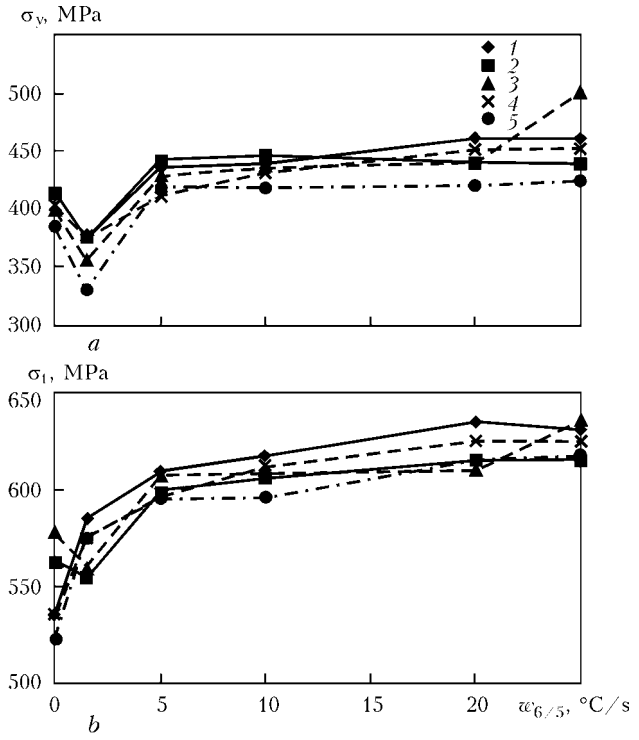

Figure 3. Dependence of yield strength (*a*) and tensile strength (*b*) of steel 06GBD on cooling rate of HAZ metal at different thickness δ = 12 (*1*), 14 (*2*), 20 (*3*), 32 (*4*) and 40 (*5*) mm

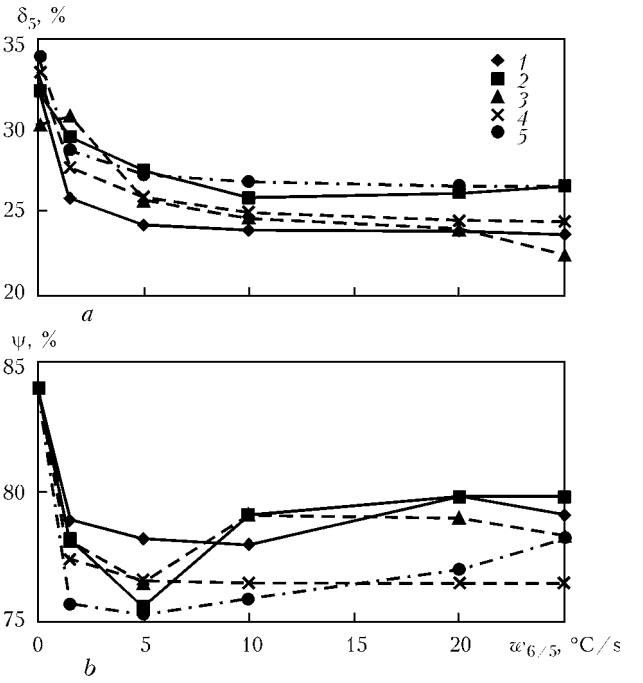

Figure 4. Dependence of relative values of elongation (*a*) and reduction in area (*b*) of HAZ metal of steel 06GBD on cooling rate of metal of different thickness δ = 12 (*1*), 14 (*2*), 20 (*3*), 32 (*4*) and 40 (*5*) mm

minimal cooling rates of welded joints do not drop lower than 10 °C/s.

The resistance of welded joints to formation of cold cracks was evaluated according to the results of tests of Implant and Tekken specimens and technological butt samples «rigid contour welding». To conduct tests according to the Implant method the cylindrical specimens-inserts of 6 mm diameter with screw notch were used manufactured of roll metal of steels 06GBD and 06G2B of different thickness. The cooling rate of HAZ metal of the Implant specimens (in the range of 5–80 °C/s) was adjusted changing the energy input of welding and elongation of binding beads. The content of diffusive hydrogen $[H]_{diff}$ in the metal deposited using electrodes UONI-13/55 (during determination by chromatographic method) was measured from 5 to 15 ml/100 g. The axial static loading of specimens-inserts was applied after welding and their cooling down to the temperatures of 100–150 °C. The maximal tensile stress from the outer loading σ_{cr}, at which no cracks are formed during 20 h in Implant specimens, was accepted as the criterion for resistance of HAZ metal to delayed fracture.

As a results, it was established that σ_{cr} of steel 06G2B Implant specimens 30 mm thick at the cooling rates, characteristic for welding modes without preheating ($w_{6/5} \leq$ 25 °C/s), and $[H]_{diff} \leq 10$ ml/100 g are at the high level ($\sigma_{cr} \geq \geq 0.8\sigma_y$ of the base metal).

This proves that probability of cold crack formation in HAZ metal of welded joints of the investigated steels is low. However, when the welding modes are not favorable, the cold cracks

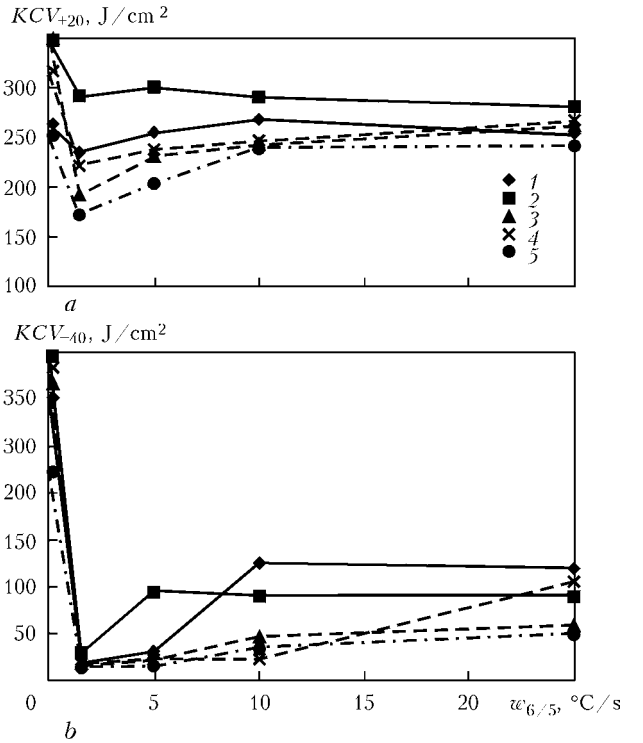

Figure 5. Dependence of impact toughness *KCV* for T_{test} = = +20 (*a*) and –40 (*b*) °C of steel 06GBD HAZ metal on cooling rate at different thickness of rolled metal δ = 12 (*1*), 14 (*2*), 20 (*3*), 32 (*4*) and 40 (*5*) mm

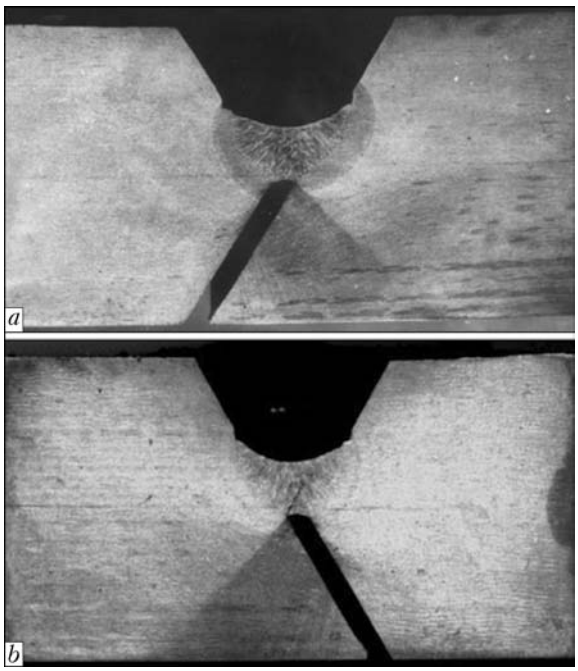

Figure 6. Sections of Tekken samples produced using electrodes UONI-13/55 at $[H]_{diff}$ = 10 (*a*) and 15 (*b*) ml/100 g

can be formed in the weld metal. Thus, at the increase of cooling rate of welded joints up to 60–80 °C/s, characteristic of welding under the conditions of low climatic temperatures, and increase of $[H]_{diff}$ content up to 15 ml/100 g it is possible to prevent the cracks formation having applied the preheating up to 60–90 °C. It is comparable with the data obtained while testing the Tekken samples of steel 06G2B.

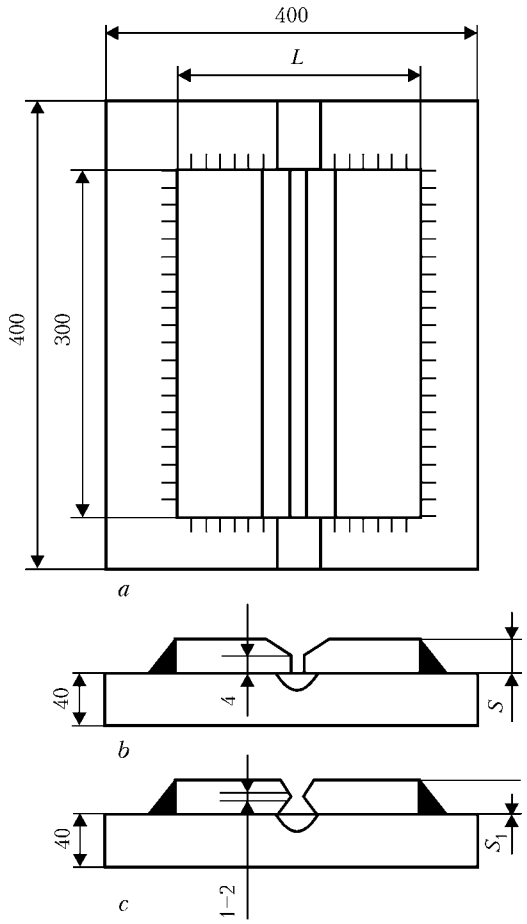

Figure 7. Diagrams of rigid butt joints for investigation of resistance to cold crack formation (technological sample «rigid contour welding»)

It was established that at content of diffusive hydrogen in weld metal not exceeding 10 ml/100 g, the welded joints of steel 06G2B have a good resistance to delayed fracture. Cracks in the Tekken samples are absent (Figure 6, *a*). At higher concentrations of $[H]_{diff}$ the probability of cold cracks formation in welded joints is extremely high, which is evidenced of the test results of Tekken samples, produced using electrodes UONI-13/55 with high content of diffusive hydrogen ($[H]_{diff} \approx$ 15 ml/100 g). Under such welding conditions the cracks in the samples are originated already directly after completion of producing the root bead (during 3–5 min after completion of welding). The process of crack propagation occurs also intensively. Within 5–10 min after formation it was detected at the surface of weld in its end part, and within 2 h after completion of welding it affected the whole its section. The crack originated and propagated exclusively along the weld metal (Figure 6, *b*). It is indirectly proved by the earlier obtained results of tests of Implant specimens, which evidence of high resistance to delayed fracture of HAZ metal of steel 06G2B.

The resistance of multilayer welded joints of steel 06GBD to cold cracks formation was evaluated according to the results of tests of technological samples «rigid contour welding» (Figure 7, *a*). The sample represents a massive plate of 400 × 400 × 40 mm size, on which the butt joints of thickness S = 12, 14 and 20 mm with V- (Figure 7, *b*) and X-shaped edges preparation (Figure 7, *c*) for the thicknesses S_1 = 12, 14, 20, 32 and 40 mm, were mounted and welded-on around the whole perimeter. In the samples the obligatory gap of 1.5–2.0 mm is provided, which serves as a concentrator of stresses in welding of joints with 2–4 mm root face to provide technological lack of penetration.

The samples of the width L = 300, 200 and 100 mm were welded at different temperatures and welding modes, meantime controlling the thermal effect using heat source, namely, rate and time of cooling. The rigidity of technological sample was controlled changing the width of plates to be welded.

As the criterion for tendency to delayed fracture the presence/absence of cracks in weld and HAZ metal is served.

The mechanized welding of rigid butt joints of the specimens of steel 06GBD of 100 mm width and thickness of 12, 14 and 20 mm with V- and X-shaped edge preparation were performed in the shielding gas mixture of Ar + 18 % CO_2 using wire Sv-08G2S of 1.2 mm diameter under the conditions of I_w = 180–200 A, U_a = 24–26 V and v_w = 10–12 m/h. The automatic welding of rigid butt joints of specimens 20, 32 and 40 mm thick with X-shaped edges preparation was performed by wire Sv-10NMA of 4 mm diameter under the flux AN-22 at I_w = 500–550 A, U_a = 32–34 V and v_w = 22–26 m/h (root beads). The same conditions were applied also for the next welding of specimens 20 mm thick. The welded joints of steels of 32 and 40 mm thickness were further welded using the more powerful conditions: I_w = = 550–600 A, U_a = 32–34 V, v_w = 20–22 m/h and I_w = 700–750 A, U_a = 32–34 V, v_w = 24–26 m/h, respectively.

The process of cracks initiation and propagation in the samples was controlled by the method of acoustic emission using the device IKD 128. For this purpose the special sensors were mounted on the specimen directly after welding. After welding all samples were subjected to holding for not less than 48 h. Then, they were inspected visually (using magnifying glass with five-fold magnification) to determine the presence/absence of cracks at the surface of welded joint. At the final stage of testing the samples «rigid contour welding», the macrosections were manufactured and examined under the microscope Neophot-2 at ten-fold magnification.

The obtained results evidence also of sufficiently high resistance of welded joints of steel 06GBD to delayed fracture. Even at maximal rigidity of samples (the specimens of 100 mm width) the cold cracks were not revealed in macrosections in mechanized welding in mixture of gases, as well as in automatic submerged arc welding (Figure 8).

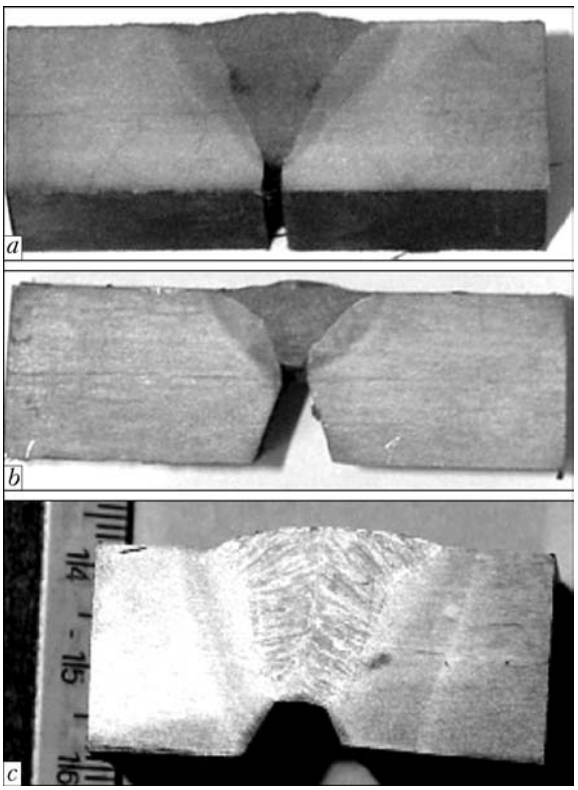

Figure 8. Typical macrosections manufactured of technological samples «rigid contour welding» of steel 06GBD: *a*, *b* — mechanized welding in shielding gases; respectively, V- and X-shaped preparation of edges 12 mm thick; *c* — automatic submerged arc welding; X-shaped preparation of edges 20 mm thick

Basing on the carried out tests of effect of the thermal cycles of welding on the structure and properties of HAZ metal of welded joints of steel 06GBD, the rates of cooling in the temperature range of 600–500 °C were established, and modes of automatic submerged arc welding were calculated (Table 4).

The investigations, carried out at the E.O. Paton Electric Welding Institute and shop conditions, showed that in welding of steel 06GBD the producing of joints with mechanical properties equal to those of base metal is provided by the welding consumables produced by the industry: wire Sv-08G2S in combination with shield-

Table 4. Recommended modes of automatic welding of butt joints with edge preparation of steel 06GBD of strength class C390 under the flux using wire of solid section of 4 mm diameter, and relative energy inputs and cooling rates of weld and HAZ metal

δ, mm	Welding mode			$q_{h.i}$, J/cm	$w_{6/5}$, °C/s, at initial temperature of welded joint, °C			
	I_w, A	U_a, V	v_w, m/h (cm/s)		+5	+20	+120	+160
40	700–750	30–34	25 (0.7)	24,600–29,870	25.6–21.4	24.5–20.2	15.7–12.8	12.7–10.2
32	550–600	30–34	20 (0.555)	24,380–30,133	22.4–20.5	21.5–19.7	14.0–12.0	11.5–9.6
20	550–600	30–34	20–22 (0.555–0.611)	22,141–30,133	24.5–14.4	22.8–12.9	12.8–6.1	9.01–4.20
14	450–500	30–32	26 (0.722)	15,325–18,166	27.0–18.6	25.1–16.2	11.8–7.6	8.1–5.3
12	450–500	30–32	28 (0.777)	14,241–16,879	21.5–14.3	19.4–12.8	8.9–5.7	5.9–3.8

Table 5. Mechanical properties of welded joints of steel 06GBD of the strength class C390 produced using automatic arc welding under the flux AN-47 and wire Sv-10NMA of 4 mm diameter

δ, mm	Shape of edge preparation	σ_t, MPa	α_{bend}, deg	*KCU*, J/cm^2				*KCV*, J/cm^2				HV_{max}
				Weld center		HAZ		Weld center		HAZ		
				+20	−40	+20	−40	+20	−40	+20	−40	
40	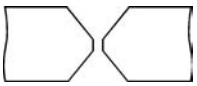	528	180	183.5	93	330	330	142	64	305	300	208
32	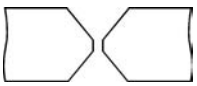	534	180	160	101	334	315	146	56	300	298	208
20	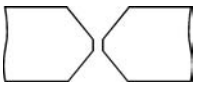	550	180	196	102	347	344	122	40	No data	No data	208
14		566	180	194	95	326	314	157	43	306	300	208
12		582	180	166	110	290	289	142	55	298	296	201
12		560	180	214	91	330	322	123	41	305	295	192

ing gas mixture Ar + 18 % CO_2, and also wire Sv-10NMA in combination with the flux AN-47. The typical values of mechanical properties of welded joints of the steel 06GBD of different thickness are given in Table 5. It should be noted that welding consumables mentioned above provide required level of mechanical properties also on steel 06G2B of the strength class C440.

The recommended welding modes and welding consumables found application in manufacture of critical welded metal structures of tanks of steel 06G2B of the high capacity for oil and oil products, and also in manufacture of bridge metal structures of steel 06GBD. The experience of service of these structures of sparsely-alloyed steels 06G2B in Ukraine and Belarus under the normal climatic conditions proves the high reliability and correct application of welding technologies.

1. Mikhoduj, L.I., Kirian, V.I., Poznyakov, V.D. et al. (2003) Sparsely-alloyed high-strength steels for welded structures. *The Paton Welding J.*, **5**, 34–37.
2. Grabin, V.F., Golovko, V.V., Kostin, V.A. (2004) Morphological peculiarities of microstructure of weld metal from low-alloy steels with ultralow content of carbon. *Ibid.*, **7**, 15–20.
3. Goldshtejn, M.I., Gladshtejn, L.I., Golovanenko, S.A. (1977) Carbonitride strengthening of low-alloy steels. *Stal*, **9**, 833–837.
4. Poznyakov, V.D., Barvinko, A.Yu., Barvinko, Yu.P. et al. (2012) Cold resistance and lamellar fracture resistance of welded joints on steel 06GB-390. *The Paton Welding J.*, **3**, 35–39.
5. Ivashchenko, G.A., Demchenko, Yu.V. (1990) Principles of choice of chemical composition of higher strength and cold resistance steels for welded structures. In: *Advanced methods for producing of structural steel and cast iron welded joints*. Kiev: PWI, 110–116.
6. Pilyushenko, V.L. (1987) Influence of microalloying on service characteristics of steels. *Stal*, **10**, 24–26.
7. Grigorenko, G.M., Kostin, V.A., Orlovsky, V.Yu. (2008) Current capabilities of simulation of austenite transformations in low-alloyed steel welds. *The Paton Welding J.*, **3**, 22–24.
8. Sarzhevsky, V.A., Sazonov, V.Ya. (1981) Unit for simulation of welding thermal cycles on the base of MSR-75 machine. *Avtomatich. Svarka*, **5**, 69–70.

Received 07.02.2013

CRACKS IN WELDED JOINTS OF LARGE DIAMETER PIPES AND MEASURES FOR THEIR PREVENTION

A.A. RYBAKOV, T.N. FILIPCHUK and **L.V. GONCHARENKO**
E.O. Paton Electric Welding Institute, NASU
11 Bozhenko Str., 03680, Kiev, Ukraine. E-mail: office@paton.kiev.ua

Considered are the cases of failure of main gas pipelines, including after long-term operation, caused by presence of crack-like defects in the welded joints of pipes which were formed at their manufacture. Analysis of main reasons of appearance of such defects in weld metal and heat-affected zone is provided considering the peculiarities of technological processes of manufacture and welding of pipes. It is shown that cracks can have different orientation and origin, being formed immediately in the process of welding or at later stages of manufacture during performance of adjacent operations, for example, pipe expanding. Their formation is caused by series of technological reasons, for example, movement of welded edges of pipe in process of assembly, incorrect selection of consumables (welding wire, flux), local change of weld metal chemical composition or its structural inhomogeniety due to entering of exogenous particles in weld, increased flux humidity etc. Measures for prevention of appearance of crack-like defects in welded joints of pipes are described. Research results can be used in tube-welding production for improvement of welding technology and control of tubular products, as well as inspection of pipelines in process of their operation. 9 Ref., 1 Table, 9 Figures.

Keywords: *arc welding, main oil-gas pipelines, welded joints, failure, cracks, reasons of formation, prevention*

Main reasons of accidents of linear part of main oil-gas pipelines, as shown by statistical data [1, 2], are such called constructional (formed during construction-assembly works) and service (mainly, corrosion, including stress-corrosion) defects. It is assumed that failures of pipelines caused by construction reasons are the most often in the initial period of their operation [2]. In contrast, increase of pipeline operation significantly raises amount of failures due to corrosion damages.

At the same time, as study of series of failures on main pipeline indicates, their failure, including after long-term operation, can be related with defects formed in the process of pipe manufacture, in particular, with presence of crack-like defects in the welded joints.

Thus, main zone of failure at accident on gas pipeline of 820 mm diameter, the consequences of which are shown in Figure 1, became an extended crack in a mill longitudinal weld of the pipe. Crack length made 850 mm, depth was 4–6 mm (Figure 2). Defect propagation lied in the limits of outside weld along the whole length. Crack surface is damaged by surface corrosion, whereas, out of defect, i.e. zone of failure devel-

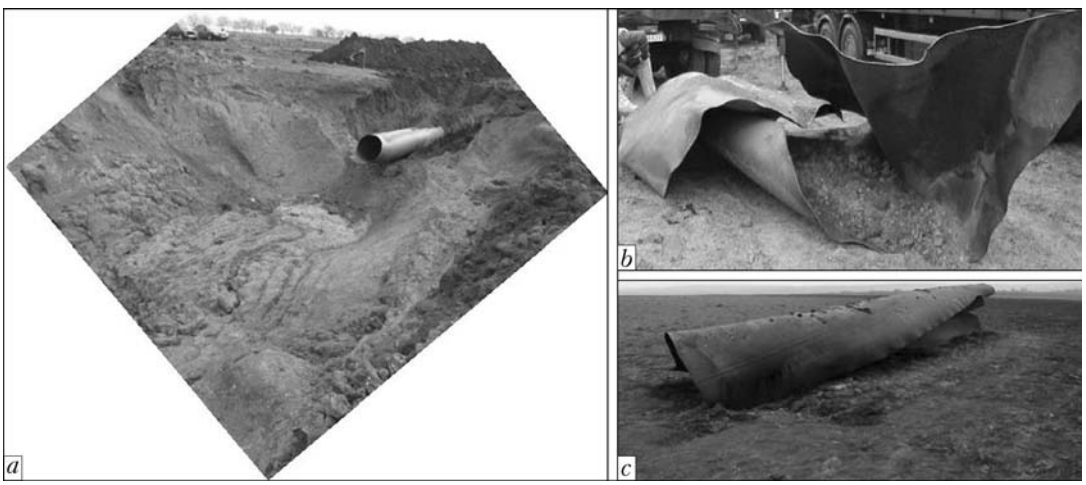

Figure 1. Pipeline failure (*a*), and fragments of failed pipes (*b*, *c*)

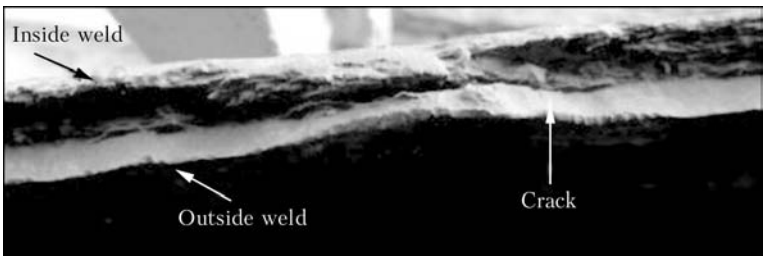

Figure 2. Crack in outside longitudinal weld on failed pipe of 820 mm diameter

opment (final break), there are no fracture corrosion damages, that is additional confirmation of crack formation during the pipe manufacture. Failure of pipeline took place after 35 years of its operation at 4.5 MPa pressure (operating pressure of the pipeline was 5.4 MPa). The pipes are manufactured from 17GS steel of 9 mm thickness.

Defect, classified as «metal loss», was found in the welded joint of main gas pipeline of 1420 mm diameter, constructed in 1983 from pipes of 15.7 mm wall thickness (X70 type steel) during in-tube diagnostics. Through crack in which transported gas leaked out (Figure 3) was detected in longitudinal weld of the pipe at test probing. Gas leakage started at pressure more than 3 MPa, the crack was closed at lower pressure. Additional non-destructive testing of this weld detected one more crack which reached the surface of only inside weld. Fractographic examinations of surface of these defects allow stating that they were also formed in the process of pipe manufacture.

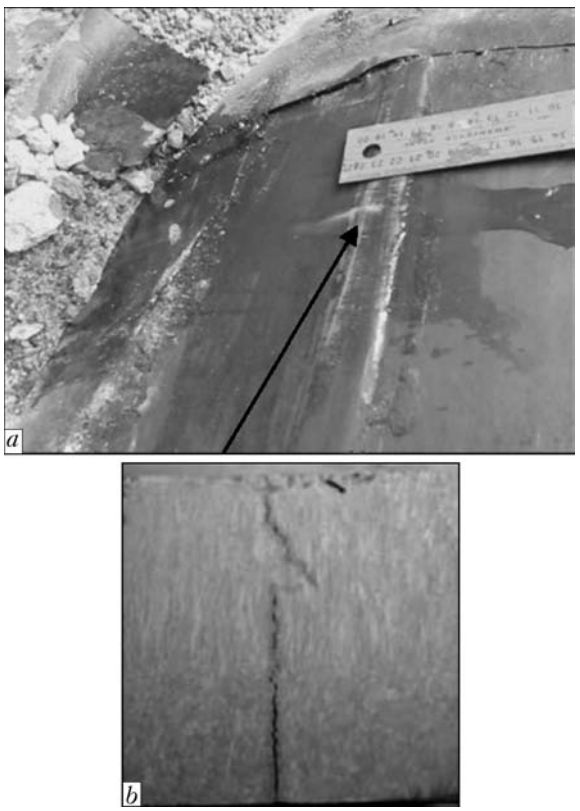

Figure 3. Through transverse crack in weld metal of pipe of 1420 mm diameter: *a* — appearance of pipe with crack in weld from side of external surface; *b* — marcosection of weld metal with crack (arrow indicates gas outflow from crack in longitudinal weld)

Failure of series of pipes of 1220 × 19 mm size from steel K60 (Figure 4) took place at hydraulic testing of newly constructed oil pipeline. At that, 12.4 MPa pressure was registered (mill testing pressure was 13.3 MPa). The pipes fractured along the near-weld zone of longitudinal mill weld on length, approximately, 1.6 m. Examination of fracture pattern in zone of failure on scanning microscope allowed determining that it propagated from external surface of the pipe to internal one, and, mainly, by toughness mechanism. It was determined that lamellar tearing along the HAZ of longitudinal weld became the reason of pipe failures (Figure 4, *b*).

Thus, described cases of pipeline failure were caused by presence in the welded joints of crack-like defects which had been already formed at stage of manufacture. Analysis of conditions and reasons of appearance of indicated defects in the welded joints of pipes is given below considering applied technological processes of their manufacture (in this case longitudinally welded pipes of

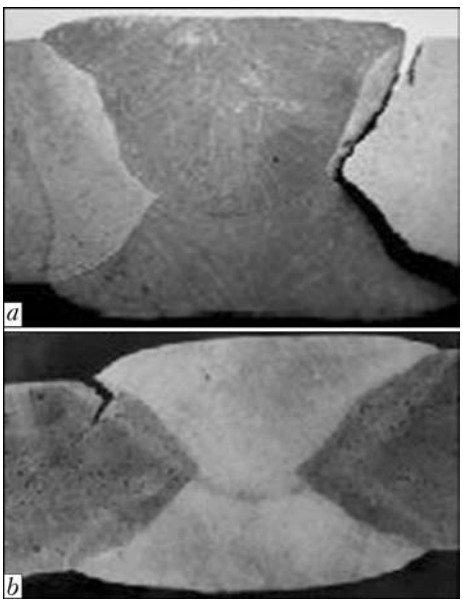

Figure 4. Failure in the near-weld zone of 1220 mm diameter pipe: *a* — failure character; *b* — lamellar tearing in HAZ metal

large diameter made using submerged arc welding are analyzed). Studied defects were conditionally joined in separate groups based on general characteristics and main reasons of their formation for convenient representation of material.

Longitudinal solidification cracks. Cases of formation of this type of cracks, similar to crack which became a reason of described above failure of 820 mm diameter gas pipeline, have been already known at the early stage of development of large diameter welded pipe production [3]. They mostly appeared in application of outdated two-layer welding technology. Using this technology, longitudinal weld of longitudinally welded pipe was made successively in two layers from external and internal surfaces of the pipe. At that, the first one, as a rule external layer was performed in assembly-welding mill in a process of assembly of edges of tubular billet that under excessive deformations of these edges provides the conditions for formation of hot solidification cracks. In 1960s longitudinally welded pipes of up to 1220 mm diameter were manufactured applying such a welding technology and in great number used for construction of main pipelines. Figure 5 shows longitudinal cracks by example of welds of 820 mm diameter pipes from 14KhGS steel. Coarse columnar crystallites can be seen on the surface of crack that verify their hot origin.

Three-layer welding technology was developed and realized at the beginning of 1970s in tube-welding production, firstly for spirally-welded pipes and then for longitudinally welded pipes of large diameter, during which the edges of tubular billets in the moment of their matching are welded in shielding gas by assembly (technological) weld [4]. The latter then completely re-welded by external and internal working layer made under the flux. Such a technology allowed eliminating formation of longitudinal cracks in welds related with movement of welded edges.

It should be noted that current normative documents provide for obligatory application of pipes being welded using three-layer technology with preliminary edge joining by technological weld in construction of critical oil-gas pipelines. In our opinion, this requirement is to be stipulated in contracts for pipe supplying. As for old pipelines, the possibility of presence of such defects in them is not eliminated, including due to absence of sufficient means of non-destructive testing of pipe welded joints in period of their construction.

Longitudinal crack-like defects related with shrinkage porosity in welds. Defects of this type (Figure 6) are formed in submerged multiarc welding with increased speed due to, as indicated

Figure 5. Longitudinal crack in outside weld of pipe from 14KhGS steel caused mainly by force factor: *a* — appearance from side of outside weld; *b* — fracture surface

in work [5], isolation of tail part of the weld pool and solidification of remaining portions of liquid metal under conditions of complicated shrinkage. Depth of shrinkage porosity (shown by arrow in Figure 6, *a*) is usually not significant (0.3–0.4 mm). However, cracks, which sometimes accompany porosity, can have large depth. Such cracks are located along the weld center and have, as in previous case, intercrystalline character. Work [5] shows that possibility of formation of shrinkage porosity rises with in-

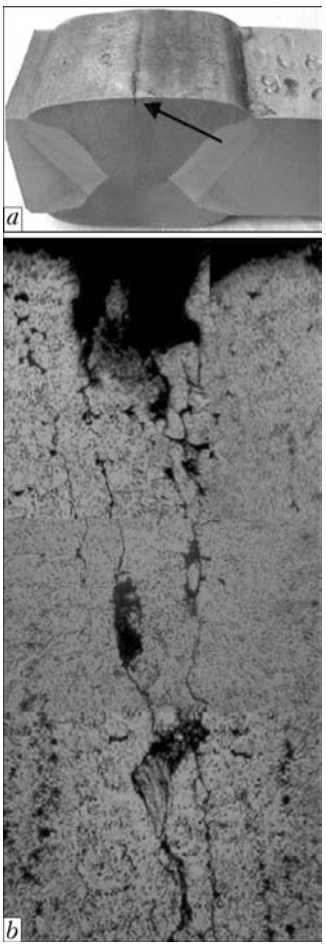

Figure 6. Macrosection with shrinkage porosity along the weld center (*a*), and microstructure (×250) of this zone (*b*)

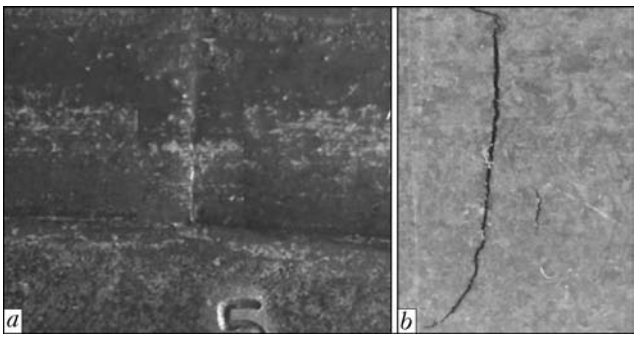

Figure 7. Cold transverse cracks formed in welds with hardening type structures: *a* — transverse crack on external weld surface; *b* — longitudinal macrosection

crease of speed of multiarc welding and application of fused flux of average and coarse grain size. If agglomerated flux is used for pipe welding, no shrinkage porosity is observed, as a rule.

Cold transverse cracks can be formed in welds as a result of effect of two main factors [6–8], i.e. formation of hardening structures in weld metal, and/or presence of excessive hydrogen. Figure 7 shows appearance of cold transverse crack in the longitudinal pipe weld caused, mainly, by structural factor. It is determined, that cracks of this type in weld metal of pipes from typical microalloying steel of K56–K65 strength class appear due to its increased alloying, first of all, by manganese, molybdenum, niobium and vanadium, that promotes formation of hardening type structures of high strength *HV*49-280–350. Such cracks in double-sided welded joint of pipes, nucleate, mostly, in metal of local brittle zones of the first weld with increased strength, which are formed in reheating during performance of the second weld. The failure, preferably, has intecrystalline character.

Peculiarities of formation of *cold transverse hydrogen cracks* were studied by example of welded joints of 914 mm diameter pipe from X65 steel (Figure 8). Cracks reached the surface of outside, inside or both welds. No specific differences of structure in metal of crack formation zone from usual one were found. Hardening structures in the welds were absent. No polyganizational boundaries, which could testify increased weld microalloying, were also detected. Vickers hardness of the weld metal did not exceed critical level from point of view of crack formation (*HV*49-260). At the same time, investigations using scanning microscope showed accumulation of small pores in the crack zone, that is indicative of its hydrogen origin (see Figure 8). Similar pores were found in area of the through crack which became the reason of failure of gas pipeline of 1420 mm diameter mentioned above.

Data of work [8] confirm an idea of delayed character of formation of hydrogen transverse cracks in metal of pipe welds. Therefore, their detection immediately in the process of pipe manufacture is difficult.

Application of increased humidity flux as well as accelerated cooling of welded joint before ultrasonic testing is the possible source of increase concentration of diffusible hydrogen in weld metal at pipe manufacture.

Different orientation cracks of metallurgical origin, caused by local change of chemical composition of weld metal of pipes, can be formed by different reasons, mainly, due to entering of exogenic particles in the weld metal. There are cases, for example, of crack appearance in the weld due to its local enrichment by carbon and manganese and formation of structural constituents with high hardness. Such cracks, in particular, were found in the pipe welds in application of fused flux AN-60 and AN-67B due to its contamination by particles of furnace lining in the process of manufacture [9]. Cracks of this type of different orientation were located in outside as well as inside weld, have filament character and, mainly, small sizes. However, in series of cases, they were propagated along the whole weld

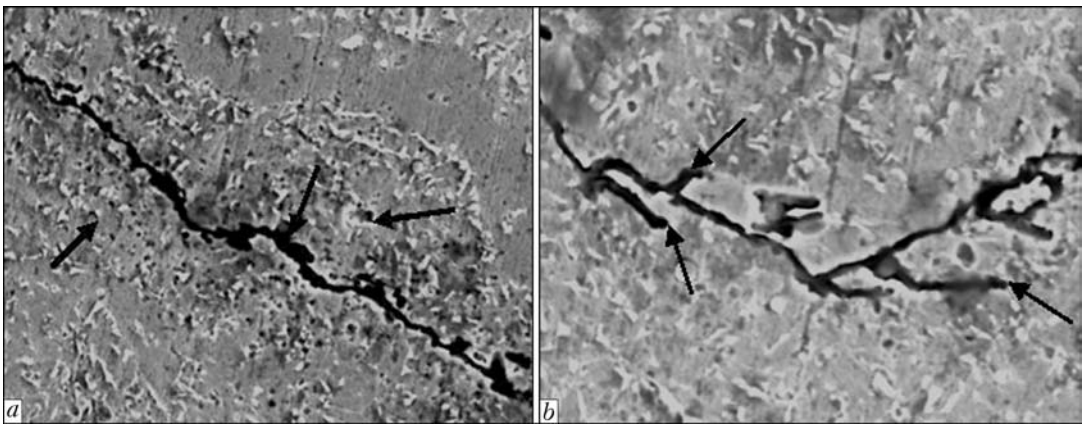

Figure 8. Hydrogen-induced cracks in weld metal of pipe made by submerged arc welding (×1400): *a* — accumulation of pores in crack zone; *b* — examples of stopping of microcrack development by pores

section. Crack formation in the weld metal of pipes can also be caused by coarse nonmetallic (slag) inclusions of exogenic character from contaminated flux in its re-usage and inequality separation.

Cases of crack formation in places of local enrichment of weld metal of pipes by copper and sometimes zinc (Figure 9) were registered. Cracks were nucleated in the surface layers of welds and propagated normal to its axis up to 15 mm depth. Contamination of the weld metal by specified elements can be related with fusion of tips and contact dies of welding machines including due to breaking of stability of submerged multiarc welding process, for example, at increased arc voltage that results in shunting of arcs by slag crust. Cracks formed at that have relatively small dimensions, that make difficult their detection using non-destructive methods.

Cracks in repaired sections of pipe weld, where correction of found defects (pores, slag inclusions, lacks of penetration etc.) was performed with their preliminary removal and further multipass mechanized submerged multilayer welding, are formed, as a rule, due to unfavorable structural characteristics of metal of «repair» weld. Cracks, mainly, develop in longitudinal direction and nucleate, as a rule, in the last layer of «repair» weld and then propagate in metal of previous layers of this weld and HAZ.

It is determined that studied cracks can be related to cold ones and their formation is caused by progressive increase of weight fraction of alloying elements (manganese, silicon, molybdenum, chromium etc.) from layer to layer during performance multipass welds using consumables applied, usually, for these purposed in pipe production. For example, application of flux AN-60 and Sv-08G1NMA wire for repair of defective area of the longitudinal weld of pipe from 10G2FB steel resulted in increase of content of manganese in the last (fourth) layer of «repair» weld up to 1.97 %, silicon — up to 0.98 and molybdenum — up to 0.53 % (in the first layer of this weld quantity of indicated elements was in the level of 1.96, 0.45 and 0.16 %, respectively). Excessive level of alloying of metal of the last weld layers resulted in formation of areas of upper bainite structure with high hardness, reduced ductility and toughness, enrichment of ferrite matrix by silicon, also reducing its ductility, and formation of developed system of polygonization boundaries with microcracks. Issues on optimizing of chemical composition and structure of metal in sections of pipe welds subjected to repair will be considered in detail in our next publications.

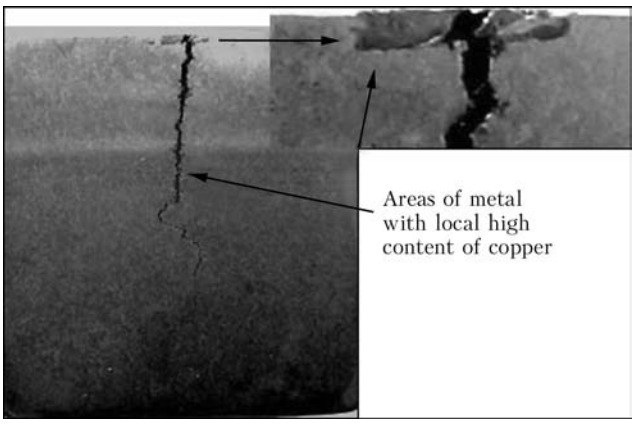

Figure 9. Cracks in weld metal in areas of local enrichment by copper (fragment of crack (×6) is shown in right upper angle)

Cracks-tears in the near-weld zone, similar to shown in Figure 4, can be formed during performance of expanding operation of pipes, necessary for providing their required dimensions. Appearance of such cracks is a result of effect of series of factors, i.e. excessive deviations of pipe profile in area of welded joint from circularity before expanding, non-smooth transfer of weld reinforcement to base metal, and unfavorable structural characteristics of metal in areas adjacent to weld caused by welding heating. Cases of formation of cracks-tears are mostly observed in a period of mastering of production of new grade pipes or pipes of higher level strength. Small dimensions of these defects and location in area of geometry concentrator complicate their detection using non-destructive testing methods. Namely, cracks-tears formed in expanding of pipes at the near-weld zone became a reason of considered earlier failures of main pipeline of 1220 mm diameter.

Therefore, study of reasons of failures of main pipelines and investigations of technological welding and allied processes performed at tube-welding plants allowed determining peculiarities of location, reasons and mechanisms of formation of crack-like defects in welds on the pipes designed for application in construction of main pipelines. System of measures on reduction of possibility of appearance of such defects and increase of reliability of testing methods was developed considering these data and partially realized in acting tube-welding productions. For example, as was previously mentioned, three-layer welding technology (with preliminary performance of assembly weld) is virtually everywhere used in manufacture of pipes of critical designation instead of outdated two-layer welding. Welding of pipes is performed only using ceramic flux instead of fused one, in which presence of separated particles of furnace lining and other foreign particles is possible. Accelerated

Recommended measures for prevention of appearance of crack-like defects in welds on large diameter pipes made by submerged arc welding

Cracks	Measures for prevention of crack formation
Longitudinal solidification cracks in outside welds caused mainly by effect of force factor	Application of three-layer welding technology with preliminary joining of pipe edges by assembly (technological) weld Forming of pipe billets eliminating excessive deformations of edges in assembly
Longitudinal cracks in metal of pipe welds related with shrinkage porosity	Improvement of pipe shape (elimination of «saddle», limitation of weld width) Limitation of slope angle «downhill» of a mill for welding of inside pipe welds in the range not more than 20 min Application of ceramic flux Control of flux quality
Cold transverse cracks of hydrogen origin or caused by formation of hardening structures in weld metal	Control of flux humidity (flux humidity should be not more than 0.03 %) Limitation of weld metal alloying (first of all, not more than 0.3 % Mo and not more than 0.03 % Nb) Elimination of operation of accelerated cooling of welded joints before US testing (if this operation is necessary, time between finish of welding and start of cooling should be not less than 1 h, and weld temperature — not more than 80 °C) Control of hardness of metal of the first weld for new grades of pipe steel and consumables, including for the purpose of detection of local zones of increased hardness (more than *HV* 260) in its root
Cracks of different orientation of metallurgical origin in weld metal	Application of agglomerated flux and control of its quality Quality control of surface of welding wire Registration of parameters of welding process and control of its stability Control of condition of nozzles
Cracks in repair sections of mill welds performed with the help of multilayer welding	Application of welding wire with limited content of molybdenum (up to 0.3 %) and nickel (up to 0.6 %) as well as aluminate-basic agglomerated flux Certification of welding process for repair of pipe welded joints
Cracks-tears in the near-weld zone	Control of pipe billet and welded joint shape before expanding (deviation of pipe surface profile from theoretical circle in area of welded joint should not exceed 0.15 % D_{out}) Improvement of weld shape (for example, transfer angel of weld to base metal should not be less than 120°) Limitation of expanding value (up to 0.9 %), in particular, for thick-wall pipes of increased strength Additional limitation of maximum allowable concentration of alloying elements, in particular, carbon (depending on strength level), molybdenum (not more than 0.2 %), niobium (not more than 0.05 %), including for pipe steel of increased strength, for example, X80

cooling of welds before ultrasonic testing is eliminated at most pipe plants. Equipment and scheme of testing of welded joints of pipes are improved to significant extent, including due to increase of number of US transducers etc. Detailed list of measures, recommended for prevention of appearance of crack-like defects in welds of large diameter pipes made using submerged arc welding, is given in the Table.

At the same time, in our opinion, increase of guarantee of absence of crack-like defects in pipe welds in addition to technological measures and improvement of means and testing methods, requires setting of additional requirements to technological process of their production in customer normative documents for pipes, for example, limitations of flux humidity, entering of norms of maximum allowable concentration of alloying elements in steel and weld metal, control of applied consumables and shape of pipe billet before expanding, registration of parameters of welding process and its certification before pipe production, etc.

Results of these investigations can be also used for improvement of methods for diagnostics of main pipelines.

1. Kuznetsov, V.V., Lyapin, A.A., Monakhov, R.E. (2007) Comparative analysis of statistical data on accident rates in main pipelines of Russia and Western Europe. *Neft, Gaz and Bizness*, **1/2**, 49–56.
2. Mazur, I.I., Ivantsov, O.M. (2004) *Safety of pipeline systems*. Moscow: Elima.
3. Mandelberg, S.L., Rybakov, A.A., Sidorenko, B.G. (1972) Resistance of pipe steel welded joints to solidification cracks. *Avtomatich. Svarka*, **3**, 1–4.
4. Mandelberg, S.L., Rybakov, A.A., Fajnberg, L.I. et al. (1972) CO_2 welding of assembly longitudinal welds of large diameter pipes. *Ibid*., **11**, 56–58.
5. Mandelberg, S.L., Semyonov, S.E. (1962) Formation of shrinkage cavities on weld surface in submerged multiarc welding with higher speed. *Ibid*., **6**, 17–20.
6. Mandelberg, S.L., Buslinsky, S.V., Bogachek, Yu.L. (1984) Influence of hydrogen on cold crack formation in welding of pipe steels. *Ibid*., **2**, 2–5.
7. Makarov, E.P. (1981) *Cold cracks in welding of alloy steels*. Moscow: Mashinostroenie.
8. Hrivnak, I. (1984) *Weldability of steels*. Moscow: Mashinostroenie.
9. Mandelberg, S.L. (1965) Higher speed multiarc welding with electrode weaving. *Avtomatich. Svarka*, **2**, 8–13.

Received 12.02.2013

ARC BRAZING OF LOW-CARBON STEELS

V.F. KHORUNOV, I.V. ZVOLINSKY and **S.V. MAKSYMOVA**
E.O. Paton Electric Welding Institute, NASU
11 Bozhenko Str., 03680, Kiev, Ukraine. E-mail: office@paton.kiev.ua

The article is dedicated to investigation of the process of arc brazing on thin-sheet steel 08kp (rimmed) by using brazing filler alloy BrKMts 3-1. Peculiarities of spreading of the filler alloy under conditions of tungsten-electrode arc heating using different shielding atmospheres are considered. It is shown that the best spreading is achieved in a mixture of argon with 10 wt.% of hydrogen. Heat input in arc welding and brazing was compared by the calculation method: the values of heat input (for a specific case) were 1200 and 516.7 J/cm, respectively. The possibility of decreasing the heat input by using the pulsed process is shown. Peculiarities of formation of butt and overlap joints are revealed. In brazing of the butt joints the gap can be adjusted over wide ranges (0.2–0.8 mm), and in brazing of the overlap joints this parameter is within the narrower ranges. However, in general the use of the overlap joints seems more promising. As seen from the data of optical microscopy and X-ray spectrum microanalysis, a silicide interlayer forms at the interface of the joint, where the content of silicon may exceed 10 wt.%. Structure of the seam is a solid solution with discrete precipitates of the phase with the increased silicon content along the grain boundaries. It is shown that in brazing under optimal conditions the strength value of the butt joints on low-carbon steel brazed by using filler alloy BrKMts 3-1 is 330–390 MPa. In the overlap joints the full strength value is achieved at an overlap equal to thickness of the materials joined. 11 Ref., 8 Figures.

Keywords: *welding, arc brazing, low-carbon steels, brazing filler alloy, shielding atmosphere, spreading of brazing filler alloy, coating, strength of joints*

Brazing is one of the most important technological processes of modern production. Rapid development of different industries resulted in its wide application first of all in motor car construction and in other sectors where it is necessary to join structures of thin-sheet materials, including those having protective coatings (zinc, aluminium, etc.). This can be explained by the fact that brazing as a process of formation of joints on materials is performed at a temperature below the melting point of a material being brazed.

Brazing, along with welding, is now one of the most common methods for production of permanent joints. A wide variety of the technological tasks makes it necessary to use different heating methods for brazing, the arc being among the most promising heat sources for production of the brazed joints. At present the methods of brazing using arc heating are applied for joining assemblies of thin-sheet billets, including the galvanised ones, e.g. car bodies [1–11]. However, some methods of high-temperature arc brazing, and gas-shielded tungsten-electrode arc and plasma brazing in particular, are little studied as yet.

The purpose of this study was to investigate the capabilities of arc brazing of low-carbon steels by using standard Cu-base alloy BrKMts 3-1 as a brazing filler alloy.

The special bench was prepared to conduct experiments. The bench comprised Kemppi argon-arc welding device Master TIG MLS 2300, 0.8–1.6 mm diameter wire feeder with gradual adjustment of the feed speed in a range of 0–130 mm/s (468 m/h), and device for moving the torch at a speed of 0.5–25.0 mm/s (90 m/h). Filler wire was fed to under the arc, i.e. it was not alive, which widened the ranges of adjustment of the arc brazing parameters.

To conduct the experiments, the above filler alloy was used in the form of the 1.2 mm diameter wire. Liquidus temperature of the alloy was 1020 °C. Specimens of steel 08kp (rimmed) measuring 150 × 60 × 1 mm in the horizontal position were used as substrates. The effect of heat input, gap, pulse duration and filler alloy feed speed on the weld parameters was investigated.

Naturally, it was interesting to determine how the heat input changed in transition from welding to arc brazing. As a starting point, it should be noted that parameters of welding of such a specimen in the shielding atmosphere of argon by using 1.2 mm diameter wire Sv-08G2S were as follows: I = 100 A, U = 10.8 V, v_w = 22.7 m/h, and v_f = = 10 mm/s.

The effective power of the arc was around 750 J/s, and heat input was approximately 1250 J/cm. It might be expected that in a case of using metal with a considerably lower melting point less energy would be required for formation

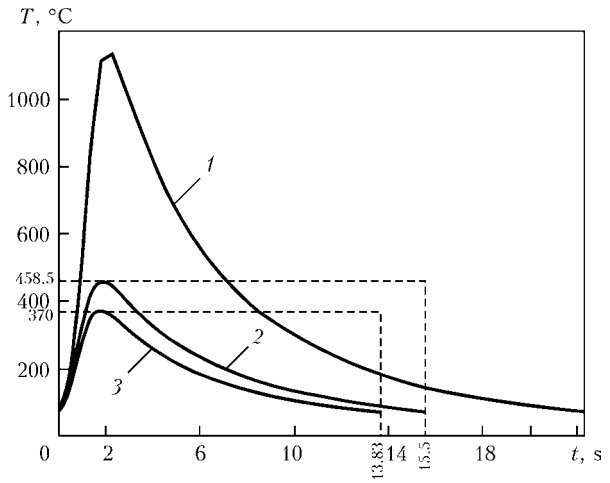

Figure 1. Thermal cycle of arc welding and brazing of steel 08kp at different process parameters: *1* — welding at I = = 100 A, U = 10.8 V, v_w = 22.7 m/h, v_f = 10 mm/s; *2* — brazing at I = 60 A, U = 9.5 V, v_b = 22.7 m/h, v_f = = 15 mm/s, δ = 0.4 mm; *3* — brazing in pulsed mode at I_{pulse} = 100 A, I_{pause} = 10 A, U = 10.2 V, v_b = 22.7 m/h, v_f = 6 mm/s, ν = 5 Hz, τ_{pulse} = 30 %, δ = 0.04 mm

of the joint. Indeed, in arc brazing the heat input was approximately 625 J/cm (I = 60 A, U = = 9.5 V, v_b = 22.7 m/h, v_f = 15 mm/s). The value of the heat input can be decreased due to using the pulsed mode. For instance, when brazing was performed in mode 3 (Figure 1), the heat input was about 416.7 J/cm.

Calculations were made by using the known formulae to evaluate changes in heat input in transition from welding to arc brazing. The ratio of thermal cycles at a point located at a distance of 0.6 mm from the seam centre is shown in Figure 1.

It follows from the given data that transition from welding to arc brazing allows a substantial decrease in heat input and, hence, reduction of the probability of burns-through and distortions in the process of formation of the joints.

Obviously, the data on behaviour of filler alloys under the arc heating conditions are lacking. In particular, no generally accepted procedure for investigation of the spreading process under the considered conditions is available. Therefore, we used the known recommendations, which were adapted to arc heating (Figure 2).

The experiments on wetting of steel 08kp were conducted in compliance with GOST 23904–79 «Determination of the Surface Area of Spreading of Brazing Filler Alloy». The specimens measuring 40 × 40 × 1 mm and the charges of filler alloy BrKMts 3-1 with a diameter of 4 mm (0.42 g in weight) were made for these experiments. A chromel-alumel thermocouple was used to monitor the temperature. The thermocouple was welded to a specimen to form a hot end. The temperature was controlled by using the TRM-202 instrument. Argon, helium and a mixture of Ar + 10 % H_2 were used as shielding gases. A filler alloy charge was placed strictly at the substrate centre to provide its uniform heating. The distance from the electrode tip to the charge was 2 mm.

The temperature of the wetting process was limited, it being 30 °C higher than the liquidus temperature of brazing filler alloys, i.e. for filler alloy BrKMts 3-1 it was 1050 °C. The wetting experiments were carried out at the direct and alternating currents with different pulse shapes. The resulting deposited beads were photographed, and the photos were processed on the computer by using the AutoCard 2002 software.

As seen from Figure 3, the spreading area strongly depends on the composition of a shielding atmosphere. The best results were achieved

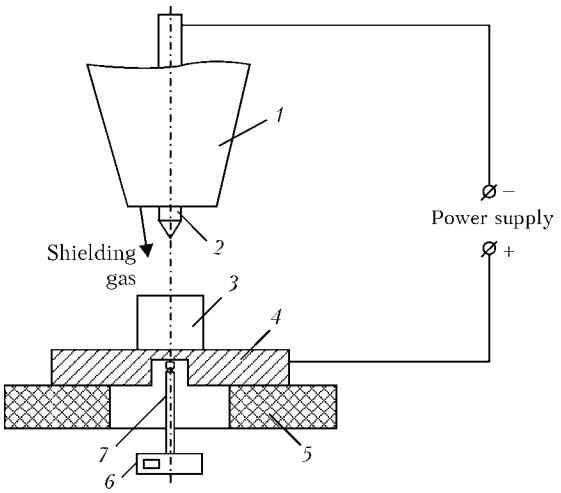

Figure 2. Schematic of the experiment on spreading of filler alloy under the arc heating conditions: *1* — nozzle; *2* — tungsten electrode; *3* — filler alloy charge; *4* — substrate; *5* — insulator; *6* — temperature recorder; *7* — thermocouple

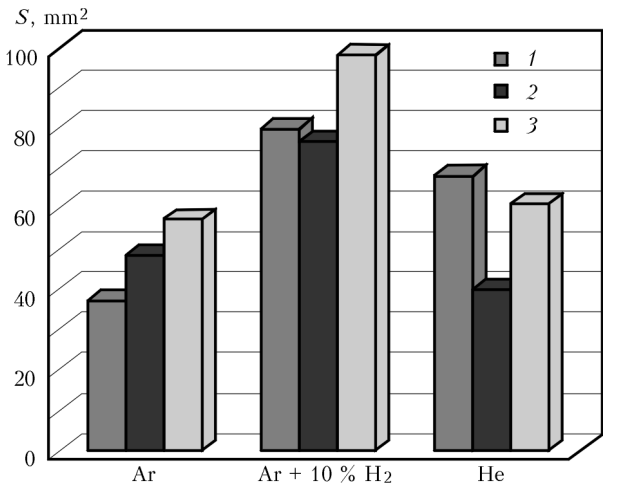

Figure 3. Diagrams of the area of spreading of filler alloy BrKMts 3-1 on steel 08kp depending on the shielding atmosphere and kind of the current: *1* — DC; *2* — AC (sinusoidal); *3* — AC with rectangular pulse shape

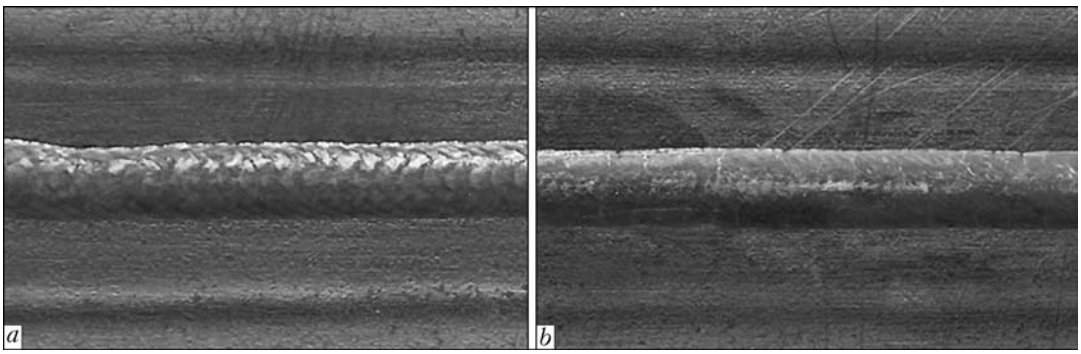

Figure 4. Appearance of the seams on butt joints brazed with filler alloy BrKMts 3-1 at different process parameters: *a* — I_{pulse} = 100 A, I_{pause} = 10 A, U = 10.1 V, ν = 5 Hz, τ_{pulse} = 30 %, v_b = 22.7 m/h, v_f = 6 mm/s, Q = 416.7 J/cm; *b* — I_{pulse} = 100 A, I_{pause} = 10 A, U = 10.3 V, ν = 10 Hz, τ_{pulse} = 30 %, v_b = 22.7 m/h, v_f = 10 mm/s, Q = 525 J/cm

in a mixture of argon with hydrogen. Moreover, the spreading area grew with increase in the electrode diameter.

From the practical standpoint, the use of helium is hardly expedient in view of its high cost, whereas it is worthwhile to pay attention to the mixture of argon with hydrogen as a promising shielding atmosphere.

Good formation of the butt and overlap joints was achieved by using the above brazing filler alloy. No spattering at all was observed in brazing of the butt joints under optimal conditions, and the seams had a smooth surface. Good formation of the brazed seams can be provided at different combinations of the arc brazing parameters, including in the pulsed mode (Figure 4). However, the integral criterion of quality of the seams is heat input. Variations of the gap within 0.2–0.6 mm in brazing of the butt joints had just a negligible effect on quality of the seams.

Examinations of microstructure of the joints brazed at different process parameters showed that in all the cases in brazing using filler alloy BrKMts 3-1 a clearly etchable interlayer formed at the interface of the joints, this interlayer looking light on a non-etched section, i.e. it had increased hardness. As the filler alloy contains

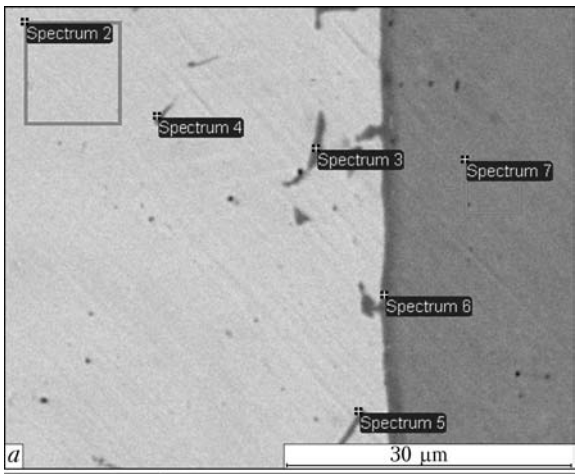

a

Spectrum No.	Chemical composition, wt.%			
	Si	Mn	Fe	Cu
2	3.87	1.13	0.89	94.12
3	12.93	2.74	40.30	44.02
4	14.74	10.15	32.33	42.78
5	10.29	1.47	47.66	40.58
6	12.04	0.83	78.91	8.21
7	0.16	0.24	99.47	0.13

b

Figure 5. Microstructure of interface of the joint on steel 08kp brazed with filler alloy BrKMts 3-1 at the following process parameters: I = 19 A, U = 8.9 V, v_b = 7.2 m/h, v_f = 2 mm/s, base metal thickness — 1 mm, filler wire diameter — 1.2 mm (*a*), and chemical composition of metal at the sampling locations (*b*)

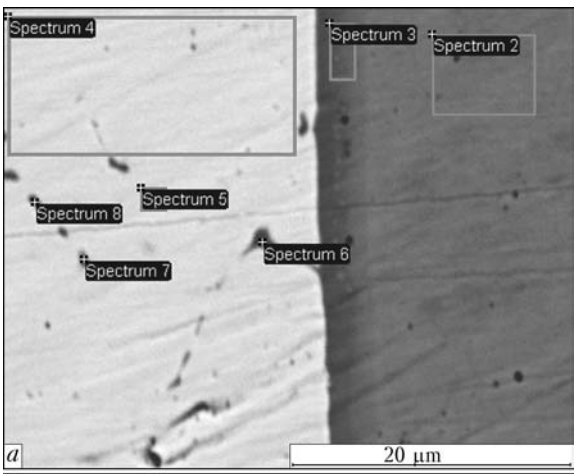

a

Spectrum No.	Chemical composition, wt.%			
	Si	Mn	Fe	Cu
2	0.15	0.26	99.11	0.48
3	10.19	0.67	84.91	4.24
4	2.41	0.92	2.53	94.13
5	3.01	0.93	1.63	94.44
6	4.93	1.26	17.32	76.50
7	3.90	1.13	4.23	90.74
8	3.43	1	2.38	93.19

b

Figure 6. Microstructure of interface of the joint on steel 08kp brazed with filler alloy BrKMts 3-1 at the following process parameters: I = 30 A (DC), U = 10.8 V, v_b = = 2 mm/s, v_f = 2 mm/s, base metal thickness — 1 mm, filler wire diameter — 1.2 mm, gap — 0 (*a*), and chemical composition of metal at the sampling locations (*b*)

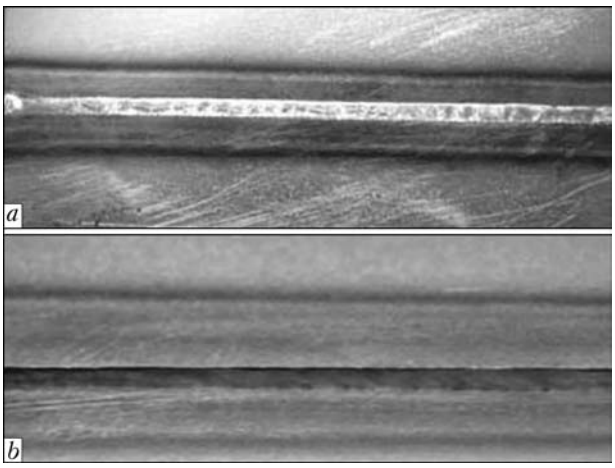

Figure 7. Appearance of the overlap joints made by arc brazing at the following process parameters: I_{pulse} = 100 A, I_{pause} = 10 A, U = 10.2 V, ν = 5 Hz, v_b = 22.7 m/h, v_f = = 6 mm/s, τ_{pulse} = 60 %: *a* — straightforward seam; *b* — reverse seam

3 wt.% Si, we assumed that it was silicide. Examinations using scanning electron microscope CamScan equipped with energy-dispersive spectrometer Energy-200 were carried out to generate data on a specific chemical composition of this interlayer.

Microstructure and results of X-ray spectrum microanalysis of the seam brazed at heat input of 591.7 J/cm are shown in Figure 5. The base metal and filler alloy preserved their initial composition practically without any change. However, the phase containing an increased amount of silicon — up to 12 wt.% solidified along the seam (at the joint interface), and this really was silicide (see Figure 5, spectrum 6). Moreover, the phase containing approximately 10–15 wt.% Si precipitated in the seam along the grain boundaries of the base metal (see Figure 5, spectra 3–5).

As heat input was increased approximately to 1125 J/cm, the width of the silicide interlayer grew (Figure 6), although the phase composition hardly changed.

The experiments on brazing of the overlap joints were carried out with allowance for the data obtained in brazing of the butt joints on low-carbon steel 08kp. As noted above, to produce the quality butt joints it was necessary to provide heat input within 416.7–583.3 J/cm. For the overlap joints this level of heat input turned out to be insufficient. The good straightforward (Figure 7, *a*) and reverse fillets (Figure 7, *b*) formed with a rise in heat input due to increase in the pulse duration approximately by 70 %.

It should be noted that the overlap joints are most characteristic of brazing, and it is reasonable to suppose that they will continue to be the key type of the joints used in industry.

Strength of the butt joints on low-carbon steel brazed with filler alloy BrKMts 3-1 was (with the removed reinforcement) 330–390 MPa. In the as-brazed state the rupture occurred in the base metal. The full strength value in the overlap joints was achieved at an overlap equal to thickness of the materials being joined.

As note above, the given experimental results on arc brazing of low-carbon steel were obtained by using the up-to-date equipment possessing wide capabilities in terms of control of the arc process. Therefore, transition to application of microplasma heating using the MPU-4 unit turned out to be ineffective, and the attempts to achieve the same results at the same heat input failed. With increase in heat input to 1275 J/cm the good formation of the seam on the arc side was achieved at a gap of 0.2, 0.4 and 0.6 mm. However, the reverse fillet formed only at a gap of 0.6 mm. Moreover, the gap was hardly filled in some places (Figure 8).

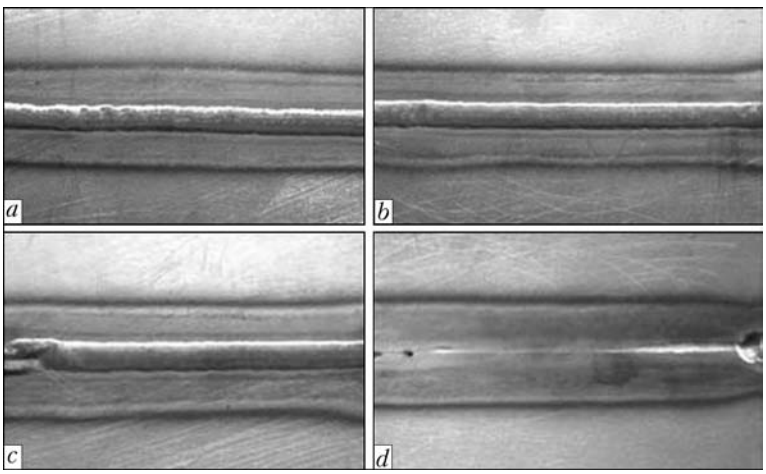

Figure 8. Appearance of the seams brazed at the following process parameters: I = 28 A, U = 15.2 V, v_b = 7.2 m/h, v_f = 4 mm/s, gap — 0.2 (*a*), 0.4 (*b*), 0.6 (*c*) and 0.6 (*d*) mm (reverse fillet)

By analysing the data obtained, it should be noted that increase in heat input within the investigated ranges did not give the expected effect in brazing of the butt joints at low currents: the amount of metal in the seam on the arc side increased gradually, whereas the reverse seam formed only at a sufficiently big gap (0.6–0.8 mm), i.e. the lower edge of the joint remained non-heated, and the filler alloy could not fill up the gap. In brazing of the overlap joints the conditions for formation of the joints were more favourable, the range of the favourable conditions being widened. For example, an attachment was made to the above Master TIG MLS 2300 unit, which allowed this process to be controlled over a wide power range. As a result, it made it possible to obtain the results close to those typical of using arc heating.

Conclusions

1. Filler alloy BrKMts 3-1 investigated in this study spreads well on steel 08kp and forms sound butt and overlap joints without a marked dilution of the base metal in the liquid filler alloy.

2. The most favourable shielding atmosphere for arc brazing using the investigated filler alloy is a mixture of argon with 10 wt.% of hydrogen.

3. The use of alloys with a melting point that is much lower than that of steel allows the level of heat input to be radically changed in production of permanent joints. For instance, in brazing of 1 mm thick plates the level of heat input is approximately 416–625 J/cm. The heat input required for welding of the similar specimens is 1166–1250 J/cm.

4. Strength of the butt joints on low-carbon steel brazed with filler alloy BrKMts 3-1 (with the removed reinforcement) is 330–390 MPa. In the as-brazed state the rupture occurs in the base metal. In the overlap joints the full strength value is achieved at an overlap equal to thickness of the materials being joined.

1. (1999) WIG-Loeten verzinkter Bleche. *Bleche Rohre Profile*, 46(**7/8**), 16.
2. Tischter, F. *Verfahren zum MSG-Loeten und Verwendung eines Schutzgases*: Appl. 19952043, Germany. Int. Cl. B23K 3/04, B23K 1/08. Fil. 28.01.1999. Publ. 03.05.2001.
3. Knopp, N., Killing, R. (2004) Hartloeten verzinkter Feinbleche mit dem Lichtbogen sicher und wirtschaftlich: Teil 2. *Der Praktiker*, **1**, 8–12.
4. Hackl, H. (1998) MIG-Loeten von verkzinten Duennblechen. *Technica* (Suisse), 47(**25/26**), 54–58.
5. Hackl, H. (1998) MIG-brazing of galvanised thin sheets and profiles. *Welding and Cutting*, 50(**6**), 102–104.
6. Hackl, H. (2001) Loeten statt Schweissen steigert Qualitaet von PK WS Stahlmarkt: Informationen ans Stahlindustries. *Stahlhaldel und Verarbeitung*, 51(**1**), 68–69.
7. Hackl, H. (2000) Loeten statt Schweissen. *Bleche Rohre Profile*, 47(**12**), 110.
8. (2003) Verzinkte Bleche MIG-Loeten. *Ibid.*, 50(**1**), 24–25.
9. Hackl, H. (2002) Beim MIG-Loeten eruebright sich das Nachverzinken. *Ind.-Anz.*, 124(**23/24**), 38–39.
10. Grzybicki, M., Jakubowski, J. (2009) Comparative tests of welding of sheets made of car body steel using the CMT and MIG/MAG methods. *Przeglad Spawalnictwa*, **10**, 32–36.
11. Rozanski, M. (2010) Modern weldbrazing methods. *Ibid.*, **9**, 24–28.

Received 05.02.2013

STUDY ON THE EFFECT OF INDUCTION HEATING TO PREVENT HOT CRACKING DURING LASER WELDING OF ALUMINUM ALLOYS

V.V. SOMONOV[1], **S. BOEHM**[2], **M. GEYER**[2] and **S. BERTELSBECK**[2]
[1]Institute of Laser and Welding Technologies of Saint-Petersburg State Polytechnical University
29 Politekhnicheskaya Str., 195251, Saint-Petersburg, Russia. E-mail: vlad@ltc.ru
[2]University of Kassel
19 Steinstrasse, 37213, Witzenhausen, Germany
E-mail: s.boehm@uni-kassel.de; m.geyer@uni-kassel.de; s.bertelsbeck@uni-kassel.de

This work is devoted to research of hot spots generated by induction heating to prevent hot cracks during laser welding of Al–Mg–Si and Al–Si aluminum alloy samples 2 mm thick. The results of numerical modeling of temperature fields and stress fields formed during the process of induction heating, as well as results of experimental validation of the simulation are shown. 25 Ref., 3 Tables, 10 Figures.

Keywords: *laser welding, induction heating, aluminum alloys, modeling, SYSWELD, thermal stresses, hot cracks*

Aluminum alloys are widely used in various fields of engineering due to their good strength characteristics in combination with low weight [1]. Thus, they have a competitive advantage compared to other materials used in industry. They are also highly resistant to corrosion [2]. It is advantageous to use the insertion of heat-treated aluminum alloys in lightweight constructions as that can reduce the total weight of the product while maintaining its strength. Usage of aluminum welded structures manufactured via the method of butt joints is significantly limited due to its ability to form cracks during the welding process [3, 4].

Today, modern lasers such as fiber ones are increasingly used to welding aluminum products. They provide a relatively high penetration with low heat input [5], reduce the strain and minimize further processing, reducing the stages of production. In laser welding of aluminum alloys, similar problems related to their ability to form cracks occur, and high-rate cooling of melt during welding process is one of the cause of cracking.

The aim of the research was to prevent the formation of hot cracks in the aluminum alloys during laser welding. Our task is to create the heating fields in the HAZ by two coaxial coils, that will create a stress field in the weld pool, which will reduce hot cracking.

Study of hot cracking during laser welding of aluminum alloys. Hot cracks are the brittle intercrystalline fractures of the weld metal and HAZ formed in the solid-liquid state at the finish of crystallization, and also in the solid state at high temperatures at the stage of the main development of intercrystalline deformation.

Cracks in aluminum materials are mainly formed during solidification of the weld metal caused by shrinkage and eutectic phase crystallization in the middle of the weld [6]. Pellini and then Clyne and Davies in their studies argue that the susceptibility to hot cracking in alloys of these groups is related to the «critical interval» that is the distance between oppositely directed growing dendrites during crystallization of the weld [7]. Feurer suggested that cracks are formed in the «soft» (quasi-equilibrium two-phase) zone if the rate of cooling of the interdendritic liquid is less or equal to the rate of shrinkage [8]. The approach to cracking of Piwonka and Flemings is based on the Poiseuille's equation which describes how the pressure gradient causes the fluid to flow in an «interdendritic way» [9].

All these theories are related to the peculiarities of crystallization of alloys. The susceptibility to hot cracking can be determined by obtaining the cooling curves for thermal calorimetry. Typical S-shaped curves test some binary alloys. The susceptibility to cracking is caused by the content of dissolved elements. The first quantitative description of the crack formation was proposed by Prokhorov in the middle of 20th century [10–12]. Prokhorov argued that mechanical tensile strain is a cause of cracking. He did not take into account the metallurgical condition in the «soft zone» and did not consider the microstructural formation during solidification of the two-phase region. Prokhorov did not quantify the criteria

for predicting susceptibility to cracking. Most of the studies on solidification cracking in welds are based on the approach of Prokhorov, but they do not consider the accumulation of strain and defects of microstructure. These criteria only consider some of the mechanical conditions, such as critical stresses or strain rate.

Rappaz [13] and other authors describe the cooling of the interdendritic liquid and solid tensile strains as normal to the direction of the growth of dendrites. In their opinion, hot cracks are formed by cavitation pressure above a critical value of stress. It can be calculated according to the physical-chemical properties of alloy and microstructural dimensions of material. The possibility of hot cracking during welding has traditionally been measured for every individual case when the stress or deformation changes occur during the process. For example, Coniglio based his research on the concept of weldability. He believes that the susceptibility to cracks is determined by the critical rate of deformation during welding and studied the dependence of crack formation on content on silicon in aluminum alloys [14].

Recently, two models of the formation of cracks have come up. They are based on integration of the cracking localization. The first of these model was proposed by Shibahara [15, 16], who proposed to build it on the physical mechanism of crack formation according to fracture mechanics of solids. The value of stresses in liquid-solid phase was taken as criteria for the formation of cracks. He used the special computer equipment and finite element method for modeling of cracking. The assumption of the existence of metallurgical conditions in the two-phase region is not taken into account. Stresses in the system are compared with the stress critical value obtained in advance by the correlation with the melt surface energy. Surface energy is the known quantity and has the unique value for the temperature. Shibahara considers this as an aspect which generates local cracks. This approach has the following disadvantages:

- experimental determination of the surface energy at high temperatures is a very complex task;
- surface energy of the melt is strongly influenced by any changes in the chemical composition;
- very small amount of surface active element in the melt can lead to excessive change in the surface energy more than 10 times;
- calculated stress in the two-phase region is sensitive to mechanical properties at high temperatures. Large systematic errors were detected in measurements on the basis of such properties as yield point. Subsequently, it can lead to significant errors in the calculation.

The second approach of modeling cracks was developed by Hilbinger [17–19]. It is based on the theory of Pellini and is implemented using the finite element method as in the previous approach. Localization of tensile stresses in the liquid film in the rest of the melt is taken into account by introducing a «liquid» element in the middle of the weld. These elements have a very low flow in the liquidus–solidus temperature range. As criteria for crack formation the maximum allowable deformation of the «liquid» element in the two-phase region is taken. Critical deformation parameters are established experimentally. The approach of Hilbinger, as well as the method of Shibahara, gives a visual representation of the origin and propagation of cracks.

So, according to theoretical ideas, hot cracks are formed at critical values of the combination of the following factors:

- temperature interval of fragility (TIF) during solidification of the weld metal;
- minimum plasticity in the TIF, δ_{min};
- high rate of welding deformation α [20].

Literature data show several ways to prevent the formation of hot cracks in laser welding. For example, addition of filler material, preheating of samples in the furnace, using protective flux during welding, preheating by parallel laser of smaller capacity to compensate the tensile stresses in weld. Magnetic field also affects the process of laser welding. As was already said, the depth of penetration can be increased, cross-section can be changed, and periodic humping-type defects in weld can be suppressed by the magnetic field [21].

The use of induction heating during laser welding has a positive effect on the technological strength of the weld. It improves the weld geometry, regulates the keyhole shape and reduces the ability to form hot cracks and other defects in weld at crystallization [22].

Modeling the process of induction heating of aluminum alloy plates. The use of computer for process simulation very often promotes cost reduction in the development of defect-free technologies sharply by reducing the amount of experimental investigations. In manufacturing today, there is also the need to create algorithms with an optimal mode of parameters for laser welding on the basis of computer models of the process, which allows obtaining welds without defects [23]. In our investigations before beginning the experiments, the process was simulated

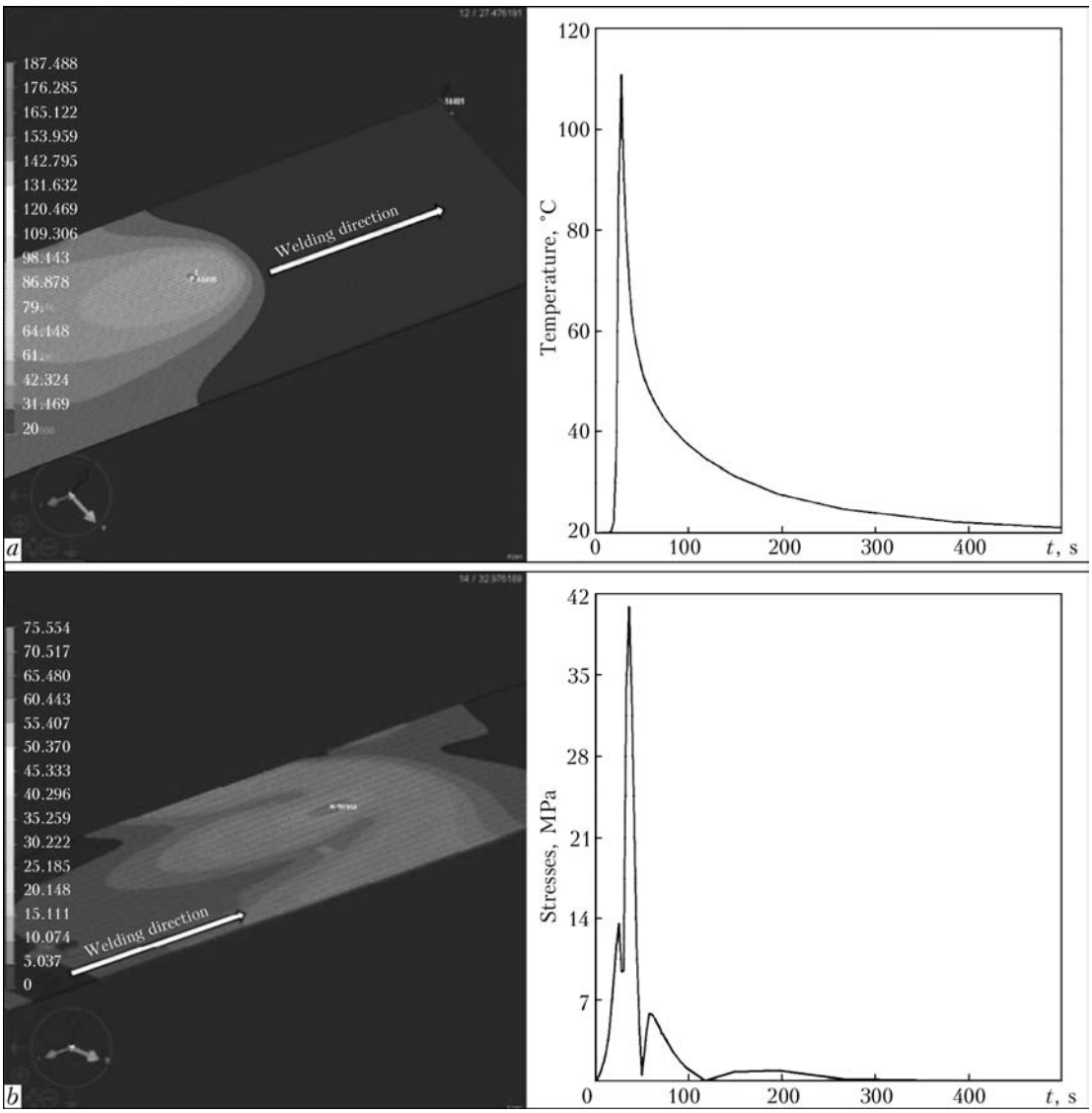

Figure 1. Example of calculated fields: *a* — temperature; *b* — stresses that occur in the sample during induction heating

by the computer program package SYSWELD 2012. Many different software packages and modeling tools exist currently. They are divided into specialized and universal programs. Specialized packages are used in the simulation of a limited number of systems and processes. Universal programs are in most cases commercial developments. With their help, it is possible to fulfill a wide range of applications, modeling a large number of physical processes and systems with complex geometry. One of these is the universal program SYSWELD.

SYSWELD is the software package that implements a finite element calculation scheme. It is used in static and dynamic analysis of structures subjected to physical and geometrical problems (2D and 3D problems). SYSWELD also solves the problem of linear and nonlinear stability of structures; simulates electromagnetic fields, hydro-gasdynamic, acoustic, and other processes.

The main objective of the research was to improve the technology of laser welding of aluminum alloys by preventing or reducing the formation of hot cracks. This was achieved by thermally induced compressive stress in the weld area. This was generated by induction heating on the plate surface, running parallel with the laser welding.

In the course of the simulation of the heating of the samples, the level of emerging internal thermal stresses was monitored [24].

The temperature and thermal stress fields, arising as a result of induction heating of the samples, were investigated with the help of numerical models created in SYSWELD. When building the model, it was taken into account that the efficiency of the setup for traditional method of induction heating of metal parts in a variable electromagnetic field does not exceed 60 % [25]. The process of induction heating from one side of the aluminum alloy plate in the course of its movement was modeled. The preparation

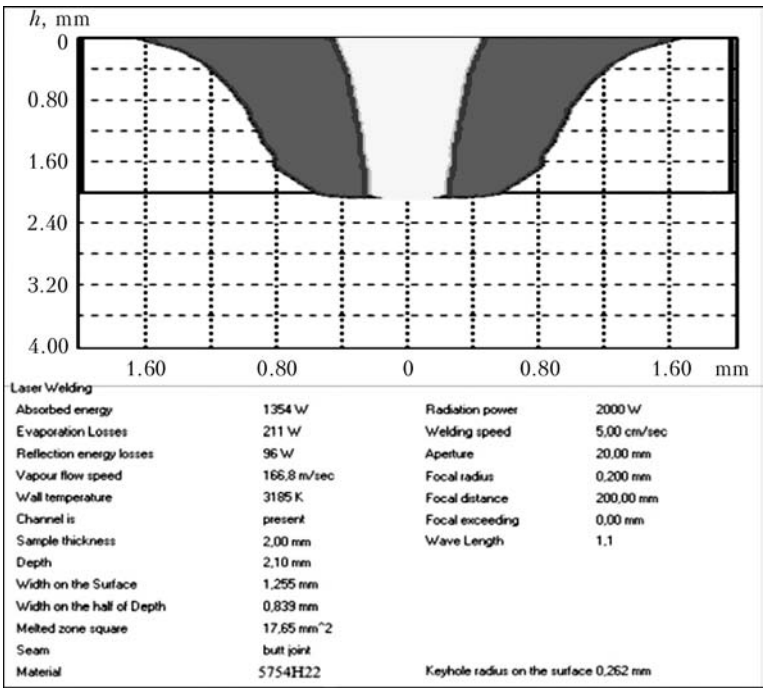

Figure 2. Results of simulation of laser welding of the 5754-H22 Al–Si alloy by software package LaserCAD

of the file for the calculation included the creation of 3D geometrical model of the sample with characteristics of the induction heat source, cooling modes, conditions of fixing and parameters of the heating process. The results of calculation were two files. The first file shows how the temperature field changes in time. The second file demonstrates the chronological variation of the stress fields. An example of results of the calculation of temperature and stress fields that occur in the sample with induction heating is presented in Figure 1.

As the bottom border of required temperature stress, the limit of elasticity was selected. Plastic deformation of the metal begins when the stresses are equal to the elastic limit which for aluminum alloys is more than 30 MPa. The main objective of the study was to obtain the parameters of induction heating at which in the near-weld zone the thermal stresses will compensate the tensile stresses in the weld. Then the results of the simulation were validated experimentally.

The laser welding process has been modeled, and optimal parameters of the full penetration of the plate are determined. Simulation was carried out using the software package LaserCAD

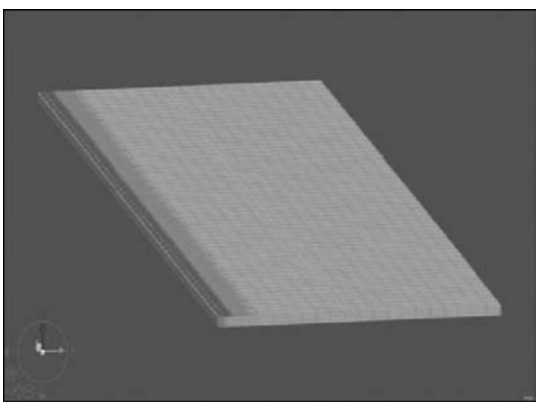

Figure 3. 3D geometrical model of laser welding of the 6082-T4 Al–Mg–Si alloy 2 mm thick with induction heating of HAZ built in software package SYSWELD 2012

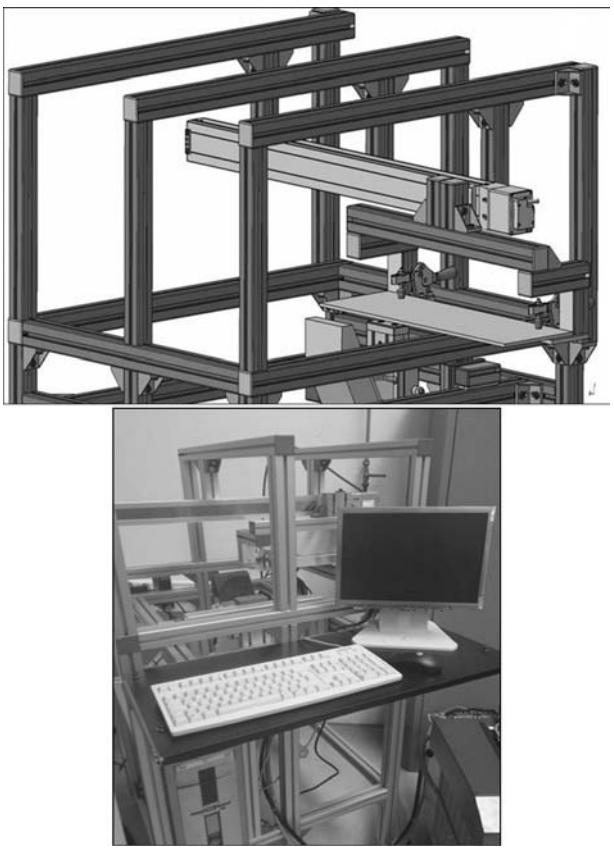

Figure 4. Experimental stand used

Table 1. Chemical composition of investigated aluminum alloys according to GOST 4784–97, wt.%

Alloy	Russian analogue	Si	Fe	Cu	Mn	Mg	Cr	Zn	Ti	Al
5754	AMg3	0.5–0.8	0.5	0.1	0.3–0.6	3.2–3.8	0.05	0.2	0.1	Others
6082	AD35	0.7–1.3	0.5	0.1	0.4–1.0	0.6–1.2	0.25	0.2	0.1	Same

Table 2. Mechanical properties of aluminum alloys investigated

Alloy	Type of processing	$\sigma_{0.2}$, MPa	σ_t, MPa	σ_{sh}, MPa	δ, %	*HV*
6082	T4	170	260	170	19	75
	T6	310	340	210	11	100
	0	60	130	85	27	35
5754	0	100	215	140	25	55
	H22	185	245	150	15	75
	H24	215	270	160	14	80

developed at the St.-Petersburg State Polytechnic University. An example of the simulation results is shown in Figure 2.

In the future, it is also planned to model the process of laser welding with induction heating by two inductors located at equal distance to the weld. To reduce the necessary computing power and calculation time the process will be simulated only for half of the weld. The image of the 3D geometrical model is presented in Figure 3.

Materials and experimental research. In the experiments, flat samples of 600 × 150 × 2 mm in size from Al–Si–Mg–Mn alloys AA6082-T4 and Al–Mg alloy AA5754-H22 were used. Chemical composition and mechanical properties of the materials are presented in Tables 1 and 2. Before experiments, the plates were cleared from grease and dirt with acetone.

The specially designed experimental stand was used for this study (Figure 4). It has the IFF GmbH coaxial inductor KI-112-U-30° (Figure 5). The components of the stand and their characteristics are presented below:

Maximum travel speed of the Oriental Motors linear drive with frame of stand built from aluminum profiles, mm/s 2000
The IFF GmbH equipment for induction heating
Pulse generator EW100W:
- maximum power, kW 10
- pulse power, % 0–750
- pulse frequency, kHz 8–20

Operating temperature of chiller, °C 18–30
Coaxial coil KI-112-U-30°:
- maximum time of process at maximum pulse power, s 0–100
- coil gap, mm 0.2–0.5
- heating temperature, °C 0–300

The heated plates move at a speed equal to speed of welding, which was calculated with the help of computer simulation. Online measurements of the temperature in three different zones and measurements of the linear change of plate sizes were made during the experiments. The change of temperature was recorded with the help of the Greisinger Electronic GmbH 2-channel temperature meter GMH 3250 and the Mastech

Figure 5. Coaxial coil KI-112-U-30° with pulse generator EW100W and chiller

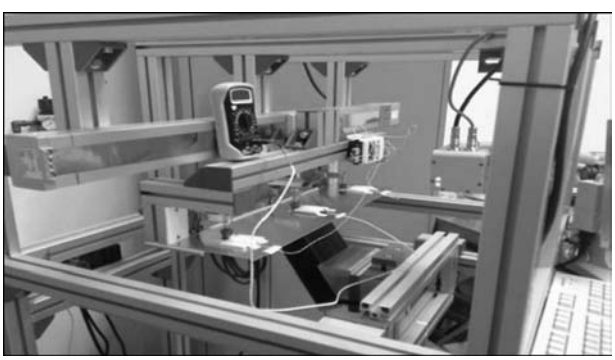

Figure 6. 2-channel temperature meter GMH 3250 and potentiometer IAS838 for measuring the temperature during induction heating of plate

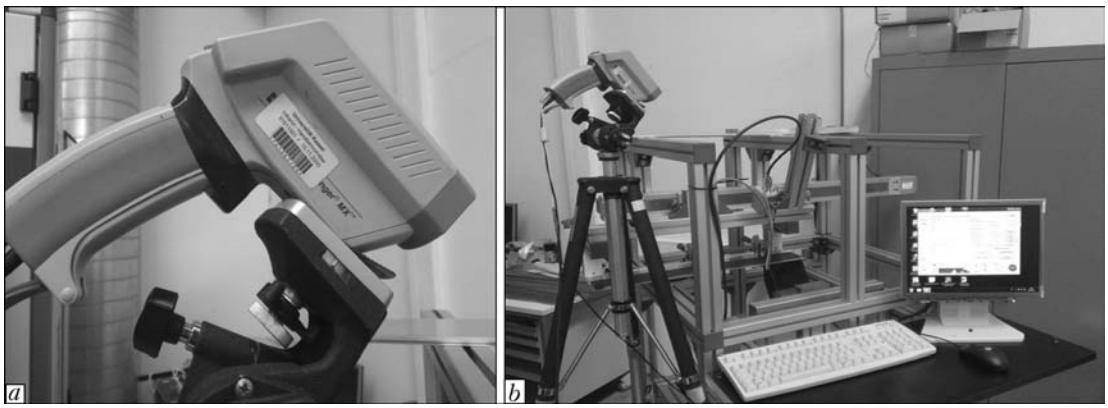

Figure 7. Infrared thermometer Raynger MX4 (*a*) for measurement of the temperature field (*b*)

potentiometer IAS838, functioning as a temperature measurement tool (Figure 6).

The temperature field movement was also registered via the Raytek GmbH high performance infrared thermometer Raynger MX4 (Figure 7). The images of the temperature fields, obtained in the course of the experiments, are presented in Figure 8.

In future it is planned to carry out an experimental verification of modeling results for laser welding using radiation generated from the IPG ytterbium fiber laser YLS 10000 with maximum output power of 10 kW (Figure 9). The movement of the beam will be carried out by the Reis Robotics robot (Figure 10).

Some of the results of temperature measurements are given in Table 3.

As is seen from the Table, induction heating process parameters are divided into two stages: parameters of preheating the coil (step 1), and main parameters of heating the plate in movement (step 2). For induction heating the following parameters were chose from the results of simulation and experiments for step 1 and 2, respectively:

frequency of pulse in inductor f_1 = 12.5 and f_2 = 13.0 kHz; power of pulse in percentage of

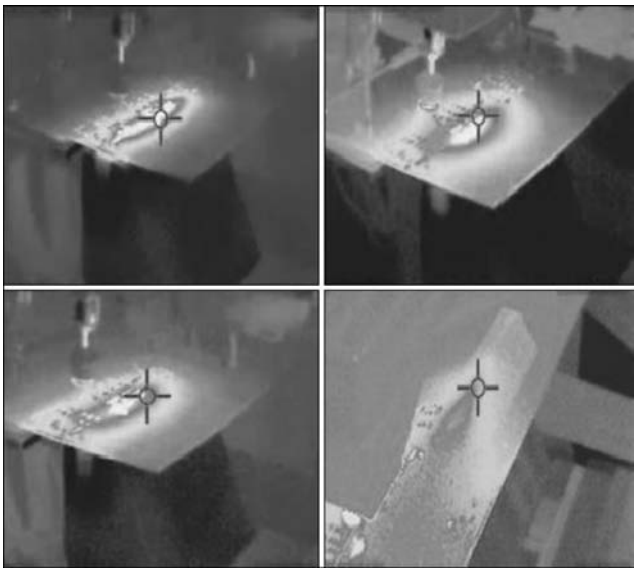

Figure 8. Images of temperature fields obtained

Figure 9. Ytterbium fiber laser YLS 10000

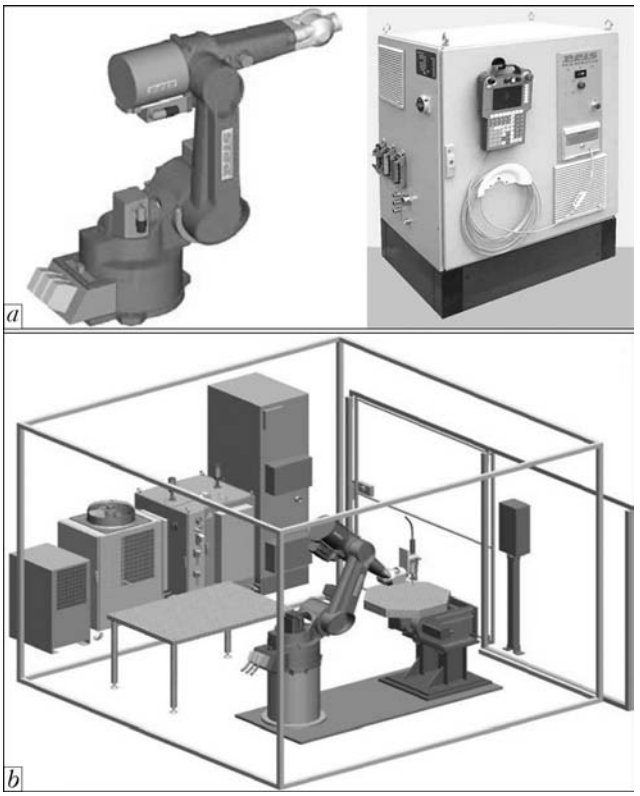

Figure 10. Robot REIS RV60-60 (*a*), and general arrangement of the equipment for laser welding (*b*)

Table 3. Results of experiments

№	Travel distance l, mm	T_{set}, °C	Regulation time, s	Step 1			Step 2			
				f_1, kHz	PWM_1, %	t_1, s	f_2, kHz	PWM_2, %	t_2, s	v, mm/s
1	500	300	1	12.5	750	10	13	600	10	50
2	500	300	1	13.5	750	10	15	700	10	50
4	500	300	1	12.5	750	10	13	600	10	50
5	500	300	1	12.5	750	10	15	600	10	50
11	483	300	1	12.5	750	5	15	700	10.5	50
12	483	300	1	12.5	750	5	13	700	10.5	50
13	483	300	1	12.5	750	5	13	700	10.5	50

Table 3 (cont.)

№	Direction of heating, and distance between inductor and welding line, mm	Gap before heating, mm			Temperature before heating, °C			Temperature during heating, °C		
		g_1	g_2	g_3	T_1	T_2	T_3	T_1	T_2	T_3
1	From right to left, 60	1	0.90	0.25	21.4	21.5	22	237.4	86.7	40
2	Same	1.50	1	0.70	35.2	28	25	246.2	93.9	53
4	From right to left to right, 60	0.50	0.50	0.50	23.1	24.4	26	297.8	86.6	52
5	Same	1	0.30	0.25	21.4	21.4	21	266.8	96.4	42
11	From right to left, 40	0.25	0.25	0.25	24	23.3	22.9	146	122.7	83
12	Same	0.25	0.25	0.25	26	24.9	23.7	143	141.3	97.4
13	»	0.25	0.25	0.25	28	27.1	25.4	144	142.7	97.8

generator maximum power PWM_1 = 750 and PWM_2 = 700 %; generation time t_1 = 5 and t_2 = = 10.5 s.

For step 1: the set of maximum of temperature generated T_{set} = 300 °C.

For step 2: the travel distance with movement l = 483 mm, v = 50 mm/s, gap between sheet and inductor before heating g = 0.25 mm. Recorded temperature was 100–140 °C. As result thermal stresses generated in welding were 38–50 MPa, that is similar to the results of computer simulation.

Results showed that the rate of heating up to high temperature depends on number of reheating of the sample. This is possible due to the change in material structure and its susceptibility to induction heating after heating up to higher than 140 °C. The closer the edge, the less power is needed for heating and generation of the necessary stresses. However, it is impossible to place the inductor closer to the plate edge because it will cause high rate deformations of the plate used. It is impossible to keep the constant parameters of heating the plate in process of its movement.

Conclusion

At this stage of research, the process of induction heating of the plates 2 mm thick of aluminum alloys AA6082-T4 and AA5754-H22 has been studied. Temperature and stress fields were simulated, and parameters of induction heating, creating thermal stresses in the plate and equal to stresses in the weld, were found.

It has been reported that the level of thermal fields depends on the heat source power at the stage of preheating and on the gap between the surfaces of the inductor and aluminum plates, and rate of heating depends on the impact and alloy original structure. Experiments, carried out at multiple induction heating with the subsequent air cooling after each heating of the plates, showed that after each heating process the average recorded temperature increased by a few degrees.

Authors thank the accompanying Ministry of Education and Science of the Russian Federation for his excellent support. The research was funded in the program «Michail Lomonosov» of DAAD and Ministry of Education and Science of the Russian Federation. This assistance is gratefully acknowledged.

1. Lang, A. (1997) Schweissen von Aluminiumwerkstoffen im Fahrzeugbau. In: *Jahrbuch Schweisstechnik*.
2. Ostermann, F. (2007) *Anwendungstechnologie Aluminium*. Berlin; Heidelberg: Springer.

3. Cam, G., dos Santos, J.F., Kocak, M. (1997) *Laser and electron beam welding of Al-alloys*: Rev. Geesthacht: GKSS-Forschungszentrum.
4. Brune, E. (2005) Schweisser Maschinenmarkt. *Schweissen von Aluminiumwerkstoffen*, 106(**25**/**26**).
5. Thomy, C., Seefeld, T., Vollertsen, F. (2005) Schweissen mit Hochleistungsfaserlasern. *Werkstatttechnik*, **10**, 815–820.
6. Ploshikhin, V. et al. (2005) Integrated mechanical-metallurgical approach to modeling solidification cracking in welds. In: *Hot cracking phenomena in welds*. Berlin: Springer.
7. Clyne, T.W., Davies, G.J. (1981) The influence of composition on solidification cracking susceptibility in binary alloy systems. *British Foundry*, **74**, 65.
8. Feurer, U. (1977) Influence of alloy composition and solidification conditions on dendrite arm spacing, feeding and hot tearing properties of aluminum alloys. In: *Proc. of Int. Symp. on Engineering Alloys* (Delft, The Netherlands), 131–145.
9. Piwonka, T.S., Flemings, M.C. (1966) Pore formation in solidification. *Transact. of Metallurg. Soc. of AIME*, **236**, 1157.
10. Prokhorov, N.N. (1952) *Hot cracking during welding*. Moscow: Mashgiz.
11. Bochvar, A.A., Rykalin, N.N., Prokhorov, N.N. et al. (1960) On problem of «hot» (crystallization) cracks. *Svarochn. Proizvodstvo*, **10**, 5–7.
12. Prokhorov, N.N. (1962) Technological strength of metals at crystallization during welding. *Ibid*., **4**, 1–8.
13. Rappaz, M., Drezet, J.-M., Gremaud, M. (1999) A new hot-tearing criterion. *Metallurg. and Materials Transact. A*, **30**, 449–455.
14. Coniglio, N. (2008) *Aluminum alloy weldability*: *Identification of weld solidification cracking mechanisms through novel experimental technique and model development*: BAM-Diss. Berlin.
15. Shibahara, M., Serizawa, H., Murakawa, H. (2000) Finite element method for hot cracking analysis under welding using temperature-dependent interface element. In: *Modeling of casting, welding and advanced solidification processes IX*. Aachen: Shaker, 844–851.
16. Shibahara, M., Serizawa, H., Murakawa, H. (2001) Finite element method for hot cracking analysis using temperature-dependent interface element. In: *Mathematical modeling of weld phenomena 5*. London: IOM Commun., 253–267.
17. Bergmann, H.W., Hilbinger, R.M. (1998) Numerical simulation of centreline hot cracks in laser beam welding of aluminum close to the sheet edge. In: *Mathematical modeling of weld phenomena 4*. London: IOM Commun., 658–668.
18. Hilbinger, R.M., Bergmann, H.W., Koehler, W. et al. (2001) Considering of dynamic mechanical boundary conditions in the characterization of a hot cracking test by means of numerical simulation. In: *Mathematical modeling of weld phenomena 5*. London: IOM Commun., 847–862.
19. Hilbinger, R.M. (2000) *Heissrissbildung beim Schweissen von Aluminium in Blechrandlage*. Bayreuth: Universitaet Bayreuth.
20. Vasiliev, V.I., Illiashchenko, D.P., Pavlov, N.V. (2010) *Introduction to fundamentals of welding*. Tomsk: TPU.
21. Lindenau, D. (2007) *Magnetisch beeinflusstes Laserstrahlschweissen*: Diss. Stuttgart.
22. Goebel, G. (2007) *Erweiterung der Prozessgrenzen beim Laserstrahlschweissen heissrissgefsshrdeter Werkstoffe*: Diss. Dresden.
23. Rapoport, E.Ya. (1993) *Optimization of processes of induction heating of metal*. Moscow: Metallurgiya.
24. Grigoriants, A.G., Shiganov, I.N., Chirkov, A.M. (2004) *Hybrid laser welding technology*: Handbook. Moscow: N.E. Bauman MGTU.
25. Korshikov, S.E., Zaikina, N.V., Rybalko, G.S. (2010) Simulation of temperature fields and thermal stresses during heating of aluminum billets rotated in the direct current magnetic field. In: *Bull. of Samara STU*, **2**.

METALLURGICAL PECULIARITIES OF PLASMA-ARC WELDING OF CHROME-BRONZE

V.M. ILYUSHENKO[1], **Yu.G. NOVOSELTSEV**[2] and **S.L. BUSYGIN**[2]
[1]E.O. Paton Electric Welding Institute, NASU
11 Bozhenko Str., 03680, Kiev, Ukraine. E-mail: office@paton.kiev.ua
[2]Siberian Federal University
26 Kirenski Str., 660074, Krasnoyarsk, RF. E-mail: rector@kgtu.runnet.ru

Arc welding of parts from chrome-bronze is related with weld metal susceptibility to hot cracking. Given are the results of investigations on finding the measures for prevention of formation of hot microcracks in metal of chrome-bronze BrKh08 welds of large thickness performed by plasma-arc welding. It is shown that the main reason of defect formation in the weld metal is entry of air oxygen in plasma arc that results in intensive oxidation of chromium in a weld pool and transfer of weld metal to zone of maximum brittleness of Cu–Cr alloys. Considering that one slag coverage is not enough for large volume of liquid metal pool formed in plasma-arc welding over the flux layer using powerful modes (I_w = 1000–1400 A, U_a = 48–55 V) in order to obtain quality weld, additional alloying of weld metal by chromium and small additions of titanium being efficient deoxidizer is concluded to be reasonable. Special filler wire of PPBrKhT 12-2 grade was developed for this purpose. Its application in combination with selected flux allowed successfully solving the task of industrial manufacture of moulds for metallurgical electro-furnaces. 9 Ref., 5 Figures.

Keywords: *chrome-bronze, plasma-arc welding, solidification, structure, cracks*

Obtaining of quality welds in manufacture of large-size welded structures from chrome-bronze BrKh08, such as moulds of electrometallurgic furnaces, requires providing of initial thermal conditions for metal heating up in order to form weld pool. Limited power capacity of simple arc welding does not allow compensating a heat transfer into metal being welded and, as rule, requires application of preliminary and concurrent heating. This disadvantage was removed in development [1–3] of process of plasma-arc welding of copper and chrome-bronze which allows providing significant specific heat input into welded joint and regulating power and gas-dynamic parameters of plasma jet in a wide range.

Plasma gas is tangentially entered in plasmatron for plasma jet stabilizing that promotes vortex condition of gas flow and entering of certain amount of air in arc zone. This, in turn, results in liquid metal oxidation, due to which chromium being present in a base metal (BM) (0.8–1.2 %) burns out in the weld pool up to 0.1–0.2 %, and weld metal enters in the zone of maximum brittleness (Figure 1). Hot microcracks (Figure 2) are initiated in the formed weld metal. They are not detected by X-ray penetrant fluid and dye penetrant methods of testing, but develop and

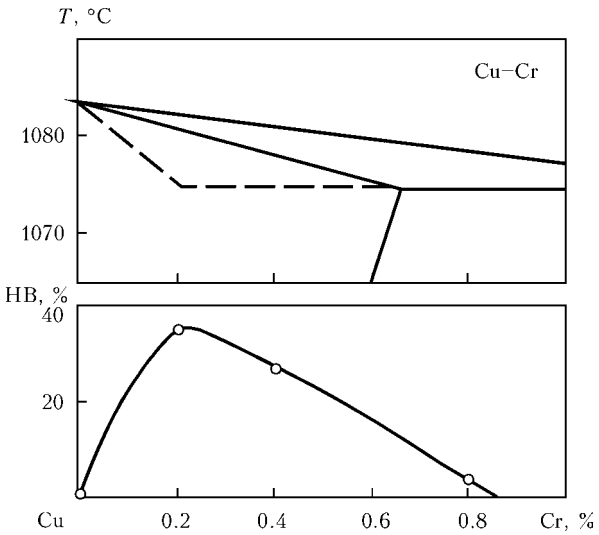

Figure 1. Effect of chromium on threshold of hot brittleness (HB) of alloys of Cu–Cr system [4]

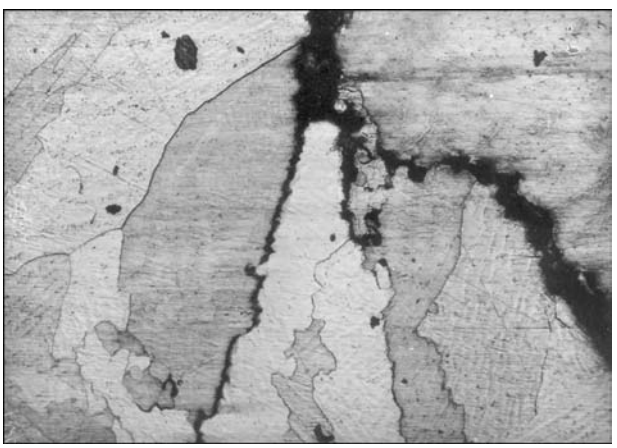

Figure 2. Microcracks in metal of weld on bronze BrKh08 (×300)

appear in further technological operations accompanied by deformations and heating of part.

Estimation of susceptibility to crack formation of Cu–Cr alloys with different chromium content performed on procedure, described in work [5], using specimens of «fishbone» type, showed that the metal with chromium content in 0.5–1.0 % limits (Figure 3) has the minimum susceptibility to crack formation.

It is known that margin of technological strength in welding (resistance to hot crack formation) depends on relationship of three characteristics, i.e. brittlement temperature range (BTR), strain capability in this interval, and intensity of increment of plasto-elastic deformation with temperature reduction (rate of strain).

BTR value is determined by chemical composition of alloy, dendritic segregation, dimension and size of crystallites, rates of cooling and strain. Approximately, it can be evaluated on constitutional diagram considering solidification nonuniformity and effect of impurities. Ductility of alloy in BTR depends on ratio of volumes of solid and liquid phases, sizes and shape of crystallites, character of liquid phase distribution, chemical and corresponding structural microinhomogeniety and strain rate.

Strain rate is determined by thermal coefficient of linear expansion, rigidity of welded joint, character of temperature distribution (determining the level of strain concentration) as well as forming of parts being welded.

Analysis of cracks, formed in plasma-arc welding of copper and chrome-bronze, showed that they are intercrystalline with oxidized surface and have solidification character. Investigations performed at the E.O. Paton Electric Welding Institute showed that solidification cracks were induced by presence of detrimental impurities (bismuth, tellurium, sulfur, oxygen etc.) [5, 6]. Negative effect of these impurities is conditioned by their general physical-chemical properties, i.e. limited solubility in copper, formation of fusible eutectics, surface activity in relation to copper. Therefore, mechanism of influence of detrimental impurities on susceptibility to formation of solidification cracks is related with effect of adsorption decrease of ductility and strength (mechanism of liquid-metal brittleness) [7].

Rapid increase of concentration of detrimental impurities took place at last stages in solidification of single-phase alloy and work on crack nucleation is reduced due to their surface activity. In solidification of binary-phase alloy, liquid is still remaining at the last stage and no enrichment with detrimental impurities takes place. Therefore, copper is necessary to be alloyed by elements promoting formation of binary-phase alloy, for example, chromium in specific concentrations, in order to increase resistance to formation of solidification crack.

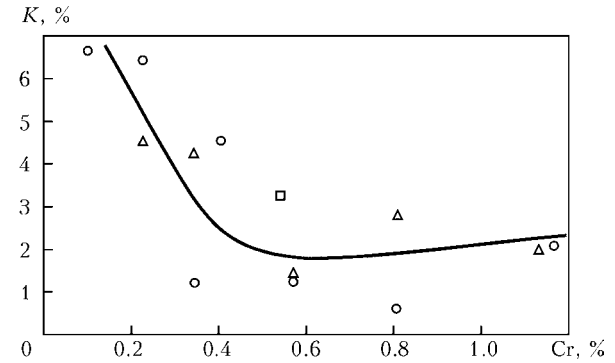

Figure 3. Dependence of technological strength of chrome-bronze on chromium content

Chromium has limited solubility in copper in solid solution (chromium solubility achieves 0.65 % at 1072 °C temperature of eutectic) and being one of the elements insignificantly reducing electric- and heat conduction of copper [8]. Therefore, compensation of waste of chromium and additional alloying of weld metal in such a way that chromium content in it being at the level of BM is necessary in plasma-arc welding of chrome-bronze for prevention of formation of solidification cracks. It also to be noted that chromium is efficient conditioning agent (Figure 4), that reduces enrichment of grain boundaries with detrimental impurities.

Special filler flux-cored wire PPBrKhT 12-2 [2] containing around 10–15 % Cr, which provides necessary additional alloying of the weld metal by chromium, was developed for compensation of chromium waste. Entering of 1.5–3.0 % Ti (efficient deoxidizing agent) in the wire promotes deoxidation of metal of weld pool, as well as reduction of chromium waste. Besides, as follows from results of investigation [9], microalloying of welds of chrome-bronze BrKh08 by 0.04–0.07 % Ti also increases their crack resis-

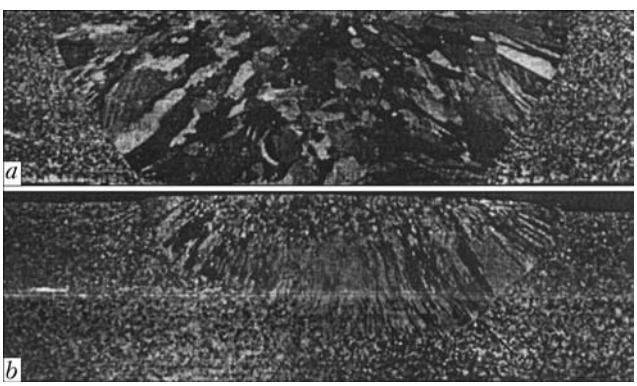

Figure 4. Microstructures of metal of weld from BrKh08 bronze with 0.2 (*a*) and 1.2 (*b*) % Cr

Figure 5. Mould for vacuum electric-arc melting titanium ingots of bronze BrKh08 40 mm thick

tance and rises strain capability of the welded joints.

The simplest method of feeding of filler wire in welding zone under manufacture conditions is its laying along the joint with further filling up by flux layer.

Considering that plasma-arc welding of copper and chrome-bronze of large thicknesses (up to 40–50 mm) is made on powerful modes (I_w = = 1000–1400 A, U_a = 48–55 V) and formed liquid metal pool has significant dimensions (more than 80 × 160 mm for 40 mm thickness metal), protection of such volume of molten metal from air influence is not simple task. Solving it by additional gas shield at the expense of plasmatron structure being already sufficiently complex is not easy. Besides, increase of consumption of inert gas for protection of molten metal from air results in its splashing from the pool. In this connection, plasma-arc welding is carried out over the flux layer, height of which makes 15–20 mm. Binary mixture of fluxes of AN-26 and AF-4A grades in 10:1 ratio was selected in experimental way, where addition of chloride flux slaking refractory oxide film Cr_2O_3 improves separability of slag crust.

Industrial technology of plasma-arc welding of chrome-bronze of large thicknesses, which was successfully mastered in manufacture of unique welded moulds of metallurgical electro-furnaces (Figure 5) was developed on the basis of investigations performed.

1. Ilyushenko, V.M., Sedov, V.E., Anoshin, V.A. (1977) Improvement of technology of plasma-arc welding of parts from copper and chrome-bronze. *Svarochn. Proizvodstvo*, **11**, 31–32.
2. Gurevich, S.M. (1981) *Reference book on welding non-ferrous metals*. Kiev: Naukova Dumka.
3. Novoseltsev, Yu.G. (2008) *Technological peculiarities of plasma welding of large dimension structures from copper and its alloys*. Krasnoyarsk: KGU.
4. Novikov, I.I. (1966) *Hot brittleness of non-ferrous metals and alloys*. Moscow: Nauka.
5. Ilyushenko, V.M., Anoshin, V.A., Bondarenko, A.N. et al. (1980) Study of effect of impurities and alloying elements on hot crack formation in copper welding. In: *Proc. of 1st All-Union Conf. on Relevant Problems of Welding of Non-Ferrous Metals*. Kiev: Naukova Dumka, 217–221.
6. Ilyushenko, V.M., Anoshin, V.A., Zherdev, A.M. et al. (1985) About effect of impurities on susceptibility to crack formation in copper welding. In: *Proc. of 2nd All-Union Conf. on Relevant Problems of Welding of Non-Ferrous Metals*. Kiev: Naukova Dumka, 335–337.
7. Glikman, E.E., Goryunov, Yu.V. (1978) Mechanism of liquid metal brittleness and other developments of Rehbinder effect in metallic systems. *Fiz.-Khimich. Mekhanika Materialov*, **4**, 20–30 .
8. Smiryagin, A.P. (1956) *Inductrial non-ferrous metals and alloys*. Moscow: Metallurgizdat.
9. Shipulin, A.P., Zobnina, G.K., Bosak, L.K. et al. (1974) Effect of titanium on weld metal plasticity in submerged arc welding of BrKh08 alloy. *Svarochn. Proizvodstvo*, **4**, 25–27.

Received 13.02.2013

INFORMATION SYSTEMS FOR SELECTION OF ARC WELDING PROCESS PARAMETERS (Review)

O.V. MAKHNENKO and **I.I. PRUDKY**
E.O. Paton Electric Welding Institute, NASU
11 Bozhenko Str., 03680, Kiev, Ukraine. E-mail: office@paton.kiev.ua

Existing software programs allowing selection of optimal technological parameters of arc welding of structural steels are considered. Analysis of advantages and drawbacks of the considered software programs in terms of their application by a welding technologist for development of a welding technological process in production was carried out. As to their functional capabilities, the considered software programs belong to different groups of software products. Software «Vertical» with module «System for Calculation of Welding Parameters» belongs to the CAD group. Software programs «Magsim», «System for Computer Analysis of Weldability of Steels», «VirtualARC», «Welding Simulation Suite» and «Simufact Welding» can be regarded as specialised engineering analysis systems for simulation of technological processes. This group of the software products includes commercial general-application software programs for finite element analysis, such as «Abagus», «Ansys», «LS-Dyna», «Catia» etc., which are close to the special systems in their functional capabilities of simulation of the welding and heat treatment technological processes. Purposes of further upgrading of the computer systems developed by the E.O. Paton Electric Welding Institute for selection of consumables for arc welding of structural steels were formulated on the base of analysis of advantages and drawbacks of the best known software products in the field of modelling of the welding technology. 17 Ref., 10 Figures.

Keywords: *software, mathematical modelling, technological process, welding, welding consumables, heat treatment*

The current scientific and technical progress has led to a wide application of computer technologies at a stage of preparation of production. Many special software products allowing virtual reproduction of various technological processes are being developed all over the world.

Reduction of the terms of development and increase of requirements to the quality of fabrication of welded structures resulted in the elaboration of a number of computer programs that facilitate and accelerate the efforts of the welding engineer or welding technologist in design of new welded structures and welding technologies. These software products can be conditionally subdivided into two main groups: systems for computer-aided design of technological processes (CAD TP), which as a rule are integrated with the 3D modelling systems for addressing design problems, and engineering analysis systems for simulation of the welding technological processes.

The E.O. Paton Electric Welding Institute developed the «Arcweldsys» welding software (system for selection of consumables for arc welding of structural steels), which is intended for reduction of the scope of experiments on specimens in selection of welding consumables for a specific welded joint by using the mathematical modelling tools [1]. This article analyses advantages and drawbacks of the best known software products in the field of modelling of the welding technology and formulates the purposes of further upgrading of the computer system developed by the E.O. Paton Electric Welding Institute for selection of consumables for arc welding of structural steels.

The CAD TP group includes software «Vertical» with module «System for Calculation of Welding Parameters» (Figures 1 and 2) developed by the «Ascon» Company (Russia) for integrated automation of the work performed by

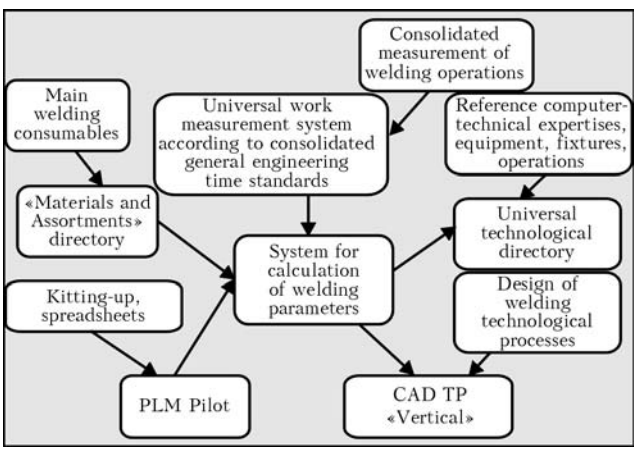

Figure 1. Schematic diagram of module «System for Calculation of Welding Parameters»

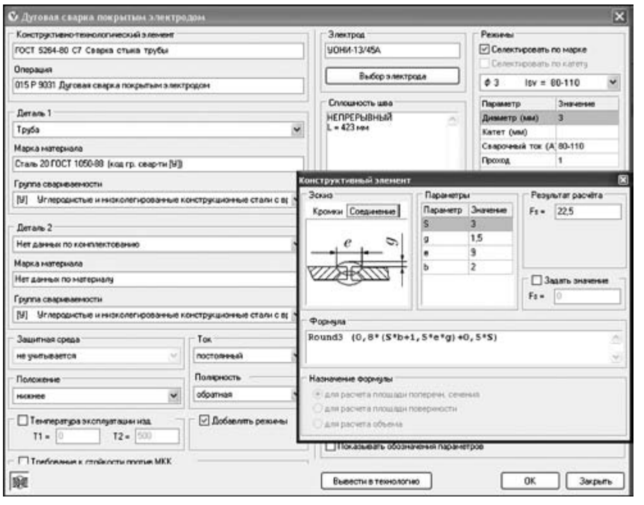

Figure 2. «Vertical» software window

the welding technologist in design of the welding technological processes [2–4]. The earlier installed 3D modelling system «Compass» or other similar system is required for operation of CAD TP «Vertical». The module operates in the CAD structure and solves the following problems: computer-aided selection of parameters for the main welding processes, computer-aided selection and calculation of the rate of consumption of welding consumables, and calculation of consumption of the power and main time for a manufacturing step.

In design of the welding technological processes and selection of the process parameters, the module allows for structural elements of the welds, position of the weld in space, materials used, characteristics of the equipment and other necessary parameters. The method of welding of parts can be specified for the entire weld or separately for each welding pass. The possibility exists of automated selection of welding consumables allowing for the requirements to intercrystalline corrosion and conditions of operation of a welded structure.

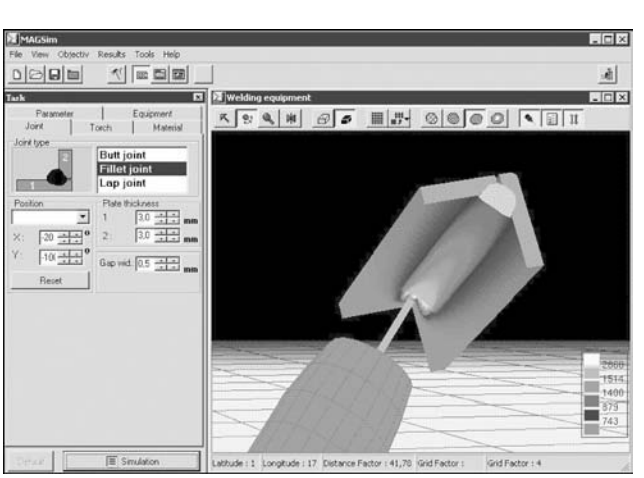

Figure 3. «Magsim» software window

Selection of welding consumables and technological parameters of welding is performed on the basis of the information bank of knowledge that includes corresponding directories «Materials and Assortments» and «Universal Technological Directory» (see Figure 1). In fact, the module is a calculation-information system, which is not intended for modelling of the welding process. Large quantity of service functions that facilitate drawing up of the documents on a welding technological process makes this software very convenient for the welding technologist in production. Drawbacks of software «Vertical» with module «System for Calculation Welding Parameters» include the probability of problems in selection of the welding technological parameters in a case of using new consumables or welding methods, for which the data and knowledge bases have no data, as well as the high labour intensity and cost of application of this system in production related to the need to install the 3D modelling system and CAD TP «Vertical», which also adds to the high cost.

Software «Magsim» (Figure 3) for numeric analysis, diagnostics and parametric optimisation of the gas metal arc welding process was developed as a result of the collaborated investigations conducted by the Tula State University (Russia) and the Aachen Technical University (Germany) [5–7]. Software «Magsim» can be classed with the engineering analysis systems for simulation of the technological processes. This software allows the welding engineer to simulate the effect of the welding process parameters on the quality of formation of a welded joint in order to reduce the quantity of experimental specimens. The software makes it possible to statistically estimate the effect of deviations of the technological parameters during welding on the quality of the weld, as well as automatically define the optimal parameters.

The main drawback of «Magsim» is that the welding simulation results are limited only to the problem of formation of a welded joint, although for development of the welding technology in production, in addition to this information, the welding engineer also needs other technological data, such as mechanical properties of the welded joint, risk of formation of hot and cold cracks, etc.

The highest-capacity specialised system for simulation of the welding and heat treatment technological processes is a package of the software products joined into the «Welding Simulation Suite» rule box [8, 9]. The developer of this system is French Company «ESI Group»,

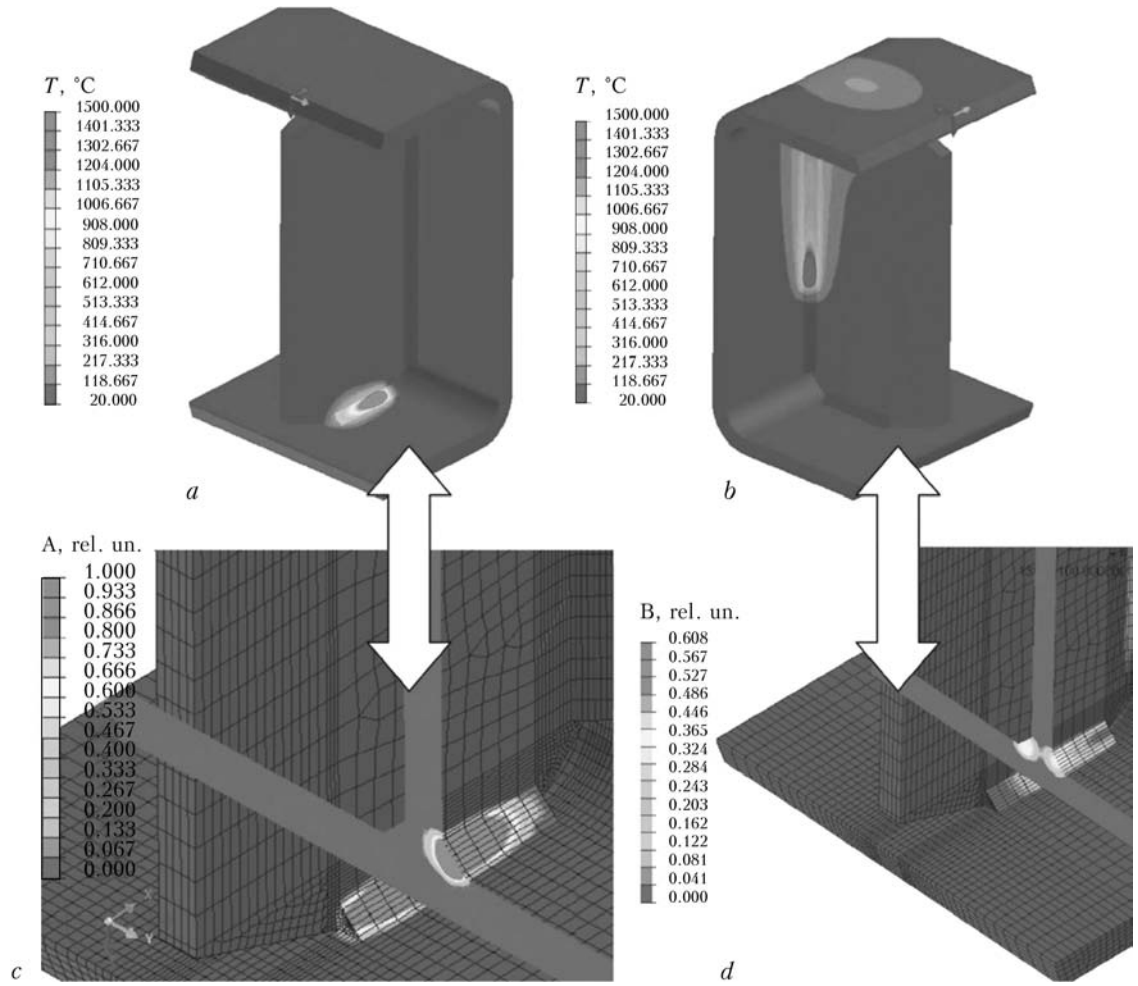

Figure 4. Results obtained with software «Sysweld/Visual-Weld»: *a*, *b* — distribution of thermal fields; *c*, *d* — relative content of austenite (A) and bainite (B) in weld

which is one of the leaders in development of CADs and simulation of the technological processes. The said software package includes:

- software «Sysweld/Visual-Weld» for simulation of the local regions of welded structures;
- software «Weld Planner» for simulation of the process of welding of thin-sheet structures;
- software «Pam-Assembly» for simulation of the processes of assembly-welding of large-size structures of a complex geometry.

Software «Sysweld/Visual-Weld» allows simulating welding and heat treatment processes, temporary and residual stresses and strains in a weldment or welded structure, mechanical characteristics and strength of the materials subjected to technological processing (Figure 4). Simulation of the welding processes includes all types of the welding technologies allowing for mechanical, thermal and metallurgical properties of materials. The models and data bases included into software «Sysweld/Visual-Weld» allow the thermal-metallurgical processes to be analysed for steels and aluminium alloys. The software operates with the thermokinetic diagrams describing the phase transition process (Figure 5).

The software has the possibility of developing a geometric model of a weldment or welded structure built in some CAD environment. Results of the calculations, including on stresses and strains, can be exported for further calculations to other calculation modules developed by the «ESI Group» Company, such as:

- «Systus» for investigation of initiation and propagation of fatigue cracks;
- «Pam-Stamp» for analysis of the process of stamping of welded sheet parts;
- «Pamcrash» for analysis of fractures in welded structures.

Software package «Welding Simulation Suite» is characterised in many cases by excessive capabilities and complexity for the welding engineer in production, requires special knowledge on application of calculation methods and long-time training of a user, and has a high cost.

Module «Simufact Welding» [10] is another specialised system for simulation of the welding processes. It is included into system «Simufact» (Simufact Engineering GmbH, Germany) [11] for general engineering analysis of different technological processes. First of all, this module is

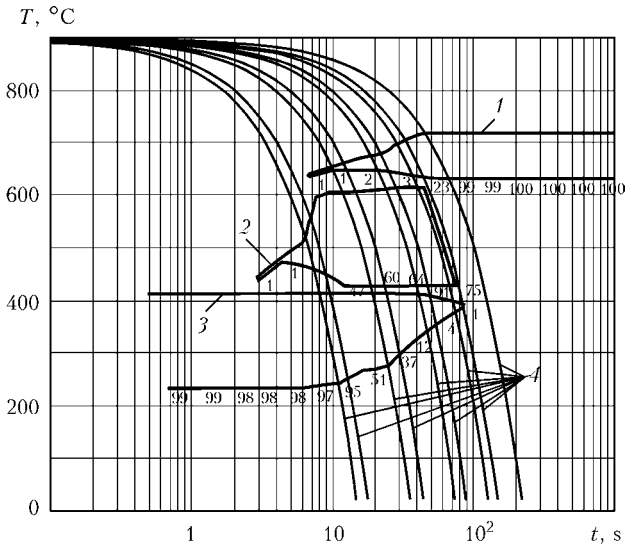

Figure 5. Presentation of thermokinetic diagram in software «Sysweld/Visual-Weld»: *1–4* — phases 1–4, respectively

intended for prediction of welding distortions. Also, it allows evaluating properties of the penetration zone (PZ) and HAZ. The problem-oriented user interface helps the welding engineer to conduct sufficiently complicated simulation of the physical-metallurgical processes occurring during welding. The software is based on a combination of analytical approaches and non-linear numerical simulation. According to the developer's description, the software is characterised by the following functions:

- time-synchronised monitoring of operation of several welding robots;
- prompt calculation of different variants differing in welding parameters;
- prompt change of the welding process parameters (welding sequence and speed, welding heating parameters, and clamping conditions);
- optimisation of sizes and properties of FZ and HAZ, as well as the level of welding stresses and strains.

Advantages of software «Simufact Welding» include sufficiently wide capabilities of simulation of the welding process for prediction of the quality of formation of a welded joint, including the multi-pass one, and evaluation of properties of PZ and HAZ allowing for the transformation structures, as well as temporary and residual welding stresses and strains. Despite using the complicated mathematical models, the software is oriented to an engineering application in production. A distinctive feature of this software is the possibility of optimisation of robotic welding and monitoring of synchronised operation of welding robots in production.

Commercial general-application packages of finite element analysis, such as «Abaqus», «Ansys», «LS-Dyna», «Catia» etc., are close to the specialised systems in functional capabilities of simulation and modelling of the welding and heat treatment technological processes. The latest versions of some of these packages include the specialised calculation modules for simulation of the welding processes [12].

For example, «Abaqus» is not the specialised welding software, but it can be applied for simulation of moving heat sources and analysis of thermal and mechanical processes occurring during welding (Figure 6). Analysis of the thermal processes is carried out by means of the user subprograms [13]:

- «Dflux» is applied for determination of heat transfer in welding in a case of a concentrated heat flux, which moves along the welding line, by simulating movement of a welding heat source;
- «Gapcon» is applied for activation of heat conduction between the base and filler metals, when the welding source passes through a certain element;
- «Film» is applied for activation of heat conduction to simulate the cooling process, when

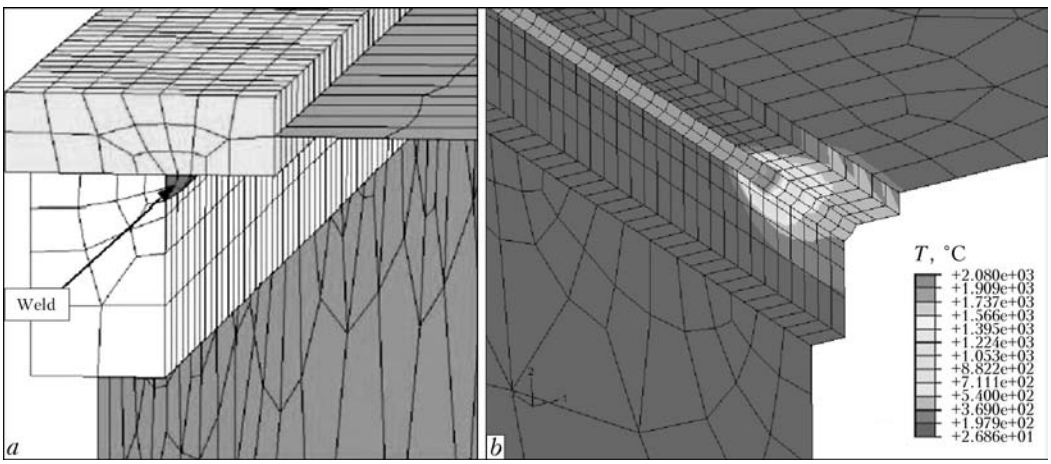

Figure 6. Software «Abaqus»: *a* — finite element model of weldment; *b* — distribution of thermal fields

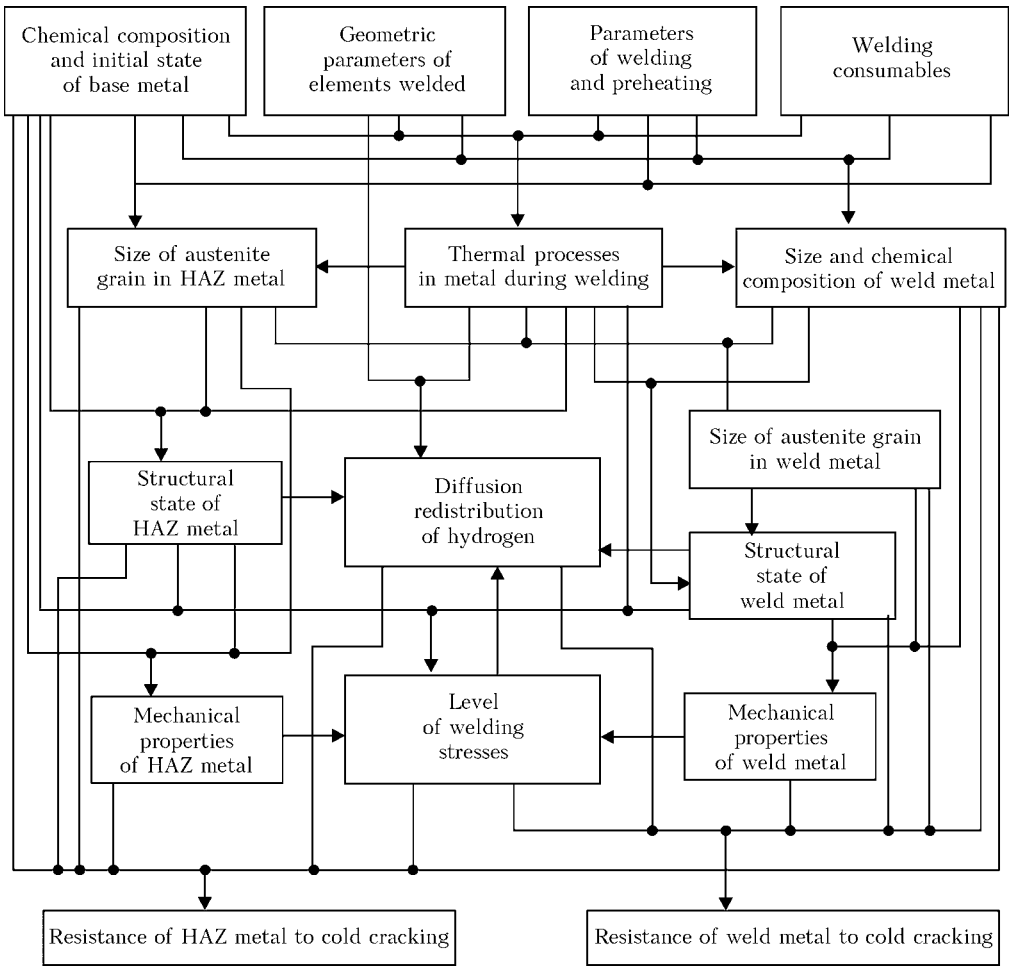

Figure 7. Schematic of interrelations of indicators of weldability of low-alloy steels with the processes occurring in metal during welding in software «System for Computer Analysis of Weldability of Steels»

the welding source passes through a certain element.

The thermal analysis results are used as the source data to solve the mechanical problem, yielding evaluation of welding stresses and strains. To simulate the thermal-metallurgical processes during welding it is necessary to develop in house or buy from a third developer the additional program modules, which allow for structural transformations occurring in steels during the welding temperature cycles. The drawbacks also include high complexity of the program, long-time training to operate it, and high cost. All these factors make software «Abaqus», as well as other commercial general-application finite element analysis software products, of little use for development of a welding technology by the welding engineer in production.

The N.E. Bauman Moscow State Technical University developed the «System for Computer Analysis of Weldability of Steels» (Figure 7) [14, 15], comprising the engineering part for prompt analysis of technological variants of welding of typical joints, which is implemented on the basis of software package «Weldability of Alloyed Steels» [16] and the data base on properties of materials.

Traditionally, selection of a rational variant of consumables for arc welding of modern structural steels involves a large quantity of experiments, in the course of which the comparative results are obtained on a number of parameters: conditions of formation and chemical composition of the weld metal or PZ, microstructure of the PZ and HAZ metals, susceptibility to hot cracking, standard mechanical characteristics (hardness, yield stress, tensile strength, elongation, reduction in area and impact toughness) in different regions of the welded joints, as well as special properties (long-time strength at corresponding temperatures, corrosion resistance, etc.). All this requires appropriate tests of each alternative variant of welding consumables and parameters for a specific base material. Considering a wide range of existing consumables for arc welding of structural steels, the substantiated experimental selection of a rational variant requires either a rich experience or numerous experiments.

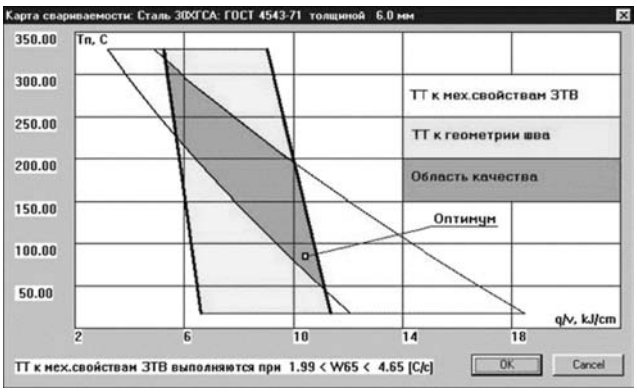

Figure 8. Plotting of the quality region in optimisation of thermal parameters of welding in software «System for Computer Analysis of Weldability of Steels»

Software «System for Computer Analysis of Weldability of Steels» makes it possible to considerably reduce the labour intensity in design of the welding technology and solve the problems of optimisation of technological parameters of the process of multilayer welding of low-alloy steels. Integrated analysis of technological variants of welding is carried out by modelling the set of the physical-metallurgical processes occurring in metal that form the weldability indicators. Optimisation of the thermal conditions of welding is performed to ensure the required combination of properties of the HAZ metal. Parameters of welding and edge preparation of the joints, which provide the preset sizes of the welds, as well as the preheating temperature to achieve the required structural state of the HAZ metal and resistance to cold cracking are determined at this stage of the calculations (Figure 8).

Software «System for Computer Analysis of Weldability of Steels» was developed with a purpose of more understandable modelling of the multilayer welding process for the welding engineer in production.

Software «Virtual ARC» (developer — Company «ABB», Switzerland), which is an efficient tool for selection of the MIG/MAG welding process equipment and parameters, was developed to facilitate adjustment of the robotic welding equipment under conditions of modern high-tech production. The software has a convenient graphical interface, combines 2D modelling, and comprises data of experimental measurements and neuron networks for prediction of formation of the weld in arc welding of low-carbon steels.

The results of modelling of physics of the arc, heat and mass transfer are used as the source data for the neural network to predict quality and size of the welds, as well as probable welding defects. According to the developer's data [17], the key functions of software «Virtual ARC» are as follows:

- planning of the technological process of MIG/MAG welding;
- adjustment of the MIG/MAG welding parameters;
- prediction of the weld shape and penetration;
- prediction of geometric parameters of the weld;
- prediction of geometric defects of welding;
- estimation of the cost of welding;
- formation of technological documents;
- optimisation of productivity and quality of the welding process.

Therefore, the main specialisation of software «Virtual ARC» is selection of the optimal welding equipment and parameters in terms of the quality formation of a welded joint in MIG/MAG welding of low-carbon steels (Figure 9). The drawbacks are that the software does not allow for structure and mechanical properties of the resulting welded joint. The class of low-carbon steels is another limitation of practical application of the software.

Early in the 2000s, the E.O. Paton Electric Welding Institute developed computer system «Arcweldsys» [1], which is intended for reduction of the scope of experiments on specimens in selection of alternative welding consumables for a specific welded joint by using the mathematical modelling tools and corresponding information support. As the source information, the system uses certificate data of a manufacturer of welding consumables concerning variants of the welding consumables recommended for arc welding of a given type of structural steel, arc welding parameters, deposition efficiency, and chemical composition of the deposited metal. These data are entered together with indication of the type of a structural steel welded (base metal) and its chemical composition into the system by a user (Figure 10).

As a result, the system gives the following information on each alternative variant to the user:

- size and shape of PZ for the root weld and subsequent passes (conditions of weld formation, risk of burn-through, etc.);
- chemical composition of the PZ metal;
- microstructural composition of the PZ and HAZ metals;
- mechanical properties (hardness, tensile strength, yield stress, elongation, reduction in area, impact toughness);

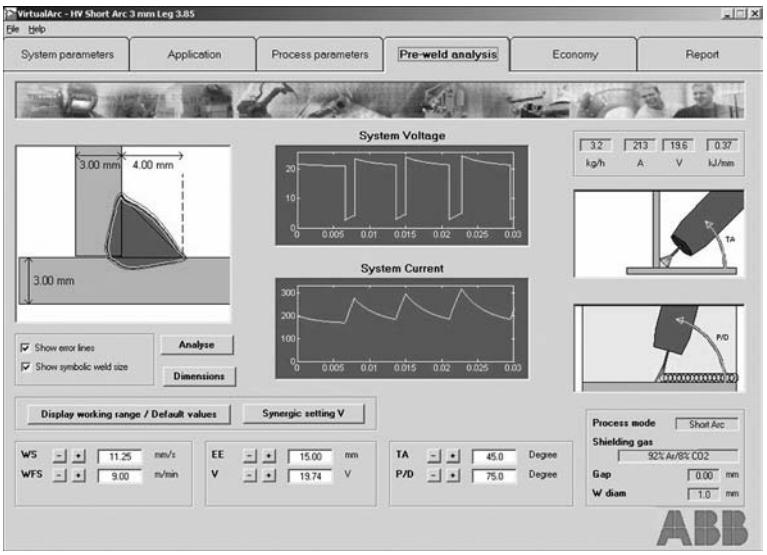

Figure 9. «Virtual ARC» software window

• *KCV* at temperatures of –20 – –70 °C in PZ and HAZ;

• risk of cold and hot cracking.

The following main drawbacks of the system were revealed in the process of its practical application: unsatisfactory accuracy of calculation of temperature fields in a case of welding at a high speed of the heat source due to using the calculation algorithms within the framework of the 2D problems, impossibility of modelling welding for such materials as stainless steel and aluminium and titanium alloys, and inconvenient software interface. At the same time, the system turned out to be rather efficient, found a number of customers in Ukraine, and was applied to perform numerous studies by specialists of the E.O. Paton Electric Welding Institute.

Based on considering advantages and drawbacks of the best known software products in the field of modelling of the welding technology, and as a result of analysis of the efficiency of application of the developed computer system, as well as allowing for the progress in modern computer engineering and calculation methods of mathematical modelling, physical-chemical and metallurgical processes occurring in welding, it was concluded that it would be expedient to further upgrade the existing version of the computer system. Such upgrading is performed on a base of redesign of mathematical models and calculation algorithms on determination of temperature fields (cycles) for different types of the welded joints, including through utilisation of 3D models, widening of the system application field to cover the class of stainless steels by adding new mathematical models and corresponding calculation algorithms on generation of extra information that is important for the welding engineer. This includes, for example, the degree of sensitisation of metal due to the welding cycle in multi-pass welding of stainless steels, updating and replenishment of data bases on properties of the base metal and welding consumables, including entering into the data bank the properties of materials, thermokinetic diagrams in the digital

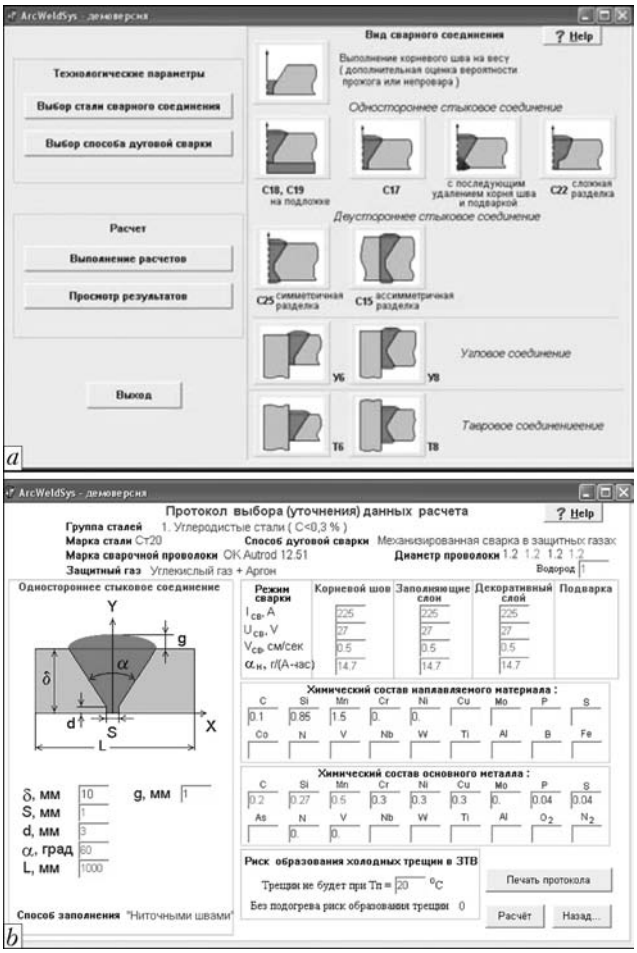

Figure 10. Interface of software «Arcweldsys»: *a* — main window; *b* — protocol of selection of calculation data

form for a more precise description of phase transformations during the thermal welding cycle, development of a more friendly and intuitively understandable user interface of the system with additional service functions for automatic drawing up of the technological documents.

Conclusions

1. Analysis of the software products available in Ukraine and abroad for modelling and simulation of the welding technology showed that now the welding engineer has high-capacity tools for design of welded structures and welding technologies.

2. The E.O. Paton Electric Welding Institute of the NAS of Ukraine developed specialised welding software «Arcweldsys» (system for selection of consumables for arc welding of structural steels), which is intended for reduction of the scope of experiments on specimens in selection of welding consumables for a specific welded joint by using mathematical modelling tools.

3. Comparison of advantages and drawbacks of the best known software products in the field of modelling of the welding technology resulted in the formulation of the purposes of further upgrading of the computer system developed by the E.O. Paton Electric Welding Institute for selection of welding consumables for arc welding of structural steels, which are meant for increasing the accuracy of the obtained prediction results and making it more convenient in operation for the welding engineer.

1. Makhnenko, V.I., Korolyova, T.V., Lavrinets, I.G. (2003) Computer system for selection of welding consumables for arc welding of structural steels. *The Paton Welding J.*, **2**, 12–17.
2. CAD TP «Vertical», module «System for calculation of welding parameters». *http*:www.ascon.kiev.ua
3. Gulyaev, V. (2012) Configurator of design-technological elements and welding parameters for CAD TP «Vertical». *Equipment and tool for professional*. Series Metal Treatment, **5**.
4. Gulyaev, V., Kharmats, I. (2008) Automation of design of welding technological processes. *SAPR i Grafika*, **4**, 90–92.
5. Magsim. *http*://comhightech.tsu.tula.ru/software/magsim-r.htm
6. Sudnik, V.A., Ivanov, A.V., Dilthey, U. (1999) Analysis of effective power of the pulsed arc in MAG welding by the mathematical modelling method with experimental verification. In: *Proc. of 2nd All-Russ. Sci.-Techn. Conf*. Tula: TulGU, 64–80.
7. Dikshev, I., Dilthey, U., Gollnick, J. et al. (2004) Die Simulationswerkzeuge des ISF: MAG-Sim, Beam-Sim, SimWeld. *Sitzung der DVS-Arbeitsgruppen I 1 und I 2*. 24.06.2004.
8. ESI Welding Simulation Suite. *http*://esirussia.ru/taxonomy/term/5
9. Bilenko, G. (2012) Modelling of welding processes in the ESI software products by an example of a locomotive part. *Metallurg*, **3**, 18–21.
10. Wohlmuth, M. (2011) Practical design of industrial welding processes. *Welding and Cutting*, **6**, 346–347.
11. SIMUFACT. WELDING. *http*://www.simufact.com
12. Pakos, R., Szymczak, M. (2010) Przeglad programow komputerowych do przewidywania odksztalcen i symulacji procesow spawalniczych na wczesnych etapach produkcji. *Przeglad Spawalnictwa*, **3**, 32–39.
13. Abaqus. *http*://abaqus.com
14. Makarov, E.L., Konovalov, A.V. (1995) System for computer analysis of weldability and welding technology of structural alloyed steels. *Svarochn. Proizvodstvo*, **3**, 6–9.
15. Konovalov, A.V. (2004) Software for numerical analysis of indicators of weldability of low-alloy steels in multilayer welding. *Nauka i Obrazovanie*, **10**.
16. Kurkin, A.S., Makarov, E.L. (2010) Software package «Welding» — a tool to solve the problems of welding production. *Svarka i Diagnostika*, **1**, 16–23.
17. VirtualARC. *http*://www.abb.ua

Received 10.01.2013

MODERNISATION OF ELECTRON BEAM WELDING INSTALLATION ELU-20

L.A. KRAVCHUK, A.V. KUSHNERYOV and **V.I. KOZHUKALO**
E.O. Paton Electric Welding Institute, NASU
11 Bozhenko Str., 03680, Kiev, Ukraine. E-mail: office@paton.kiev.ua

The electron beam welding installation of the universal type ELU-20, designed by National Institute of Aviation Technologies (NIAT, Russia), in most cases does not provide meeting the modern requirements, specified to the technology and equipment. On order of users the E.O. Paton Electric Welding Institute developed and created specialized complex for EBW with automatic systems of control and application of distributed computer systems on the base of the installation ELU-20. Such approach allowed realization of a number of technological capabilities on automatic control of parameters of welding electron beam, programmable movement and inclination of electron beam gun, visual programming of trajectory of a butt in the real time mode, during the operation of vacuum system of pumping-out. «Windows» as the oriented interface of the user provided graphical plotting and editing of programs for welding, 3D display of specimens of the product and trajectories of the butt during welding process. 2 Ref., 3 Figures.

Keywords: *electron beam installation, vacuum chamber, electron beam gun, pumping-out system, coordinate axes of movement, inclination and rotation, computer control, interface, video monitoring, focusing, programming of butt trajectory, master-program, cutoff voltage*

As the experience of application of the universal installation of ELU-20 type, designed by the NIAT, showed that the necessity in its modernization arose in most cases to meet the nowadays requirements of leading branches of industry. In the first turn it concerns the vacuum pumping-out system, high-voltage power source, welding EB gun, system of control of parameters of welding electron beam, system of butt tracking and visual monitoring of welding process and also mechanism of movement and inclination of a gun, loading carriage and rotators of a product.

On order of the user (OJSC «Motor Sich», Zaporozhie) at the E.O. Paton Electric Welding Institute a specialized complex on the base of installation ELU-20 was designed and manufactured for EBW with automatic control system (ACS) and using the distributed computer systems [1]. Such approach provided the realization of the following technological capabilities:

- movement along the five axes (three coordinates X, Y, Z for movement of EB gun, coordinate VG of inclination of a gun, axis of rotation of rotator);
- simultaneous synchronous movement along any three coordinate axes with linear interpolation;
- synchronous movement with control of parameters of welding electron beam;
- conductance of welding in both modes: automatic and manual welding;
- «Windows» is the oriented interface of the user providing graphical designing and editing of programs for welding, 3D display of specimens and trajectories of butt in the welding process;
- combining of several subprograms into one program;
- visual programming of a butt trajectory in manual, semi-automatic and automatic modes;
- automatic control of vacuum system and high-voltage power source;
- logging of all the commands of control and parameters of welding process in graphical and tabulated form;
- diagnostics of single subsystems (vacuum system, high-voltage power source, movement system, parameters of welding process).

Vacuum chamber of rectangular shape with inner sizes of 3000 × 2000 × 2000 mm (length × × width × height) and volume of 12 m^3 is equipped with one door, hinge-hanged up on the door suspension beam (Figure 1). The door can move along the beam using electric drive, opening the space for delivery of loading carriage to the position of welding. The front wall of vacuum chamber (on the side of welding operator) is equipped with inspection windows and also lighting and monitoring camera. On the rear wall the mechanisms of movement of welding EB gun along the coordinates X, Y, Z and gun inclination VG and also vacuum pumping-out system are located.

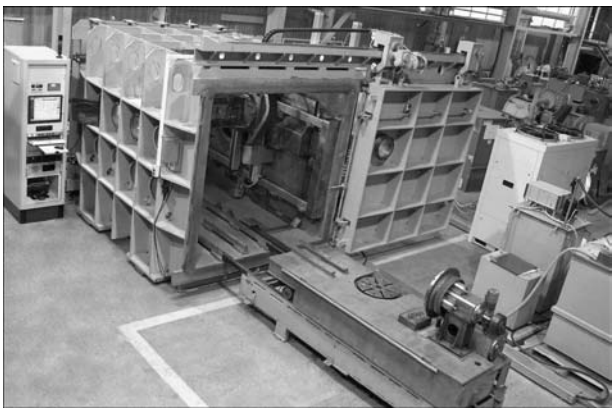

Figure 1. Appearance of EB installation ELU-20 after modernization

The unit of updated EB gun from the components of the equipment ELA-60B with a collector of secondary-emission signal of the video monitoring system RASTR [1, 2], turbomolecular pump, vacuum sensors and screen of thermal protection of a gun is mounted on the rotary beam for the gun inclination in the plane XZ (coordinate VG) (Figure 2). The movement of EB gun along the coordinates X, Y, Z is performed using linear modules. The control of movements is performed from the Siemens drive SINAMICS S210, providing the accuracy of positioning of not worse than ±0.05 mm. The application of ceramic high-voltage isolator and metallic tungsten cathode of 3 mm diameter in EB gun allowed obtaining the current of electron beam in the range 0–500 mA and life of cathode of not less than 40 h at accelerating voltage 60 kV.

The vacuum pumping-out system of the installation designed and manufactured on the base of modern vacuum equipment provides necessary rarefaction in welding chamber and EB gun in automatic mode at the computer control (Figure 3). The time of reaching the working pressure in the chamber ($1 \cdot 10^{-4}$ mm Hg) and gun ($5 \cdot 10^{-5}$ mm Hg) amounted to not more than 30 min. «Windows» as the oriented interface at the control on commands of welding operator allowed realizing the following operation modes of the vacuum system:

- «Pumping out» — the mode of pumping out of air from the vacuum chamber and gun both during preparation for welding as well as directly in the process of its fulfillment;
- «Expectation» — the guard mode allowing preserving safe state of the machine under vacuum at switched-on diffusion pumps;
- «Letting-up» — the mode of ventilation of vacuum chamber and gun before the ready state of opening the door of vacuum chamber;
- «Stop» — the mode of interruption of operation of vacuum system with switching-off of diffusion pumps;
- «Manual» — the mode of manual control of the equipment of vacuum system during search and elimination of failures;
- «Cold pumping-out» — switching-on of «Pumping» mode without switching-on of diffusion pumps.

The program of automatic control of vacuum system follows and displays the condition of the equipment on the screen of the monitor of ASC using designations of state of valves, shuttles and vacuum pumps.

To obtain the image of welding site on the ASC monitor in the real time mode the RASTR video-monitoring device was applied. The image of a surface of the item being welded is formed according to signals from the sensor of secondary-emission electrons, mounted on the EB gun in direct vicinity from the site of welding (see Figure 2). The clear image of welding process with formation of a face bead of weld is displayed on the ASC monitor and as compared to traditional optic monitoring systems it is not subjected to influence of vapors of the metal being welded. The application of additional computer which solves the problems of recognition of a butt on the image of product surface, obtained from the RASTR video monitoring device and also from human–machine interface, provided the fulfillment of functions of automatic visual designing of trajectory of a butt, correcting of butt deflection and tracking the butt.

«Windows» as the oriented interface of the user allows plotting the master-programs of welding process for different configurations of products in a form of diagrams and tables. The master-program can include up to five subprograms — «Cleaning», «Partial Tacking», «Full Tacking», «Welding», «Finishing Welding». In

Figure 2. Unit of modified welding EB gun with the mechanisms of movement along coordinates X, Y, Z and inclination on the coordinate VG

tables the values of welding current, focusing current, welding speed, value of operating distance from the end of EB gun to the product, type and amplitude of technological scanning, amplitude and direction of deflection of gun are preset. During performance of EBW process in the automatic mode the possibility of manual correction of the following parameters is foreseen: welding current in the limits of ±10 %, focusing current in the limits of ±5 % of the program mode. Welding according to the program can be performed in the mode of pulse current modulation with presetting the frequency of tracking the pulses and length of a pulse.

The subprogram «Cleaning» is applied for cleaning of surfaces of abutted edges of a product from contamination and oxides using sharp-focused low-power electron beam. The value of focusing current for location of electron beam focus on the surface of a product is determined using the video-monitoring system RASTR. The mode of cleaning using electron beam is usually performed at the speed of movement of 10 mm/s with a beam scanning around the circle of 10 mm diameter and welding current of 15 mA.

The interface of welding operator provides the possibility of presetting the two types of rotators: horizontal rotator W_x (horizontal axis of rotation) and vertical rotator W_z (vertical axis of rotation). During compiling and correcting of welding programs using rotators the speed of rotation and direction of rotation are indicated in the table.

The transition to software conductance of the process of EBW under shop conditions sets forth the more severe requirements both to equipment as well as to technological process. To provide the reproduction of geometry of welds the following procedure of testing the welding EB gun can be applied. Except of information about parameters of electron-optical system (accelerating voltage, beam current, focusing current, bombardment current, filament current) the monitor of ASC gives the value of cutoff voltage on the gun controlling electrode. On following the change in cutoff voltage for a definite value at a rated beam current, the welding operator can predict the working efficiency of tungsten thermal cathode and timely determine the need in its change.

Technical characteristics of electron beam installation ELU-20 after modernization

Dimensions of the installation, mm:	
length	9000
width	7700
height	3100
Inner sizes of vacuum chamber, mm:	
length	3000
width	2000
height	2000
Working pressure in vacuum chamber, mm Hg	not more than $1 \cdot 10^{-4}$
Working pressure in EBG, mm Hg	not more than $1 \cdot 10^{-5}$
Time of reacheng the of working pressure in vacuum chamber and EBG, min	not more than 30
Time of letting the air into vacuum chamber, min	2
Movement of EBG along the coordinates, mm, not less than:	
X–X	2000
Y–Y	900
Z–Z	800
Time of movement of EBG along coordinates X–X, Y–Y, Z–Z, mm/s	1.66–25
Accuracy of EBG positioning along coordinates X–X, Y–Y, Z–Z, mm	±0.05
Angle of EBG rotation in the plane XOZ, deg	0–90
Number of rotators for products being welded, pcs:	
with horizontal axis of rotation	1
with vertical axis of rotation	1
Speed of rotation of faceplates of rotators, rpm	0.06–12
EBG and equipment ELA-60B:	
accelerating voltage, kV	60
range of adjustment of welding current, mA	0–500
working distance of electron beam, mm	100–400
frequency of technological scannings of beam, Hz	not more than 1000
angle of beam deflection, deg	±3.5
operation life of cathode, h	40
welding in pulse mode at frequency, Hz	5–600
RASTR system of monitoring and tracking of butt:	
accuracy of alignment of electron beam with butt, mm	±0.1
magnification of the object being monitored	×5

Figure 3. Vacuum system of pumping out of installation ELU-20 with off-line water cooling of vacuum pumps, EB gun and power source («Lahntechnik» chiller of the type BL-365-16, Germany)

1. Paton, B.E., Nazarenko, O.K., Nesterenkov, V.M. et al. (2004) Computer control of electron beam welding with multi-coordinate displacements of the gun and workpiece. *The Paton Welding J.*, **5**, 2–5.
2. Nazarenko, O.K., Shapoval, V.I., Loskutov, G.A. et al. (1993) Monitoring of EBW process and automatic butt tracking. *Avtomatich. Svarka*, **5**, 35–38.

Received 24.01.2013

MACHINES BASED ON LATHES FOR MILL ROLL SURFACING

V.I. TITARENKO, V.N. LANTUKH and **A.S. KASHINSKY**
SPE REMMASH Ltd.
74 Sovkhoznaya Str., 52005, Yubilejny, Dnepropetrovsk distr., Ukraine. E-mail: remmash_firm@ukr.net

Enterprises of a number of industries periodically need application of automatic arc surfacing for repair of wearing parts and components with using specialized machines. The work deals with approaches applied by a small enterprise in development and manufacturing of welding-surfacing equipment based on lathes of various types. Examples of fitting such machines and their application in surfacing of mill rolls are given. Upgrading and retrofitting of surfacing equipment fleet in this case involve minimum expenditure. 3 Ref., 6 Figures.

Keywords: *arc surfacing, worn parts and components, specialized machines, lathe, design and manufacture, upgrading, mill rolls*

Automatic arc surfacing is extensively applied in many industrial enterprises, so that the problem of replacement of completely rundown surfacing machines or expanding their fleet is urgent now. There is practically no serial production of such machines, and some enterprises apply surfacing machines based on lathes of various types for these purposes. Lathe type is selected, depending on the purpose and dimensions of the surfaced parts. Machines are fitted with automatic welding machines of A-1406, A-1416 type, and rectifiers with respective parameters [1, 2].

SPE REMMASH specializing in development and manufacture of welding-surfacing equipment, over the recent years has accumulated experience of development and upgrading of machines for mill roll surfacing, cooperating successfully with metallurgical plants of Ukraine. Development and manufacture of such surfacing equipment was performed using approaches applied by REMMASH in development of any installation [3]:

- analysis of current surfacing technology of the potential customer, development of its improvement variants with application of new surfacing consumables;
- analysis of the currently available similar machines;
- application of modular principle of machine fitting;
- more concrete determination of machine parameters to suit customer requirements;
- incorporating the principles of versatility into the machine;
- maximum fitting of the machine with required auxiliary equipment and rigging;
- maximum involvement of partner enterprises in equipment design and manufacture;
- involvement of customer specialists in the process of equipment development and manufacture.

Application of these approaches enables REMMASH performing «turnkey» manufacturing and commissioning of surfacing machines based on lathes in a short time.

As an example we can mention upgrading of the machine for surfacing rolls of billet mills of OJSC F.E. Dzerzhinsky DMK (Dneprodzerzhinsk, Ukraine). Before that rolls of these mills had been surfaced for a long time using surfacing machine based on roll-turning machine, developed internally by the works. Many years of operation led to extensive wear of the main components of the machine that resulted in a considerable lowering of surfacing operation quality.

Specialists of REMMASH and Chief Millman Service of OJSC Dneprovsky Metallurgical Works developed the concept and technical assignment (TA) for upgrading the currently available surfacing machine. TA defined the following main tasks:

- base roll-turning machine should be used only for fastening and rotation of mill rolls being surfaced;
- automatic surfacing machine should be fixed and should move in the mechanism, having no rigid mechanical coupling with the roll-turning machine; possibility of their removal from the zone of operation of hoisting mechanism for roll positioning and taking off should be envisaged;
- system of surfacing process control should incorporate a mechanism of automatic displacement of automatic surfacing machine nozzle for surfacing pass width;

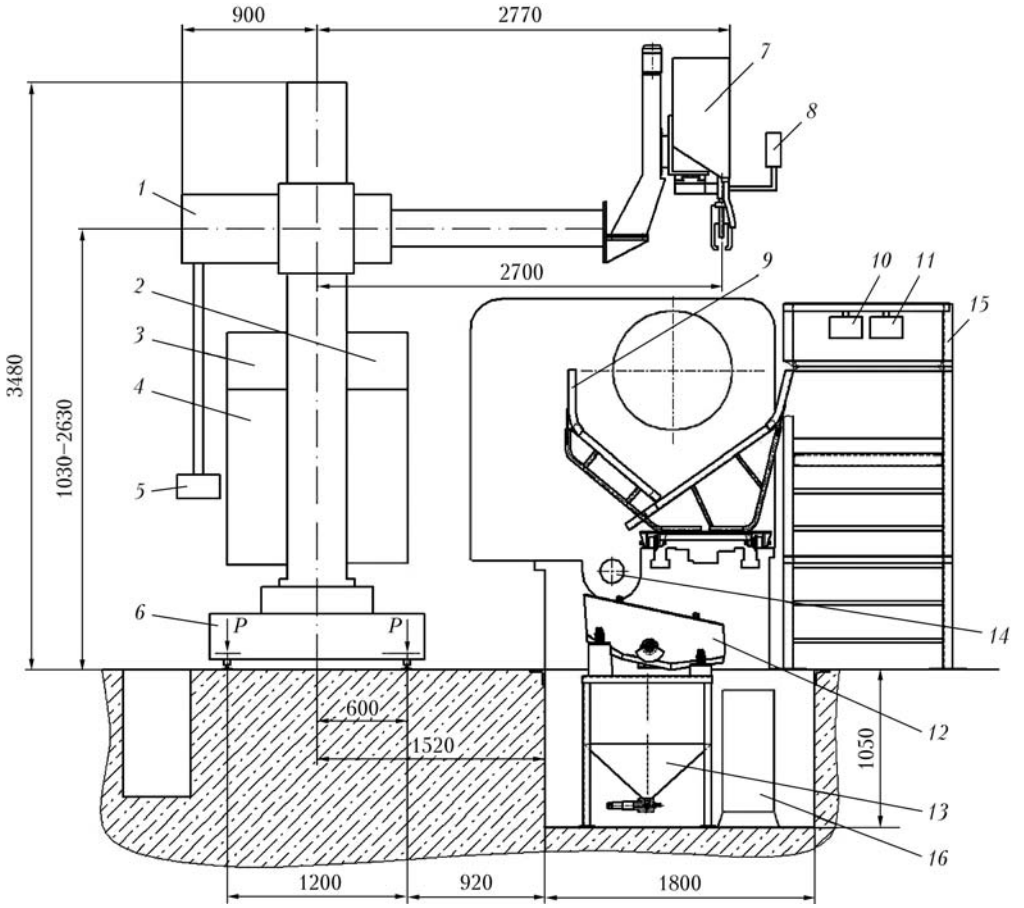

Figure 1. Schematic of upgraded machine for surfacing mill rolls of billet mills (here and in Figures 3, 5 and 6 for designations see the text)

• device for flux collection and feeding should ensure removal of unused flux, its cleaning from slag crust and reliable feeding into the flux hopper of automatic surfacing machine for reuse;

• during development and manufacture of new units and components, it is necessary to take into account the possibility for further upgrading of the machine.

Proceeding from the tasks defined in TA, a configuration of units and assemblies was proposed, which in combination with the base roll-turning machine allowed manufacturing a high-technology machine for surfacing mill rolls of billet mills (Figure 1). Mobile rotary column with cross-piece *1* was proposed as a device for fastening and displacement of automatic surfacing machine A-1406. Carriage *6*, on which the column is mounted, moves over rails, mounted in parallel to the longitudinal axis of the machine and mill rolls fastened in the machine. The column with the automatic machine can be moved into the working position before surfacing each roll pass. This enables removing the automatic surfacing machine from the working zone that is important at roll positioning and taking off.

The function of working displacement for surfacing width along the axis of the roll being surfaced was transferred to upgraded A-1406 automatic surfacing machine *7*, for which purpose the electric circuit of the automatic machine was improved. Flux feeder in the automatic surfacing machine was also replaced. KIU-1201 welding rectifier *4* was used as arc power source.

Flux feeder includes: carriage *9*, moving along machine bed guides into the surfacing zone (to collect the mixture of unused flux and slag); screw conveyor *14*; vibrating sieve *12*; storage hopper of sifted flux *13*; ejector ensuring flux feed by compressed air into the flux hopper of automatic surfacing machine; and slag collection container *16*.

Before surfacing start, carriage *9* is mounted under the roll being surfaced. During surfacing the used mixture of flux and slag is poured into the carriage, from which it comes to the receiving windows of screw conveyor. Conveyor feeds a mixture of slag and flux onto the vibrating sieve, which separates the mixture into slag pouring into the container for slag collection and the sifted flux, falling into the storage hopper. From this hopper the flux is fed by an ejector into the flux hopper of automatic machine A-1406 for reuse.

The machine also includes the mechanism of displacement of machine tool dead head used as

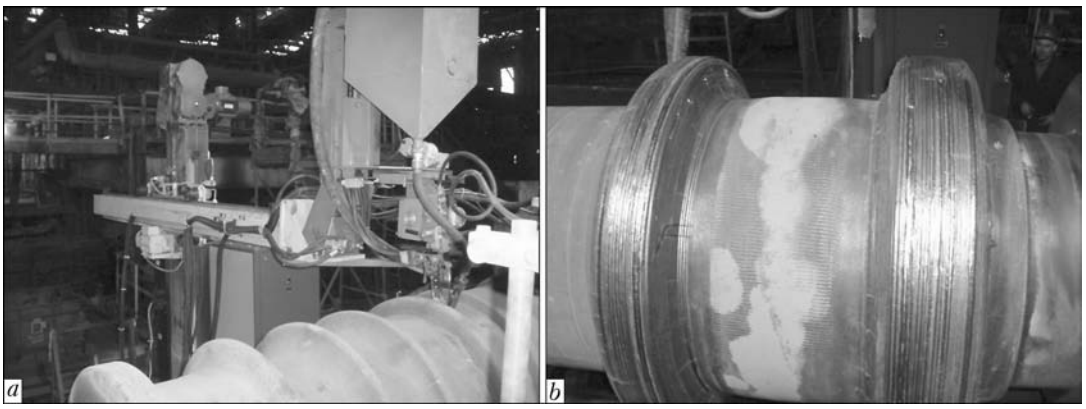

Figure 2. RM-11 machine for surfacing forming rolls of billet mills (*a*), and fragment of surfaced forming roll (*b*)

the second support for the roll being surfaced. Mechanism, consisting of electric winch and a set of blocks, allows moving the dead head when installing rolls of different length into the machine.

Machine operation is controlled from several panels, using control cabinets *2* and *3*. Main control panel *8* is fastened on automatic surfacing machine. It is used to conduct on-line control of three main units of the machine: mobile rotary column, roll-turning machine and automatic surfacing machine. Functions of auxiliary control of the machine, not requiring quick measures, in order to unload the main panel, were transferred to two more panels *10* and *11*, located on the railing of surfacing operator platform *15*. Panel *10* is used to control the vibrating sieve, screw conveyor and pre-setting displacement of the roll to be surfaced. Compressed air feed into the flux feeder ejector is switched on and controlled from panel *11*. Additional panel *5*, located in the area of the platform with control cabinets, is designed to control the rotary column during preparatory and repair operations.

Figure 2, *a*, shows the general view of RM-11 machine designed for surfacing the rolls of billet mills, and Figure 2, *b* gives the fragment of a mill roll surfaced in it.

REMMASH made for OJSC EVRAZ-Petrovsky DMZ the RM-12 machine, based on DXW 1000/3×5000 RK-1 lathe for surfacing rolls of billet and section hot rolling mills. Machine drive was upgraded and ensured roll rotation with the surfacing speed. Machine sliding carriage was removed from the working zone used for surfacing.

In addition to DXW 1000/3×5000 RK-1 lathe *1*, surfacing machine (Figure 3) also included such units as A-1416UKhL4 automatic welding machine *5* as a set with welding rectifier KIU-1201. The machine was fitted with remote control panel, which duplicates the basic elements of the stationary control panel. This allows control of the surfacing process (monitoring it) from surfacing operator's platform *7*; control of flux hopper of 250 dm^3 volume; post *8* for placing the roll of wire of up to 1 t weight; self-propelled carriage *4* for positioning and displacement of automatic welding machine based on frame *3*.

A programmable controller is used to ensure the required working speed of carriage displacement, allowing selection of the required speed in the range of 1–30 mm/min.

Device for flux and slag collection *6*, consisting of carriage and tray, is placed under the roll being surfaced and moved along the axis of DXW 1000/3×5000 RK-1 lathe.

RM-12 machine (Figure 4) was introduced at EVRAZ-Petrovsky DMZ and has been successfully used for more than two years now for surfacing the mill rolls.

Preliminary and concurrent heating, as well as tempering or delayed cooling after surfacing, are mandatory technological operations in surfacing of mill rolls from medium- and high-carbon steels. As a rule, surfacing of mill rolls is performed using induction heating or gas torch heating. Both these methods have their advantages and disadvantages, and the enterprise itself takes the decision on which of them should be used in each specific case.

For Arcelor Mittal Krivoj Rog Company, which traditionally applies inductors for roll heating, REMMASH developed and manufactured an inductor, which allows heating the mill rolls in the entire range of their diameters from 690 up to 910 mm.

Inductor (Figure 5) consists of a coil made from copper tube *4*, mobile *6* and stationary *1* magnet cores made from plates of core iron, caseframe *2* consisting of welded sectors and terminal plate *3*. Inductor coil is assembled from two sections, the ends of which are taken to the terminal plate. Cooling water is circulating inside the copper current-carrying tube (outer diameter of 14 mm, inner diameter of 10 mm). Each of the coil sections is insulated by varnished cloth, and

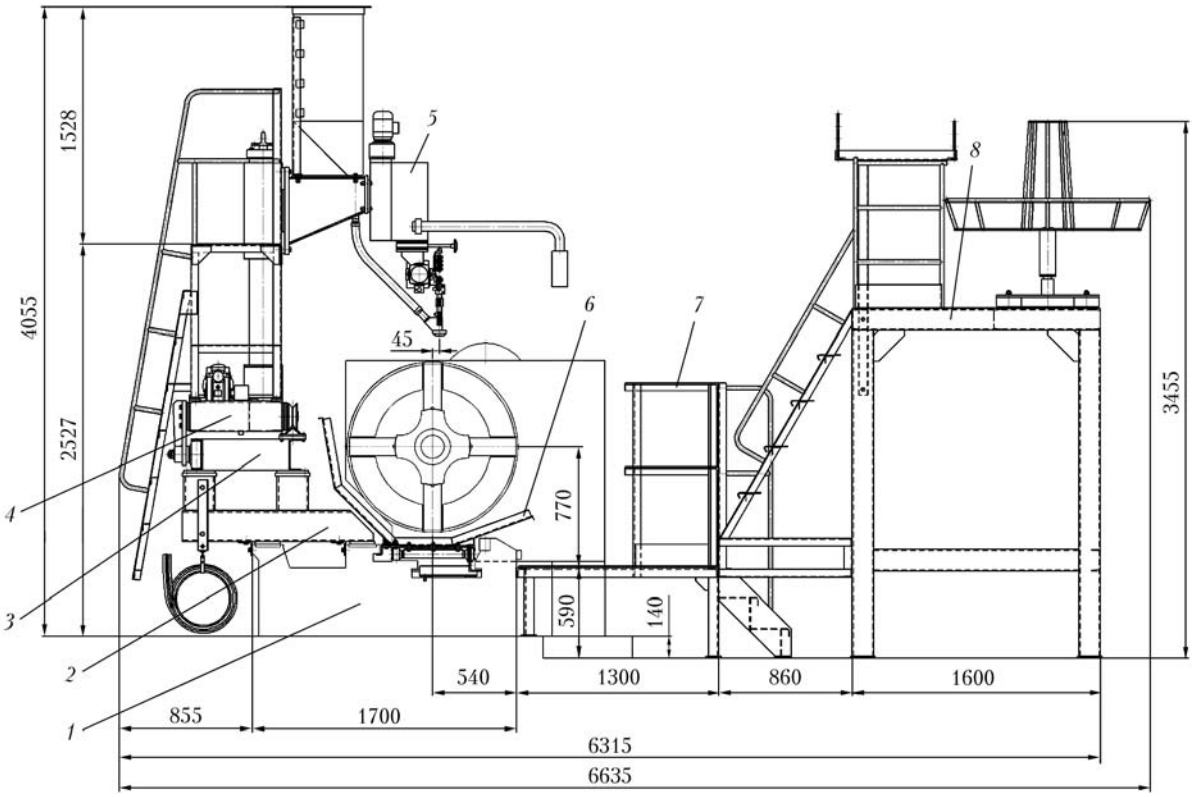

Figure 3. Schematic of RM-12 machine based on lathe DXW 1000/3×5000 RK-1

the entire as-assembled coil is insulated with asbestos cloth impregnated with varnish. Electric layers of the coil are connected in sequence, and hydraulic layers are connected in parallel. Nozzles are soldered to the start and end of each layer, which are taken to terminal plate *3*. Insulation is of class F, admissible winding temperature should not exceed 200 °C. Water flow rate at heating of a roll of 910 mm diameter up to 500 °C is equal to 7.2 l/min, and for a roll of 690 mm diameter it is 6.5 l/min. In the mode of maintaining the roll temperature during surfacing (400–420 °C), the flow rate is not more than 5.0 l/min.

Magnet cores are located in the case-frame radially in six sections around the frame circumference, every 60°. Each section consists of one stationary magnet core *6*, mounted in the frame middle part, and two mobile magnet cores *1*, mounted from two sides on the frame periphery. When items of different diameters (690–910 mm) are placed into the inductor for heating, mobile magnet cores move in the yokes to create an optimum air gap between the surface of the item being heated and end faces of mobile magnet cores. At selection of gap width between the mobile magnet cores and heated item surface, it is necessary to bear in mind that absence of such a gap is inadmissible. Excess narrowing of the gap leads to magnet core overheating, and increased width leads to longer heating time. Therefore, for each roll typesize, such a gap, at an average value of 10–20 mm, is selected experimentally. Time of heating of a roll section 490 mm long from 250 up to 400 °C is equal to 1.5 h. Main characteristics of the inductor are as follows: 380 V rated mains voltage, 260 A rated current and 0.506 power factor.

The inductor is used with success in the roll-turning shop of Arcelor Mittal Krivoj Rog Company for preliminary, concurrent and post-surfacing heating of all the surfaced steel rolls of 690–910 mm diameter.

For heating of rolls surfaced in RM-12 machine (EVRAZ-Petrovsky DMZ) a stand was developed with air torches as a heating element. The stand (Figure 6) consists of drive *1* and

Figure 4. RM-12 machine for surfacing mill rolls

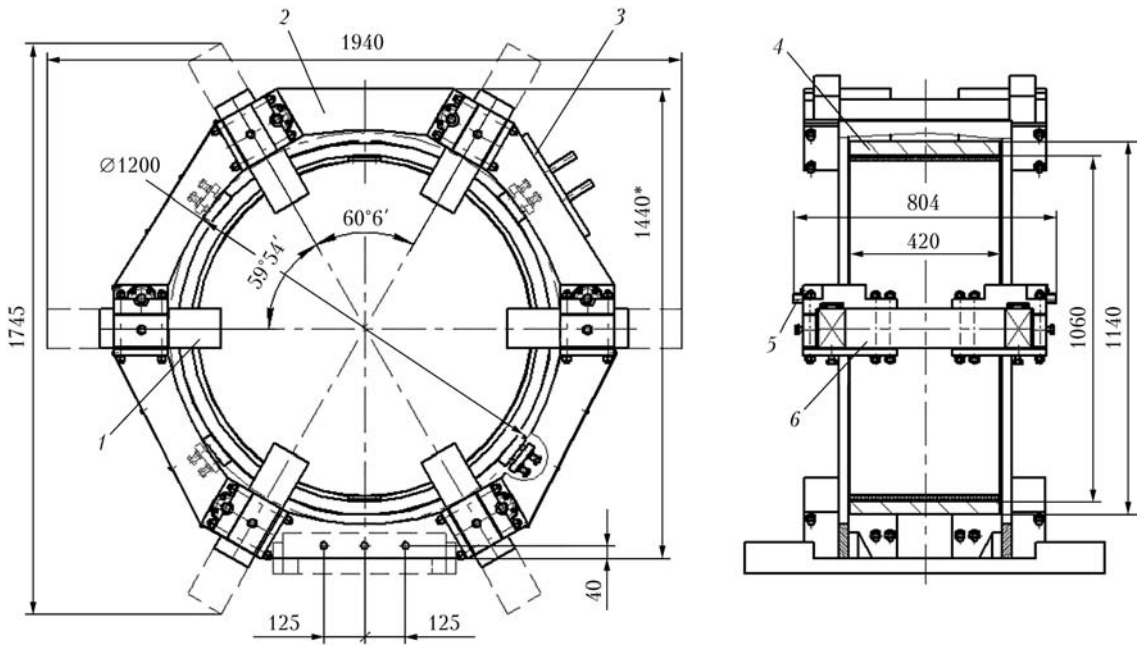

Figure 5. Schematic of electromagnetic inductor RM-6

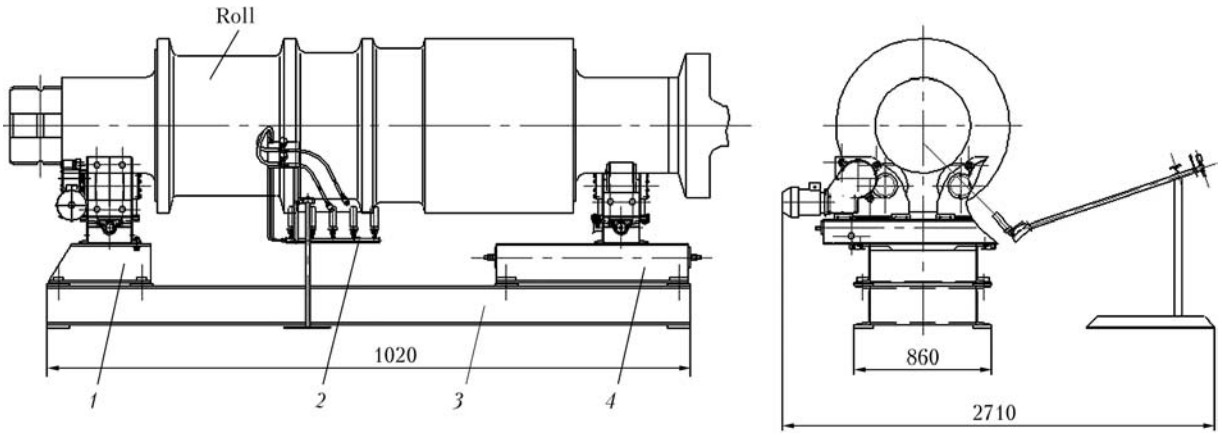

Figure 6. Schematic of RM-14 stand for heating mill rolls before surfacing

driven *4* sections of roller supports and set of air torches *2*.

Drive section is a frame, which carries two drive roller supports, as well as a screw used for bringing the roller supports together and apart at readjustment for different diameters of rolls being heated. Control of roller support rotation drives is performed from the common control cabinet, mounted on the frame. Driven section is a frame, carrying two driven roller supports, as well as a screw, the functions of which are similar to those of the screw from drive section. In addition, they have a screw mechanism for displacement in the axial direction relative to the drive section (for heating rolls of different length). The drive and driven sections are mounted on common frame *3*.

The set of air torches *2* consists of five torches GV-VK2, one collector for five torches, post and panel of torch control. Torches use natural gas (0.08 MPa pressure) and compressed air (0.3 MPa pressure). Number of air torch sets is selected by the customer or calculated by the developer (Customer provides the technical requirements on heating of mill rolls or other parts).

The approaches to development described in this paper and given examples of manufacture and introduction of surfacing equipment show one of the directions that allows upgrading and retrofitting the equipment for mill roll surfacing at minimum cost.

1. Kuskov, Yu.M., Ryabtsev, I.A., Demchenko, Yu.V. et al. (2008) Repair of rods and plungers of mine hydrosupports by submerged-arc surfacing. *Svarshchik*, **2**, 6–11.
2. Kuskov, Yu.M., Ryabtsev, I.A., Demchenko, Yu.V. et al. (2009) Hard-facing bay for repair of hydropower equipment parts in company «Sakenergoremont». *The Paton Welding J.*, **1,** 46–47.
3. Titarenko, V.I., Tkachenko, O.V., Matiko, D.Yu. et al. (2009) Experience in designing and manufacture of welding-and-surfacing installations. *Ibid.*, **3**, 18–20.

Received 30.01.2013

PLASMA-POWDER SURFACING OF POWER FITTING RODS

E.F. PEREPLYOTCHIKOV and **I.A. RYABTSEV**
E.O. Paton Electric Welding Institute, NASU
11 Bozhenko Str., 03680, Kiev, Ukraine. E-mail: office@paton.kiev.ua

Iron-based filler powder 15Kh19N9M4S5G3D was selected, and technology of mechanized plasma surfacing of sealing and cylindrical surfaces of rods (spindles) of fittings, operating in thermal and nuclear power stations, was developed. Metal deposited with this powder has the required service properties, and its price is lower compared to earlier applied for this purpose nickel alloys. Application of plasma-powder surfacing of rods of power fittings instead of coated-electrode manual arc and automatic flux-cored arc surfacing allowed improving the deposited metal quality, reducing machining tolerances, as well as lowering the surfacing costs and extending the service life of stop valves. 5 Ref., 1 Table, 6 Figures.

Keywords: *plasma-powder surfacing, surfacing powders, surfacing equipment, stop valves, rods, spindles*

Experience of application of mechanized plasma surfacing in power fitting manufacture is indicative of significant technical and economic advantages of this process compared to manual arc surfacing. In addition to higher efficiency, lower consumption of expensive and deficit surfacing consumables and better labour conditions, a higher quality of surfaced parts is also provided.

Nickel- and cobalt-based alloys are widely applied for plasma surfacing of power fitting parts. Alloys of these types have high technological and service properties. They, however, have the great disadvantage of a high cost. Less expensive iron-base alloys have been now developed for surfacing fitting parts for various purposes. However, as was mentioned above, many enterprises of CIS countries still apply manual electric arc surfacing with stick electrodes or mechanized flux-cored arc surfacing for this purpose. Arc surfacing of fitting parts is performed, as a rule, in three layers, leading to excessive consumption of surfacing consumables and prolongation of surfacing process duration [1, 2].

In batch production the fitting rods (spindles) are manufactured from 25Kh1MF steel, and their sealing surfaces are surfaced manually in 3–4 layers with TsN-12M electrodes in a copper water-cooled crucible (Figure 1). Technological process envisages billet preheating and subsequent tempering of surfaced parts. Non-uniform hardness by the height of the deposited layer, presence of slag inclusions, pores and other defects, as well as a low efficiency of manual labour — these are the factors, inherent to this surfacing technology.

PWI developed the technology of mechanized plasma surfacing of fitting parts, in particular, sealing and cylindrical surfaces of rods (spindles), with powder of iron-based alloy 15Kh19N9M4S5G3D [3]. This surfacing process allows application of thin metal layers at small penetration (5–10 %) of base metal. Dimensions of deposited beads can be adjusted in broad ranges: deposited layer thickness δ = 1–6 mm, width b = 4–50 mm. When this technology is used, the cost of filler materials is reduced, high efficiency and good quality of deposited metal are ensured, labour conditions are greatly improved and longer service life of the fittings is achieved [4].

Plasma-powder surfacing of sealing surface of the rods is performed using the diagram shown in Figure 2. To prevent pouring down of the deposited layer and to ensure sound formation of

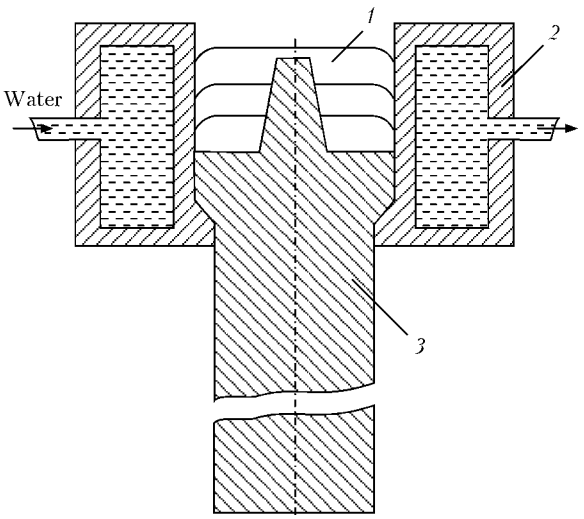

Figure 1. Schematic of manual arc surfacing of rods of DN 50 valves: *1* — deposited metal; *2* — water-cooled copper crucible; *3* — rod billet

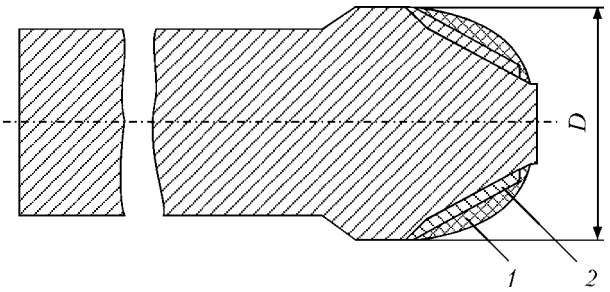

Figure 2. Schematic of edge preparation and surfacing of DN 50 rods: *1* — deposited metal before machining; *2* — same after machining

the deposited bead, the rod billet for surfacing had a protrusion of diameter D and length of 5–7 mm. Bead cross-sectional shape at optimum surfacing conditions looks like a sessile drop.

Compared to manual multilayer surfacing, plasma-powder surfacing reduces filler material consumption approximately 2 times.

In addition to conical sealing surface, also the cylindrical contact surface is wearing on the rods. As shown by verification of service durability of fittings under production conditions, the share of rod damage over this surface can be up to 15 % [5]. Currently applied strengthening methods, namely nitriding, boriding, chromium plating, thermal or electric arc surfacing do not completely meet the requirements of modern fitting engineering.

Plasma-powder surfacing gives positive results also in this case. Surfacing of cylindrical surfaces of the rods is performed along a helical line in one layer by powders based on nickel, cobalt and iron.

An important technological parameter at surfacing of cylindrical parts along a helical line is the value of plasmatron displacement from zenith [4]. Conducted investigations showed that this

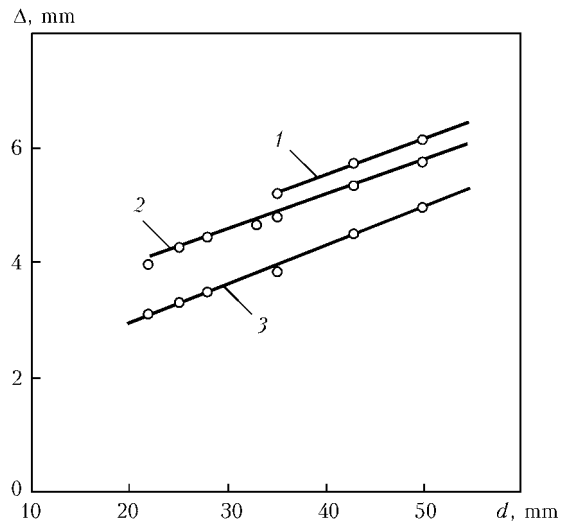

Figure 3. Influence of billet diameter d and surfacing speed on value of displacement ΔZ of plasmatron from zenith: *1* — 7.0; *2* — 5.0; *3* — 3.6 mm

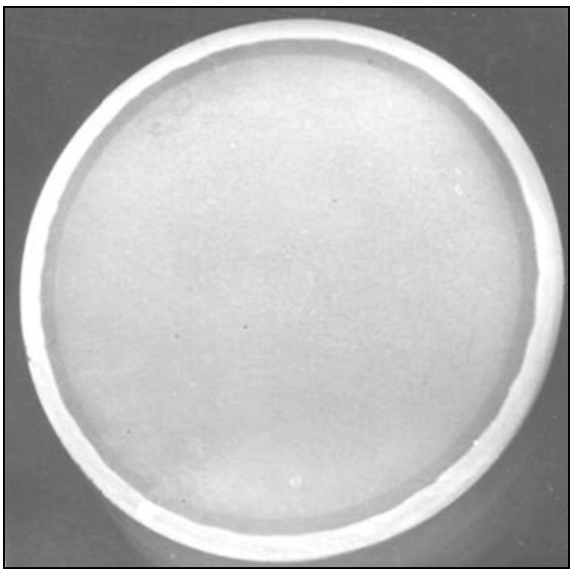

Figure 4. Transverse macrosection of cylindrical part of the rod of DN 50 gate valve surfaced by plasma-powder process

value rises with increase of billet diameter and surfacing speed (Figure 3). Increasing the diameter widens the range of optimum values of displacement. With increase of surfacing speed bead formation becomes more sensitive to the change of the value of displacement, as here the current and powder feed increase, accordingly, and, therefore, also the weld pool width. Reduction of displacement impairs formation and leads to increase of penetration.

Rods of 25–30 mm diameter are surfaced in one layer, without preheating, at the efficiency of 3 kg/h. Larger parts can be surfaced with the efficiency of up to 5 kg/h. Rod billet surface to be processed is located parallel to the edge of plasmatron nozzle at the distance of 7–9 mm. Gas flow rate is maintained within the following ranges, l/min: plasma and carrier gas — 1.5–2 each, shielding gas — 8–10. Arc current, powder feed, deposition rate and displacement from zenith are selected so as to provide the required bead dimensions and good formation of the deposited layer (Figure 4).

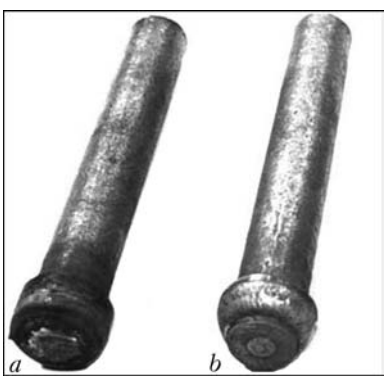

Figure 5. Billets of rods of DN 50 valves surfaced by manual arc (*a*) and plasma (*b*) processes

Main parameters of the mode of plasma-powder surfacing of sealing surfaces of rods of DN 40 and DN 50 valves

Rod diameter, mm	Surfacing current, A	Powder flow rate, g/min	Plasmatron displacement, mm	Time of one revolution, min
40	160	35	5.0	0.68
50	180	40	6.5	1

The Table gives the main parameters of the mode of plasma-powder surfacing of sealing surfaces of rods of DN 40 and DN 50 valves, and Figure 5 shows rod billets surfaced by arc and plasma-powder processes.

Under production conditions semi-automatic surfacing of the rods is performed in the machine based on A1756 unit (design of PWI Design-Experimental Technological Bureau).

The machine (Figure 6) includes A1756 unit, manipulator, bed plate, control cabinet and power source VDU-504. Manipulator consists of the bed plate, reduction gear with electric motor, pneumatic chuck and current conduit. In the initial position the pneumatic chuck is unclamped, and the manipulator is inclined towards the unit.

Main elements of plasma surfacing technology are as follows: automatic clamping of the billet, manipulator displacement using a pneumomechanical system under the plasmatron into the working position and automatic connection of billet rotation and plasma arc excitation. After completion of surfacing and issuing «Stop» command, automatic welding-up of the crater and manipulator returning to the initial condition are performed. After surfacing the batch of parts are placed into the furnace, and heat treatment is performed.

At plasma surfacing with small penetration of the base metal, the specified hardness of deposited metal is achieved already at the distance of 0.5–1.0 mm from the fusion line [3]. To ensure a high performance of parts after machining, it is sufficient to deposit a metal layer of 1.8–2.5 mm thickness. In practice this thickness is maintained in the range of 2.0–2.5 mm. Scatter of metal hardness values on one billet is not greater than *HRC* 5.

Mechanization of surfacing process with application of highly-efficient shielding of the deposited metal by argon allowed a considerable reduction of the probability of defect formation

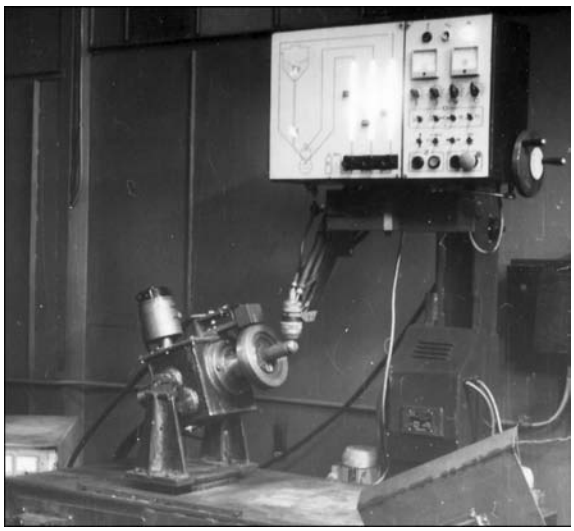

Figure 6. Unit for treatment of sealing surfaces of valve rods

(pores, slag inclusions, lacks-of-penetration), inherent to manual electric arc surfacing with stick electrodes and mechanized arc surfacing with flux-cored wires.

Technology of automated plasma surfacing with powder of iron-base alloy 15Kh19N9M4S5G3D of sealing and cylindrical surfaces of rods was developed. Metal deposited with this powder, has the required service properties and compared to nickel alloys earlier applied for this purpose, it has a lower price. It is shown that plasma-powder surfacing provides the required composition of the deposited metal already in the first layer. It also ensures excellent formation and high quality of the deposited metal.

1. Eremeev, V.V., Strelyany, Yu.V., Korbut, V.A. et al. (1979) Chemical inhomogeneity of metal deposited with different electrode consumables. In: *Properties and testing of deposited metal: Theoretical and technological principles of surfacing*. Kiev: PWI, 36–42.
2. Stepin, V.S., Starchenko, E.G. (2010) Application of dispersion hardening Cr–Ni–Si-steels for gate valve elements and surfacing of sealing surfaces of TPS and NPP fittings. *Armaturostroenie*, **3**, 66–69.
3. Pereplyotchikov, E.F., Ryabtsev, I.A. (2011) Properties of iron-based alloys for plasma-powder hard-surfacing of sealing surfaces of fittings. *The Paton Welding J.*, **9**, 27–31.
4. Gladky, P.V., Pereplyotchikov, E.F., Ryabtsev, I.A. (2007) *Plasma surfacing*. Kiev: Ekotekhnologia.
5. Pereplyotchikov, E.F., Ryabtsev, I.A. (2007) *Plasma-powder surfacing in fitting engineering*. Kiev: Ekotekhnologia.

Received 31.10.2013

CORROSION RESISTANCE OF WELDED JOINTS OF SHIP HULL MATERIALS

E.V. KOLOMIJTSEV
Company «Iliich MMK»
1 Levchenko Str., 87504, Mariupol, Ukraine. E-mail: natalya.rassokhina@ilyichsteel.com

Experience of operation of sea ferries is indicative of nonuniform general corrosion of hulls in the area of welded joints. The objective of this work was investigation of corrosion resistance of ship hull steels and their welded joints for the conditions of operation of «Sakhalin» series ferries of the second generation. Investigation procedure envisaged assessment of corrosion characteristics of ship hull materials under diverse conditions: determination of stationary electrode potentials and rate of general corrosion of low-alloyed hull steels, investigation of corrosion resistance of welded joints of these steels in rapid sea water. Obtained results allow recommending the following steels as base metal for hulls of «Sakhalin» series ferries of the second generation: for ice belt — steels of 15GB and 10GNB grades, for outer shell of hull underwater part, inner bottom and partitions — steels of A27 and D32 grades to TU-14-1-4264–87. Welding of steels 15GB, 10GNB and A27 should be performed both by nickel-containing and nickel-free consumables. Steel D32 can be welded by nickel-free consumables. 10 Ref., 6 Tables, 1 Figure.

Keywords: *corrosion resistance, hull steels, welded joints, electrode potentials, sea water, testing duration*

Over the recent decades ship service conditions became much more stringent. Ship movement speed increased, and geography and intensity of their navigation became greater. Such ships, in particular include «Sakhalin» series ferries, operated in Tatar Straight. Hulls of ferries, made from manganese steels 09G2 and 10G2S1D (ice belt), are prone to non-uniform corrosion, particularly in the near-weld zone. This leads to the need to weld up the damaged locations and replacement of the shell plates that increases the duration and cost of dock repairs, while lowering the operating effectiveness.

As ship hulls have been made welded and not riveted for more than 70 years, and corrosion resistance of welded joints quite often is greatly inferior to corrosion resistance of base metal, this necessitates performance of corrosion testing of welded joints.

There is quite extensive material on corrosion resistance of carbon and low-alloyed weldable hull steels in sea water [1–5].

Corrosion of 09G2 steel is characterized by considerable non-uniformity of surface damage. Average corrosion rate is 0.16–0.25 mm per year. With increase of sea water current speed up to 10 m/s in regions with moderate climate the rate of corrosion of low-alloyed steels can rise up to 1 mm per year [3, 4].

Corrosion wear of plates of outer shell of «Sakhalin» ferry hulls was equal to 0.3–0.5 mm per year. The greatest relative thinning was observed in the plates of bottom and bilge shell. Considerable corrosion damage was found in areas of site welds, made by manual welding, as well as in points of weld crossing and in the area of settling tank.

Enhanced selective corrosion in the form of furrows along the welds (from both sides) was observed in the metal of HAZ of slot and butt welds and welds of joining the main framework — up to 1 mm per year, and in a number of cases through-thickness rusting (blowholes) were found, which are readily visible in the Figure. Furrow fractures of HAZ metal are a consequence of enhanced corrosion of anode (hardened) zone adjacent to the weld [4].

In view of enhanced corrosion wear of outer shell of «Sakhalin» ferries after 8–10 years of operation, it was necessary to replace panels of the total area of up to 1800 m^2 and make up to 2000 m of welds.

Causes for increased corrosion wear of underwater part of «Sakhalin» ferries are as follows:

- ineffectiveness of recommended measures of anticorrosion protection at operation in the ice conditions;
- insufficient corrosion-erosion resistance of 10G2S1D, 10KhSND and, particularly, 09G2 steels.

One of the ways to solve this problem is application of new hull materials with increased corrosion resistance, as well as strict following of welding technology, including selection of welding consumables.

The objective of this work was investigation of corrosion resistance of new and currently available hull steels and their welded joints, as well as selection of optimum combinations of base materials and welding consumables to increase the resistance (fatigue life) of hulls of «Sakhalin» ferries of the second generation. Selection of low-alloyed hull steels was based on their corrosion resistance exceeding that of steel of 09G2 grade, while the welded joint resistance should be on the level of that of base metal, i.e. an optimum combination of steel grades, welding consumables and their welding technology is required.

To study the corrosion resistance of base metal and welded joints, standard samples of (10–14) × × 80 × 200 mm size to OST 5.9255–76 [6] were cut out of steel of 09G2, A27, D32, 15GB, 10KhSND and 10GNB grades.

Steels of 09G2, A27 and 15GB grades have been normalized, D32 (TU 14-1-4264–87) [7], 10KhSND and 10GNB (TU 14-1-4603–89) [8] have been subjected to quenching with tempering.

Composition and mechanical properties of the studied steels are given in Tables 1 and 2, respectively.

Welded joints were made by manual, semiautomatic and automatic welding with application of nickel-free and nickel-containing welding consumables. Table 3 gives welding consumables and welding modes.

Each variant of steel grade, welding process, and welding consumable is represented by three samples. Investigations included:

- determination of stationary electrode potential of the base metal and corrosion rate values by mass method in quiet sea water;
- determination of corrosion values of welded joints in rapidly moving artificial sea water (ASW) with strip chart recording.

Determination of stationary electrode potential was conducted in quiet ASW of oceanic composition [9] on samples of 5 × 30 × 50 mm size. Measurements were conducted with application of digital voltmeter Shch-1413, saturated calomel electrode was used as reference electrode, and then measurement results were recalculated for hydrogen electrode.

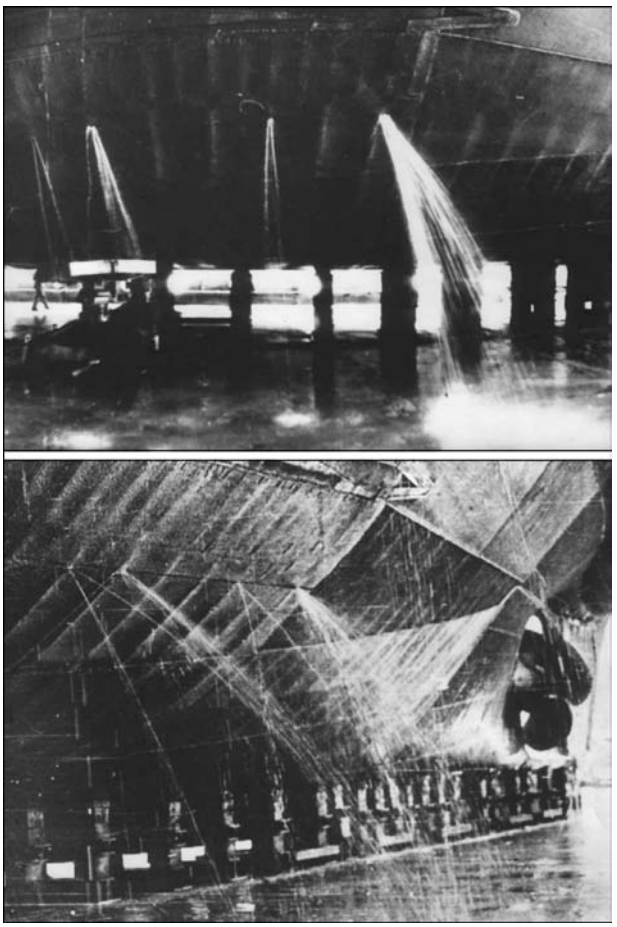

Corrosion damage (blowholes) in outer plating of underwater part of «Sakhalin» ferries of the first generation

Determination of corrosion rate in quiet ASW (testing base of 3000 h) was conducted by mass method. Then, considering the relatively uniform nature of corrosion of these steels the value was recalculated into depth index and averaged by three samples.

Results of measurement of potentials and corrosion rate of low-alloyed steels are given in Table 4.

As is seen from the Table values of electrode potentials of 10KhSND, 10GNB, 15GB, A27 and D32 steels are close and are equal from –0.45 up to –0.48 V, and for 09G2 steel they are more

Table 1. Composition of hull steels, wt.%

Steel grade (category), GOST, TU	C	Mn	Si	S	P	Ni	Cr	Cu	Al	Ti	Nb
09G2, GOST 5521–93	0.10	1.65	0.32	0.022	0.032	0.03	0.02	0.05	0.014	–	–
D32, GOST TU 14-1-4264–87	0.09	1.24	0.28	0.035	0.023	0.20	0.11	0.30	0.050	0.017	–
15GB (E36), GOST 5521–93	0.16	1.30	0.31	0.012	0.017	0.08	0.06	Traces	0.021	0.009	0.020
10KhSND (E40), GOST 5521–86	0.10	0.53	0.84	0.023	0.015	0.65	0.70	0.50	0.021	–	–
10GNB (E40), TU 14-1-4603–89	0.10	1.37	0.33	0.005	0.020	0.77	0.05	0.12	–	–	0.034
A27, TU 14-1-4264–87	0.11	0.47	0.22	0.029	0.012	0.23	0.10	0.38	–	–	–

Table 2. Mechanical properties of the studied steels

Steel grade (category), GOST, TU	Plate thickness, mm	Tensile strength σ_t, MPa	Yield limit σ_y, MPa	Relative elongation, δ, %	Impact energy KV, J, at T, °C		
					0	−40	−60
09G2, GOST 5521–86	15	523	363	34.0	–	62; 38; 50	–
D32 (E32), TU 14-14264–87	20	510	345	27.0	–	180; 190; 180	–
15GB, GOST 5521–86	16	517	365	33.6	–	62; 38; 50	–
10KhSND, GOST 5521–86	32	540	405	31.6	–	74; 69; 64	–
10GNB, TU 14-1-4603–89	10	570	468	29.3	–	–	215; 251
A27, TU 14-1-4264–87	18	435	295	35.0	124; 103	–	–

Table 3. Welding consumables and welding modes

Welding process	Welding consumables	Electrode diameter, mm	Welding modes		
			I_w, A	U_a, V	v_w, m/h
Manual	Electrodes ITS-4 S, UONI-13/45	4.0	140–160	–	–
	E-138/50N	5.0	180–200	–	–
CO_2 semi-automatic	Welding wire of Sv-08G2S, Sv-08GSNT	1.2	140–160	22–24	–
	Sv-08GSMT	1.6	180–200	22–24	–
Automatic submerged-arc	Welding wire Sv-08A, Sv-10GN, flux OSTs-45	5.0	850–900	40–42	28–30

negative from −0.48 up to −0.50 V. Corrosion rates are distributed approximately the same way, namely in 15GB, 10KhSND and 10GNB steels depth index is 0.069–0.071 mm per year; in 09G2 steel it is 0.074. Testing in quiet water of steels of category A27 and D32 was not conducted.

Thus, proceeding from obtained results, it can be noted that steels A27, D32, 15GB, 10KhSND and 10GNB have higher corrosion resistance compared to steel 09G2. For A27, D32, 10KhSND and 10GNB steels this is attributable to higher content of nickel and copper in them. For 15GB steel this point remained unclear.

Corrosion testing of welded samples was conducted in rapidly moving medium in keeping with the requirements of OST 5.9255–76.

Testing parameters were as follows: medium of ASW, medium temperature of 32±2 °C, rate of 10 m/s, and testing duration of 1000 h.

Table 4. Stationary electrode potentials and corrosion rates of the studied steels in quiet medium (ASW)

Steel grade	Stationary electrode potential, V	Depth index of corrosion rate, mm/year
09G2	−0.48 – −0.50	0.074
A27	−0.45 – −0.46	–
D32	−0.45 – −0.46	–
15GB	−0.46 – −0.47	0.070
10GNB	−0.47 – −0.48	0.071
10KhSND	−0.45 – −0.47	0.069

After testing strip chart recording of the surface of samples subjected to corrosion was performed by the method of continuous scanning with application of electron-mechanical surface contour recorder EMP-1. Profile charts of sample surface were recorded in four tracks in 1:1 scale along abscissa axis, and 200:1 along ordinate axis.

Testing results are averaged over three samples and are given in Table 5.

As is seen from Table 5, values of average corrosion rates of base metal of A27, D32, 09G2 and 15GB steels do not essentially differ from each other, and are equal to 0.94–1 mm per year at maximum rate of 1.49–2.03 mm per year.

Average corrosion rate of base metal of 10KhSND and 10GNB steels is equal to 0.62–0.70 mm per year that is essentially higher than

Table 5. Maximum and average corrosion rates of base metal of welded joints of the studied steels

Steel grade	Corrosion rate, mm/year		Index of corrosion non-uniformity
	Max	Average	
09G2	1.46	0.97	1.51
D32	1.95	0.94	2.07
15GB	1.46	0.98	1.49
10GNB	1.06	0.62	1.71
10KhSND	1.26	0.70	1.80
A27	2.03	1	2.03

Table 6. Corrosion resistance indices of metal of welded joint zones of the studied steels in rapidly-moving medium

Steel grade	Welding process	Welding consumable grade	Indices of corrosion rate of welded joint zone, mm/year						Indices of nonuniformity of corrosion		
			Base metal		HAZ		Weld metal		max BM / av BM	av HAZ / av3 BM	av weld / av BM
			Max	Average	Max	Average	Max	Average			
09G2	Manual	ITS-4S	1.24	0.83	1.49	1.18	0.74	0.53	1.49	1.42	0.64
		E-138/50N	1.31	0.86	1.46	1.16	0.71	0.41	1.52	1.35	0.48
	Semi-automatic	Sv-08G2S	1.70	1.18	1.66	1.28	1.74	1.32	1.44	1.08	1.12
		Sv-08GSNT	1.28	0.94	1.82	1.55	0.38	0.25	1.36	1.65	0.27
	Automatic	Sv-08A	1.50	1.01	1.55	1.14	1.66	1.21	1.49	1.13	1.20
		Sv-10GN	1.71	0.98	1.48	1.13	1.67	0.88	1.74	1.15	0.90
D32	Semi-automatic	Sv-08G2S	2.07	0.98	1.24	0.74	1.98	1.15	2.11	0.76	1.17
		Sv-08GSNT	1.86	0.99	1.29	0.83	0.90	0.51	1.88	0.84	0.52
	Automatic	Sv-08A	1.78	0.86	1.25	0.81	1.62	0.81	2.07	0.94	0.94
		Sv-10GN	2.07	0.94	0.84	0.60	0.92	0.48	2.20	0.64	0.51
A27	Manual	ITS-4S	2.22	1.20	1.36	0.93	2.51	1.14	1.85	0.78	0.95
		E-138/50N	1.97	1.03	1.07	0.79	0.98	0.57	1.91	0.77	0.55
	Semi-automatic	Sv-08G2S	1.93	1.01	1.18	0.73	2.70	1.78	1.91	0.72	1.76
		Sv-08GSNT	2.10	0.96	1.09	0.70	1.32	0.73	2.18	0.73	0.77
	Automatic	Sv-08A	1.75	0.83	1.24	0.79	1.78	0.83	2.11	0.95	1
		Sv-10GN	3.19	0.99	1.15	0.74	1.39	0.11	2.21	0.75	0.72
10GNB	Manual	UONI-13/45	1.03	0.55	0.77	0.57	1.30	0.77	1.81	1.04	1.40
15GB (E36)	Manual	ITS-4S	1.24	0.81	1.04	0.83	1.14	0.78	1.53	1.02	0.96
		E-138/50N	1.25	0.88	0.98	0.72	0.79	0.53	1.42	0.82	0.60
	Semi-automatic	Sv-08G2S	1.18	0.82	0.90	0.72	1.61	1.25	1.44	0.88	1.52
		Sv-08GSNT	1.75	1.30	1.49	1.25	0.98	0.77	1.35	0.96	0.59
	Automatic	Sv-08A	1.58	1.14	1.42	1.02	1.81	1.25	1.39	0.89	1.10
		Sv-10GN	1.73	0.94	1.41	1.10	1.35	0.98	1.84	1.17	1.04
10GNB (E40)	Manual	E-138/50N	1.19	0.74	0.95	0.67	1.17	0.74	1.61	0.91	1
	Semi-automatic	Sv-08GSMT	1.00	0.56	0.77	0.54	1.15	0.86	1.79	0.96	1.54
	Automatic	ITS-4S	1.08	0.59	0.78	0.54	1.20	0.66	1.83	0.92	1.12
		E-138/50N	0.95	0.57	0.55	0.42	0.84	0.53	1.67	0.74	0.93
10KhSND (E40)	Manual	ITS-4S	1.24	0.65	0.69	0.39	1.02	0.63	1.91	0.60	0.97
		E-138/50N	1.26	0.72	0.73	0.43	0.89	0.53	1.75	0.60	0.74
	Semi-automatic	Sv-08G2S	1.25	0.72	0.97	0.51	1.32	0.96	1.74	0.71	1.33
		Sv-08GSNT	1.29	0.70	0.70	0.51	0.77	0.58	1.84	0.73	0.83
	Automatic	Sv-08A	1.41	0.76	0.58	0.43	1.27	0.94	1.86	0.57	1.24
		Sv-10GN	1.16	0.65	0.58	0.43	0.64	0.51	1.78	0.66	0.78

corrosion resistance of 09G2, A27, D32 and 15GB steels.

Values of corrosion resistance of various zones of welded joints of the studied steels in rapidly moving medium are given in Table 6.

Corrosion resistance of welded joint zones was evaluated relative to corrosion resistance of base metal, considering it to be satisfactory, when the rate of weld or HAZ metal corrosion was in the ranges of 0.8–1.2 of that of base metal [10].

Proceeding from analysis of data in Table 6 the following should be noted:

• corrosion resistance of welds made by nickel-free welding consumables (ITS-4S, UONI-13/15, Sv-08G2S, Sv-08A) for all the steels is, usually, equal to or lower than that of base metal;

• corrosion resistance of welds made by nickel-containing welding consumables (E-138/50N, Sv-08GSNT, Sv-10GN) is higher or equal to that of the base metal.

Considering the corrosion resistance of HAZ metal, it can be noted that more intensive corrosion of HAZ metal is observed in 09G2 steel for all the welding processes. In other cases, corrosion resistance of HAZ metal is equal to or higher than that of the base metal. So, for welded joints of steels of 15GB and 10GNB grades equivalent resistance of HAZ metal compared to

base metal is observed, and for 10KhSND, A27 and D32 steels increased corrosion resistance of HAZ metal is found.

Thus, HAZ metal has optimum corrosion resistance in welding D32 steel by nickel-free consumables; for steels 15GB and 10GNB — in welding both by nickel-containing, and nickel-free consumables; for A27 steel — in manual welding by both kinds of consumables, and in automatic welding by nickel-free wire.

Analysis of the data on corrosion resistance of weld metal reveals that the highest uniformity of corrosion of weld and base metal in noted in the cases of combination of base metal and welding consumable with close chemical composition. At application of nickel-containing welding consumables the most favourable results were obtained for steels of 10KhSND and 10GNB grades. For steel of 09G2, A27, D32 grades the best results were obtained at application of nickel-free welding consumables.

Integral estimation of corrosion resistance of both the HAZ and weld metal leads to the conclusion that only A27, D32, 15GB and 10GNB steels meet the requirements of equivalent resistance of welded joint zones.

Considering the requirements of designers that steels of strength grade 36 or 40 are required for the ice belt, and those of grades 27 or 32 — for the outer plating of underwater part, the following materials were recommended for «Sakhalin» ferries of the second generation:

• for the ice belt: steels of 15GB (E36, GOST 5521–86) and 10GNB grades (E-40, TU 14-1-4603–89). Automatic welding can be performed both by nickel-containing and nickel-free consumables, and manual welding — by nickel-free consumables for 15GB steel and nickel-containing consumables for 10GNB steel;

• for the outer plating of underwater part, inner bottom and partitions: A27 and D32 steels, welded joints on which should be made by nickel-free consumables. Erection joint of the ice belt with the ship lower part should be made by nickel-free consumables in welding 15GB to A27 and D32 steels, or nickel-containing consumables in welding 10GNB to A27 and D32 steels.

Furtheron it is rational to conduct investigations of corrosion resistance of welded joints of steels in such a combination as D32 steel to steels of grades 15GB and 10GNB.

Conclusions

1. 09G2 and 10G2S1D steels (GOST 5521–86) in the outer plating of the hull of «Sakhalin» ferries of the first generation have insufficient corrosion resistance, that leads to the need of replacement every 8 to 10 years of up to 2000 m^2 of plating in each ferry.

2. From the studied steel grades the corrosion resistance exceeding that of 09G2 steel is found in A27, D32 (TU 14-1-4264–87), 15GB (E36), 10KhSND and 10GNB steels.

3. From the viewpoint of corrosion resistance of welded joints for operation in the hull of «Sakhalin» ferries, the following materials can be recommended:

• for the ice belt: steels of 15GB (E36, GOST 5521–86) and 10GNB grades (E-40, TU 14-1-4603–89);

• for the outer plating of underwater part, inner bottom and partitions: A27 and D32 steels to TU 14-1-4264–87.

4. Welding of steels 15GB, 10GNB and A27 by manual and automatic processes can be performed by nickel-containing and nickel-free consumables. D32 steels should be welded by nickel-free consumables.

5. The above recommendations on application of rolled stock from the concrete steel grades (A27, D32 and E36) to GOST 5521–86 and TU 14-1-4264–87 also concern all the grades within the respective strength grade (27, 32 and 36).

1. Bogorad, I.Ya., Iskra, E.V. (1973) *Corrosion and protection of sea ships*. Leningrad: Sudostroenie.
2. (1981) *Corrosion*: Refer. Book. Moscow: Metallurgia.
3. (1987) *Corrosion and protection of ships*: Refer. Book. Leningrad: Sudostroenie.
4. Chertok, F.K. (1977) *Corrosion wear and fatigue life of welded joints*. Leningrad: Sudostroenie.
5. Semenova, I.V., Florianovich, G.M., Khoroshilov, A.V. (2002) *Corrosion and corrosion protection*. Moscow: Fizmatlit.
6. *OST 5.9255–76*: Metals and coatings for shipbuilding. Methods of accelerated corrosion testing.
7. *TU 14-1-4264–87*: Rolled plates for shipbuilding.
8. *TU 14-1-4603–89*: Weldable rolled hull plates of low-alloyed steel for structures of ships and off-shore engineering facilities.
9. Tomashov, N.D. (1959) *Theory of corrosion and protection of metals*. Moscow: AN SSSR.
10. Markovich, R.A. (1980) Accelerated corrosion testing of welded joints. *Transact. of TsNII MF*, Issue 257, 25–36.

Received 15.10.2012

INFLUENCE OF TECHNOLOGICAL SCHEMATICS OF INDUCTION SURFACING ON STABILITY OF DEPOSITED LAYER THICKNESS

Ch.V. PULKA, V.S. SENCHISHIN, V.Ya. GAVRILYUK and **M.S. BAZAR**
Ternopol Ivan Puluj National Technical University
56 Russkaya Str., 46001, Ternopol, Ukraine. E-mail: v_gavryliuk@mail.ru

Induction surfacing is applied in manufacture and repair of cutting tools of agricultural machinery. Deposited layers improve the tool wear resistance. Here it is important to take into account the deposited layer thickness. The paper presents the results of investigation of geometrical characteristics of a layer of metal deposited by induction process with wear-resistant powder-like consumables by four technological schematics. It is shown that application of shields, horizontal vibration and rotation of the surfaced part improves the stability of geometrical characteristics of the deposited metal layer by 22 %, compared to traditional induction surfacing. A procedure was developed for measurement of geometrical characteristics of the metal layer deposited by induction process, which allows increasing the measurement accuracy, as well as monitoring the stability of layer thickness at development of new technological processes of induction surfacing of thin flat parts. 8 Ref., 3 Figures.

Keywords: *induction surfacing, inductor, surfacing modes, thermal and electromagnetic shields, deposited layer thickness, rotation, horizontal vibration*

In agricultural machinery engineering induction surfacing is used to improve wear resistance of shares of ploughs, cultivators, plant top cutters, etc. [1, 2]. The task of surfacing thin steel disks — top cutters of beet harvesters of a toothed shape of relatively large dimensions and complex configuration, is particularly complicated (Figure 1). Diameter of top-cutter disc is 420 mm, deposited layer width is 30 mm, thickness of base and deposited metal is 3 and $1^{+0.5}_{-0.2}$ mm, respectively [3]. Width of surfaced zone is larger than the height of the tooth proper.

Machining of the layers deposited by induction process on the tools of agricultural machinery is not performed, as a rule. For this reason it is important to select such surfacing modes, which would ensure the specified values of geometrical characteristics of the deposited layers in as-surfaced condition. This, primarily, concerns the deposited metal layer thickness, on which the wear resistance and self-wetting of the surfaced tools depend. In addition, at development of new technological processes with application of induction surfacing [3], very often it is necessary to monitor and compare the influence of a particular technological process of surfacing on geometrical characteristics of the deposited metal layer.

The purpose of this work is investigation of the influence of technological schematics of induction surfacing by wear-resistant powder-like alloys on dimensions of deposited metal layer. As the currently available methods and tools for assessment of geometrical characteristics of the deposited layers are complex in terms of design

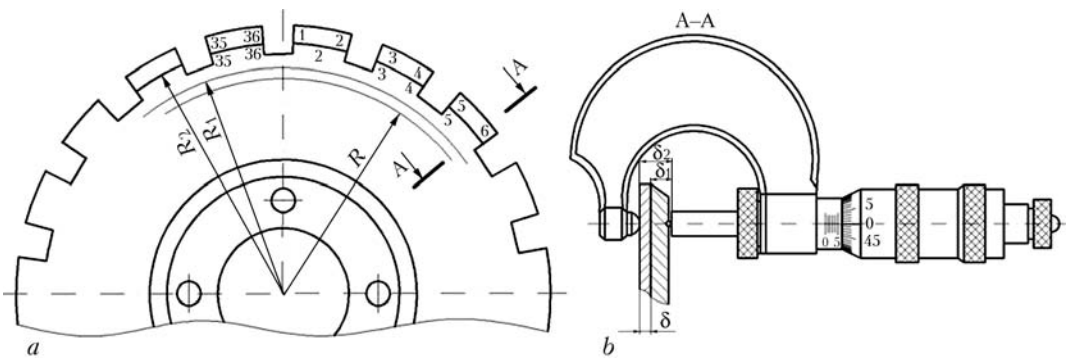

Figure 1. Schematic of configuration of plant top cutter (*a*), and cutter section along *A*–*A* with the device for deposited layer measurement (*b*)

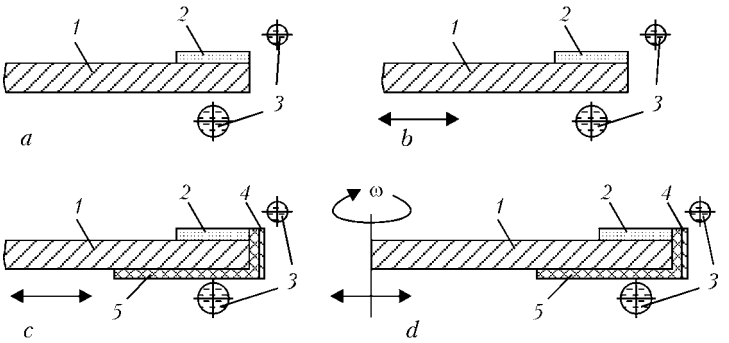

Figure 2. Schematics of induction surfacing used at investigation performance: *a* — without vibrations of surfaced part; *b* — with horizontal vibration of the surfaced part; *c* — with horizontal vibration of the surfaced part using thermal and electromagnetic shields; *d* — same, but with additional rotation of the surfaced part; *1* — part; *2* — deposited metal layer; *3* — two-turn circular inductor; *4*, *5* — electromagnetic and thermal shields, respectively (arrows show the direction of application of vibration and rotation)

[4] and give a large error at measurement, the paper deals with modern measurement tools and methods, which allow measurement of deposited metal thickness with greater accuracy and smaller error.

This work is a study of geometrical characteristics of the deposited layers for four technological schematics of induction surfacing of thin discs (Figure 2, *a–d*) [5, 6]. Deposited layer thickness was studied by the following procedure. A special device with a sphere was used to make semispherical recesses at the end face in 36 points around the circumference of radius R_2 = = 202.5 mm, as shown in Figure 1, *a*, from the side opposite to the processed surface of the disc (Figure 1, *b*). Then a micrometer, as well as another sphere of similar diameter, serving as a support for micrometer jaws (one jaw of which is semispherical, and the other has a flat surface), were used to measure the thickness of base metal δ_1 before surfacing (see Figure 1, *b*). Spheres are

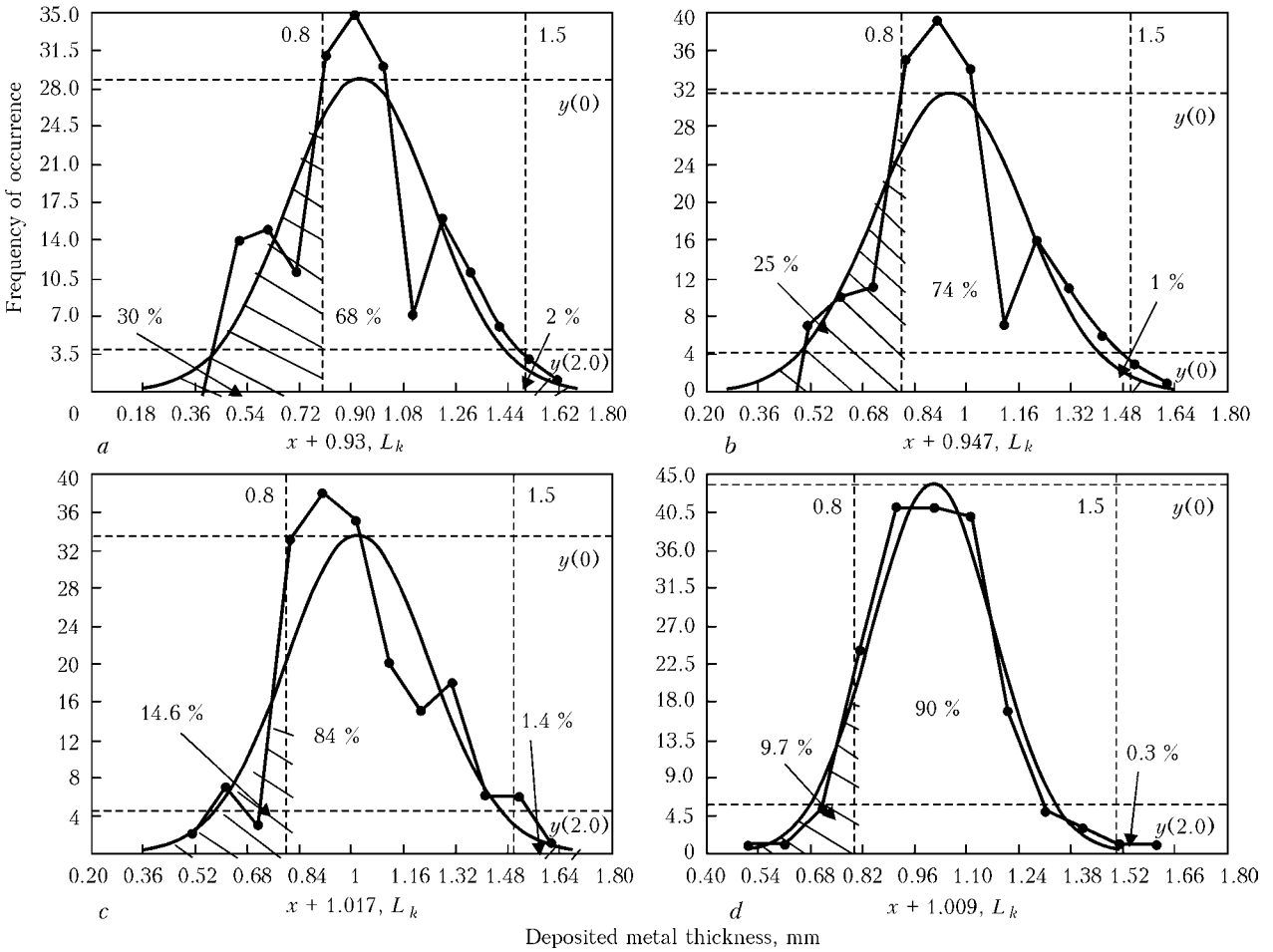

Figure 3. Curves of normal distribution of metal layer thickness (solid curve $y(x)$) and curves of dissipation of actual dimensions (broken curve) by the schematics in Figure 2, *a–d*, respectively

required to increase the accuracy of measurement of deposited metal thickness in each of 36 points, as at induction surfacing of thin discs scale forms on the surface, opposite to the processed surface, and large errors can occur at measurement of deposited metal thickness by the micrometer without spheres.

Thickness δ of the deposited layer was determined as difference of thicknesses of surfaced disc δ_2 and base metal δ_1. Investigations were performed using discs made from steel VSt3 and surfaced by induction process with powder-like alloy PG-S1 (sormite-1). Surfacing was conducted using high-frequency generator VChG-60/0.44.

Processing of the results of measurement of deposited layer thickness was performed by mathematical statistics methods [7, 8] by a specially developed algorithm.

Curves of scattering of the actual dimensions and curves of normal distribution of deposited layer thickness for the studied schematics of induction surfacing are given in Figure 3. Unhatched areas located under the curve of normal distribution, theoretically are a percentage of parts, in which the deposited metal thickness is within the tolerance range.

At induction surfacing by the schematic in Figure 2, *d*, 90 % of deposited metal thickness measurements fall into the tolerance range, that is by 22 % greater than at surfacing by the schematic in Figure 2, *a*. In this case, a more uniform thickness of the deposited layer is achieved due to simultaneous application of horizontal vibration, thermal and electromagnetic shields, as well as centrifugal forces, providing uniform distribution of liquid metal in the surfacing zone.

Conclusions

1. Developed procedure for measurement of geometrical characteristics of the metal layer, deposited by induction process, allows increasing the measurement accuracy, as well as controlling the stability of the layer thickness at development of new technological processes and modes of induction surfacing of thin flat parts.

2. Technology of induction surfacing of plant top cutters with horizontal vibration of the surfaced part, using thermal and electromagnetic shields and additional rotation of the surfaced part, improves the stability of geometrical characteristics of the deposited metal layer by 22 %, compared to traditional induction surfacing without application of shields or additional mechanical impact on the solidifying deposited metal.

1. Ryabtsev, I.A. (2004) *Surfacing of parts of machines and mechanisms*. Kiev: Ekotekhnologiya.
2. Senchishin, V.S., Pulka, Ch.V. (2012) Modern methods of surfacing the tools of agricultural tillers and harvesting (Review). *The Paton Welding J.*, **9**, 43–49.
3. Pulka, Ch.V. (2006) *Technological and energy efficiency of induction surfacing of thin steel disks*: Thesis of Dr. of Eng. Sci. Kiev.
4. Bol, A.A. (1984) Development of induction surfacing in agricultural machinery engineering. *Tekhnologiya*, Issue 3, 38.
5. Pulka, Ch.V., Shably, O.N., Senchishin V.S. et al. (2012) Influence of vibration of parts in surfacing on structure and properties of metal. *The Paton Welding J.*, **1**, 23–25.
6. Pulka, Ch.V., Gavrilyuk, V.Ya., Senchishin, V.S. (2013) Improvement of equipment and technology of induction surfacing. *Svarochn. Proizvodstvo* (in the press).
7. Kolker, Ya.D. (1976) *Mathematical analysis of the accuracy of part machining*. Kiev: Tekhnika.
8. Barabashchuk, V.I., Kredentser, B.P., Miroshnichenko, V.I. (1984) *Experiment planning in engineering*. Kiev: Tekhnika.

Received 30.01.2013

SUBSCRIPTION
FOR «THE PATON WELDING JOURNAL»

If You are interested in making subscription directly via Editorial Board, fill, please, the coupon and send application by fax or e-mail.

The cost of annual subscription via Editorial Board is $348.

«The Paton Welding Journal» can be also subscribed worldwide from catalogues of subscription agency EBSO.

SUBSCRIPTION COUPON

Address for journal delivery _____

_____

Term of subscription since _____ **20** **till** _____ **20**

Name, initials _____

Affiliation _____

Position _____

Tel., Fax, E-mail

Subscription to the electronic version of «The Paton Welding Journal» can be done at site: URL: www: rucont.ru

РУКОНТ
НАЦИОНАЛЬНЫЙ ЦИФРОВОЙ РЕСУРС

We offer for the subscription all issues of the Journal in pdf format, starting from 2009. You can subscribe to individual issues or to the entire archive including all issues over a period of 2009–2012. The subscription is available for natural persons and legal entities.

ADVERTISEMENT
IN «THE PATON WELDING JOURNAL»

in «Avtomaticheskaya Svarka» and «The Paton Welding Journal»

External cover, fully-colored:
First page of cover (190×190 mm) — $700
Second page of cover (200×290 mm) — $550
Third page of cover (200×290 mm) — $500
Fourth page of cover (200×290 mm) — $600

Internal cover, fully-colored:
First/second/third/fourth page of cover (200×290 mm) — $400

Internal insert:
Fully-colored (200×290 mm) — $340
Fully-colored (double page A3) (400×290 mm) — $500

- Article in the form of advertising is 50 % of the cost of advertising area
- When the sum of advertising contracts exceeds $1001, a flexible system of discounts is envisaged

Size of journal after cutting is 200×290 mm

Editorial Board of Journal «Avtomaticheskaya Svarka» and «The Paton Welding Journal»:
E.O. Paton Electric Welding Institute of the NAS of Ukraine
International Association «Welding»
11, Bozhenko Str., 03680, Kyiv, Ukraine
Tel.: (38044) 200 60 16, 200 82 77; Fax: (38044) 200 82 77, 200 81 45
E-mail: journal@paton.kiev.ua; www.patonpublishinghouse.com; URL: www.rucont.ru